About drugs in hydrogel drug delivery systems

Vom Fachbereich Chemie
der Universität Duisburg-Essen

zur Erlangung des akademischen Grades eines
Doktors der Naturwissenschaften

genehmigte Dissertation

von
Katarina Tomić
aus Belgrad

Tag der mündlichen Prüfung : 07.08.2008.

Die vorliegende Arbeit wurde in der Zeit von Juli 2005 bis April 2008 im Fachgebiet der Physikalischen Chemie an der Universität Duisburg-Essen unter Anleitung von Herrn Prof. Dr. W. S. Veeman angefertigt.

Vorsitzender des Promotionsausschusses:	Prof. Dr. Roland Boese
Referent:	Prof. Dr. Wiebren S. Veeman
Koreferent:	Prof. Dr. Christian Mayer

Selbständigkeitserklärung

Hiermit erkläre ich, die vorliegende Arbeit selbständig ohne fremde Hilfe verfasst zu haben und nur die angegebene Literatur und Hilfsmittel verwendet zu haben.

Katarina Tomić
22.04.2008.

Acknowledgments

First of all I would like to express my great thanks to my supervisor Prof. Dr. Wiebren S. Veeman for making it possible to start a Ph.D. study in his group, for his guidance of my work, for encouragement and extremely interesting discussions. Specially, I want to thank him for always having an open door for me, for his understanding, always positive attitude and many valuable advices, in science as well as in the life, from which I will benefit throughout my life and career.

I would like to thank DSM, Geleen, the Netherlands, for the financial support, for providing me with the materials that allowed my work to become application-oriented and for enabling me to present my results on many interesting conferences. Furthermore I would like to thank to Dr. Mark Boerakker, Dr. Victor M. Litvinov and Dr. Aylvin A. Dias for many valuable discussions throughout my research.

I sincerely thank Prof. Dr. Christian Mayer for kindly accepting to review this thesis and for his support and help during my stay at the Duisburg-Essen University.

Prof. Dr. Ronald Boese I would like to thank for the acceptance to be the chairman at my Ph.D. exam.

I owe further thanks for the technical support to Mr. Manfred Zähres and Mr. Uwe Bachorski. To Mr. Zähres I am grateful for introducing me to the NMR measurements and for his assistance during many experiments. To Mr. Bachorski I am thankful for taking care that my computer works well.

I want to thank my colleagues, Dr. Michael Vogt for his assistance at my beginning, Janine Bauer and Daniel Schunk for bringing fun in the working atmosphere and all other colleagues for a nice and pleasant atmosphere.

I owe great thanks to Gale for being all the time with me, for giving me additional motivation to stay here, for his great help and support especially at the beginning days and for everything he did for me.

Finally, I would like to express huge and special thanks to my family, my mother, father and my sister. Without them I would never be that what I am. I want to thank them for all their patience, for sharing with me both troubles and successes, for believing in me when I didn't, for endless support, love and enthusiasm. Having them makes me a rich person.

Mom deki

Dedicated to my grandfather
who taught me to read and write my first letters

Table of Contents

Chapter 1: Introduction

Drug delivery has become a major research topic in the pharmaceutical field. A drug delivery system (DDS) can be defined as device to introduce a therapeutic agent into the body[1]. It is composed of a medium or carrier and the drug to be administered in a controlled manner. The main goal of all controlled release systems is to improve the effectiveness of therapeutic agents in the body. For example, many drugs undergo degradation before they reach the action site in the body (in oral delivery certain medications are destroyed by the low pH in the stomach area). For this purpose drug carriers must fulfill some requirements. They must be able to hold the drug molecule, to release the drug under action of a stimulus (pH, temperature, dilution, electric or magnetic field,…) and to disappear after the drug delivery (removal or degradation).

The earliest drug delivery systems appeared in the 1970s and were based on polymers such as poly(lactic acid) (PLA)[2]. Since then the era of polymeric drug delivery started in which a polymer matrix is used as a rate controlling device (Fig. 1.1)

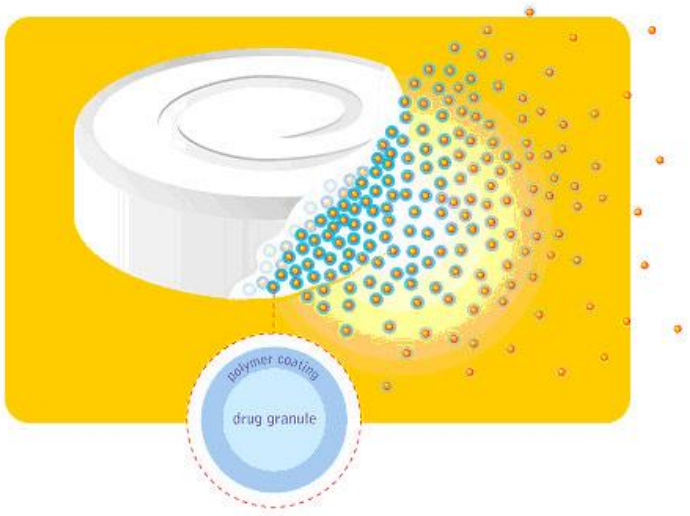

Fig. 1.1: Polymeric drug delivery[3]

There are two very important aspects to drug delivery research: the drug carrier and the control over the drug release rate.

Polymeric drug carriers can be broadly divided into two types[4]. One type comprises **non-degradable polymers** which are preferred in removable medical devices. The other type of carriers is made from **biodegradable polymers** which are favored in

permanent implants. These polymers dissolve when implanted and the release of therapeutic agent is achieved during biodegradation or prior to degradation.

An important class of materials for use as polymer matrix is formed by cross-linked polymer hydrogels. In the presence of water these polymers swell and build an open polymer network filled with water whereby the drugs are released from the matrix by diffusion[5].

A drug delivery system can also be composed without the use of a polymer network. Cyclodextrins (CDs) are most famous molecular carriers which are able to encapsulate drug molecules in their internal hydrophobic cavity[6,7,8]. CDs are very important in drug delivery and are used as solubilizing agents to enhance drug solubility and bioavailability as well as to protect drugs from enzymatic degradation and attack by various species.

The second important aspect in drug delivery is the wish to control in some way the release of the drug from the carrier. Two types of control can be achieved: **temporal control** and **distribution control**[4].

The main goal in temporal control is the delivery of a therapeutic agent at a predefined rate. That can be delivery over an extended period of time or a delivery at a specified time. For example, for those drugs which are eliminated from the body very fast it is desirable to achieve that the drug release rate from the carrier matches the drug elimination rate. In that way the drug level in the body remains constant, which can bring significant improvements in the drug therapy. This is known as **sustained drug delivery**. In other cases it is desired to achieve a burst release of the drug at a required moment. For that purpose an external stimulus has to be recognized by the delivery system that stimulates the drug release (**responsive drug delivery**). This is the case for the delivery of insulin where the stimulus is the growth of the blood sugar level.

The distribution control aims to deliver a drug to the desired location and to maintain the necessary drug level at a targeted site. The targeted drug delivery is desirable for situations where the therapeutic agent at other sites of the body can cause big unwanted side effects, like for many chemotherapeutic drugs.

For our investigations we have chosen as a drug carrier (the matrix) a group of hydrogels based on photopolymerized poly(ethylene glycol) diacrylate (PEGDA). By varying the molar mass of the PEGDA oligomers, networks can be prepared with varying

average molecular mesh sizes and chemical composition, which will affect the matrix swelling, the drug-matrix interaction and consequently the drug diffusion and the drug release rate. These polymers were made as thin films which opens their application also as coating materials. In medicine it is of great importance to develop materials for the coating of heart stents. Stents are cylindrically shaped devices which are inserted in a segment of a blood vessel to keep it open and to allow free blood flow through it (Fig. 1.1).

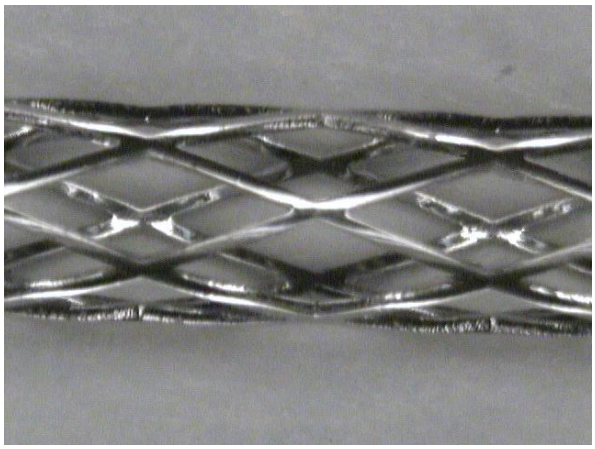

Fig. 1.1: A non-coated steel stent[9]

However, implantation of stents can cause many unwanted side effects such as inflammation or thrombosis. To prevent this coated stents are being developed in which a drug is released from the coating, the so-called drug eluting stents (Fig. 1.2).

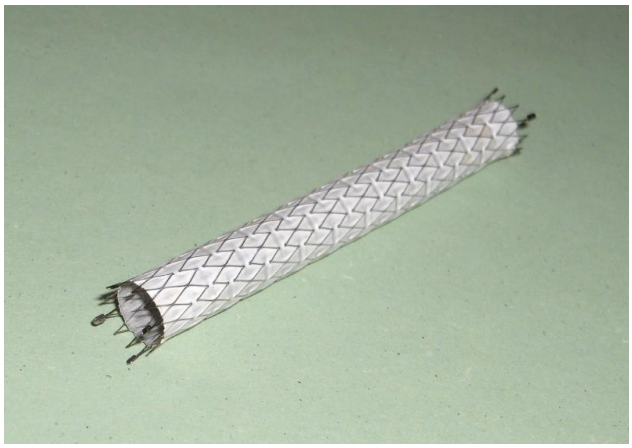

Fig. 1.2: A polymer coated stent

During insertion of a stent in a blood vessel the stent is subjected to mechanical forces and it is important that the coating is flexible enough to withstand the expansion. PEGDA films have good coating properties and for possible future application of PEGDA films as drug eluting coatings we want to investigate their behavior as drug carriers and their ability to control the drug mobility and the drug release.

PEGDA polymers are based on poly(ethylene glycol) (PEG) which makes them friendly to the human body. PEG-containing materials have been the subject of significant research for applications as controlled release devices. The PEG polymer possesses desirable properties as a drug carrier such as good water solubility, low toxicity and biocompatibility. Cross-linking of these polymers enables tuning of solute release behavior and controlled delivery of proteins[10,11], as well as small molecular weight drugs[12]. The use of photopolymerized PEG-based hydrogels for medical applications was first proposed by Hubbell et al.[13,14] The UV polymerized gels were applied for sustained and controlled release of Albumin. Later, Cruise et al.[15] studied the diffusion behavior of different biological molecules in cross-linked PEG diacrylate hydrogels. Scott and Peppas[16] developed ionizable networks from oligo(ethylene glycol) (OEG) multiacrylates and acrylic acid. They studied the swelling behavior as a function of copolymer composition and pH and demonstrated precisely tuned release behavior of the low molecular weight drug proxyphylline. Mellot et al.[17] investigated the release of a high molecular weight protein from PEGDA. Litvinov and Dias[18] investigated the structure and properties of PEGDA networks by ^{1}H NMR relaxation, ^{13}C NMR spectroscopy and dynamic mechanical experiments.

For most investigations published so far the emphasis is mainly on the direct relation between properties of the release matrix (cross-link density of the matrix, copolymer composition) and the release curve of a drug from these matrices. The drug release curve is the concentration-time curve which describes the drug release profile and from which the release rate can be determined. One can argue that the release curve indeed is the most valuable information for a drug release system. Nevertheless, a drug release curve results from a complex interplay of drug-matrix interactions, matrix swelling, drug solubility, drug and swelling solvent mobility. In this thesis we approach the problem by concentrating on the molecular drug-matrix interaction and the drug diffusional mobility

(lateral and rotational) in the matrix. The central question is the effect the matrix has on the mobility of the drug in relation to the matrix network mesh size and the drug size.

Cyclodextrins are important in drug delivery due to their ability to modify the drug release from hydrophilic matrices[19]. We also want to investigate whether it is possible to increase the retention time of a certain drug molecule in the polymer matrix by complexing the drug to a host molecule such as cyclodextrin.

We also show that for one particular insoluble drug molecule complexation with cyclodextrin leads to the formation of a novel drug delivery system without the need for a polymer matrix. This system is composed only of drug and cyclodextrin and here we report about its properties and its potential applications.

Chapter 2: Theoretical Aspects

2.1 Hydrogels

2.1.1 Composition and structure of hydrogels

Hydrogels studied here consist of polymer networks. Polymers are molecules composed of a large number of covalently bound repeating units which can be spatially arranged in different ways. If the repeating units are identical the material is termed a homopolymer. If different structural units are presented in a chain the polymer is called a copolymer. In terms of spatial arrangement polymers can be organized such that they form a linear sequence of structural units, linear polymers, such as in Fig. 2.1:

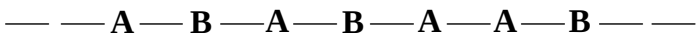

Fig. 2.1: Linear polymer

More often polymer systems are encountered where the structural units are connected to form nonlinear or branched structures (Fig. 2.2).

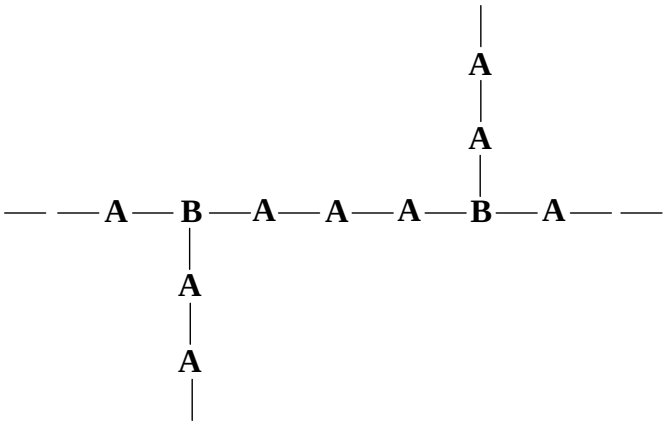

Fig. 2.2: Branched polymer

Three-dimensional (3D) network structures can be formed starting from linear polymer chains by introduction of intermolecular cross-links. The formation of cross-links joins units which belong to different molecules. A cross-linked system is presented in Fig. 2.3. There are different definitions of a polymer network, but it has to be mentioned that a cross-linked polymer and a polymer network does not necessarily represent the same thing. Not every cross-linked polymer represents a network. If the cross-linking is below a certain degree (gel point), the polymer is considered as branched. The gel point represents the state where enough polymer chains are linked. Above this limit one can talk about network structure. In chemical networks cross-links are covalent. In physical networks cross-links are formed by physical interactions. Junction points can then be caused by entanglements, crystallites or due to weak interactions (hydrogen bonding, van der Waals forces).

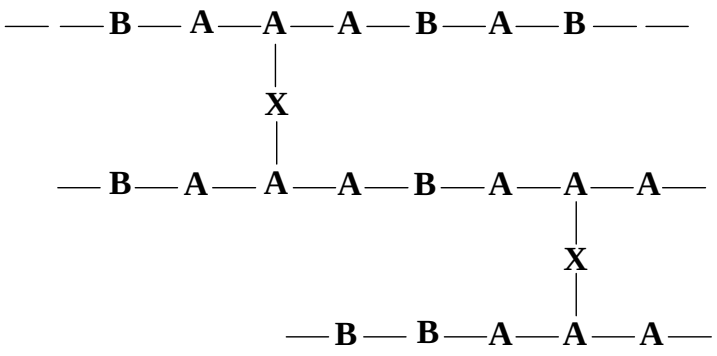

Fig 2.3: Cross-linked polymer

The properties of a cross-linked network depend on the average molecular weight between cross-links. For a better understanding of the degree of cross-linking and later the swelling behavior of polymer networks, it is important to introduce the terms “polymer molecular weight” and “degree of polymerization”. Polymers with identical chemical composition exhibit different properties depending on the length of their chains. Similarly, networks with different average chain lengths between cross-links will have a different behavior. For characterization of the polymer chain length a degree of polymerization (DP) has been introduced. The polymerization degree, DP, represents the

number of repeat units in the polymer chain. It also gives a measure of polymer molecular weight.

$$DP = \frac{M}{M_0} \tag{2.1}$$

In this equation M represents the total molecular weight of the polymer and M_0 the molecular weight of the repeating unit.

A distinction has to be made between the number average and the weight average molecular weight of a polymer. The number average molecular weight, $\overline{M}_n$, is the total weight of all polymer molecules divided by the total number of the polymers:

$$\overline{M}_n = \sum n_i \cdot M_i = \frac{\sum N_i \cdot M_i}{\sum N_i} \tag{2.2}$$

M_i represents the molecular weight of polymer chain i, N_i is the number of moles of chains i and n_i the mole fraction of chains with molecular weight M_i.

The weight average molecular weight, $\overline{M}_w$, is based on the fact that a larger polymer species contains a larger fraction of the total mass of the polymer sample than the small polymer species.

$$\overline{M}_w = \sum w_i \cdot M_i \tag{2.3}$$

w_i , the weight fraction of chains with molecular weight M_i, can be obtained by dividing the mass of species i with molecular weight M_i by the total mass of all polymer species present:

$$w_i = \frac{N_i \cdot M_i}{\sum N_i \cdot M_i} \tag{2.4}$$

The weight average molecular weight then becomes:

$$\overline{M}_w = \frac{\sum N_i \cdot M_i^2}{\sum N_i \cdot M_i} \tag{2.5}$$

The $\overline{M}_w$ is proportional to the square of molecular weight and is always larger than the number averaged molecular weight (Fig. 2.4).

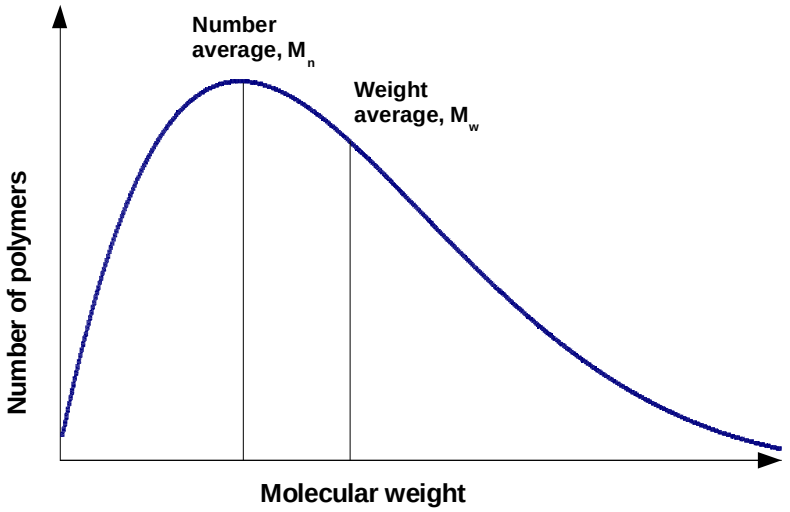

Fig. 2.4: Distribution of molecular weights in a polymer

The ratio of the weight average and the number average molecular weight describes the distribution of chain lengths, i.e. polydispersity of the sample. For most polymers this ratio is between 1.5 and 2.5. For monodisperse polymers M_w/M_n is close to 1.

For characterization of a network structure, the degree of cross-linking is a very important property. The degree of cross-linking (X) represents a measure of the extent to which a polymer is cross-linked. It can be determined as the number density of junctions (cross-links) which join the chains into a permanent structure:

$$X = \frac{\gamma}{2V} \tag{2.6}$$

γ is the number of cross-linked units, $\gamma / 2$ is the total number of cross-links and V the total polymer volume. A higher degree of cross-linking causes a restriction of chain mobility in the polymer.

2.1.2 Properties and swelling behavior of hydrogels

Hydrogels are water insoluble cross-linked network structures which are able to swell in the presence of water and thus can absorb a large amount of water. The network in a gel can be classified by the type of cross-links into physical and chemical networks.

Prediction and control of mechanical properties of hydrogels is very important for many applications. It is known that hydrogels which exhibit high swelling possess poor mechanical strength, while lowering of the swelling degree improves their mechanical properties[20]. Most of the swollen hydrogels fulfill the criteria for rubber materials. That implies that after applying mechanical stress or strain they have the ability to rapidly rearrange their polymer chains and to completely recover after removal of the stress. By decreasing the temperature this property can be lost and the gels exhibit viscoelastic behavior. Viscoelastic properties assume that after removal of deformation hydrogels need a long time for the complete recovery. If the recovery can not be completed, the materials are viscoplastic. Rubberlike properties of gels are the high extensibility, which can be achieved by low mechanical stress, and rapid recovery[21]. During swelling the thermodynamically driven swelling force is counterbalanced by the retractive force of the polymer structure and the equilibrium is achieved when these two forces become equal.
Tuning of rubber elastic behavior can be achieved by varying the ratio and type of comonomers in the gel, by changing the cross-link density and by controlling the polymerization conditions. Increasing the amount of hydrophobic components improves the mechanical properties of hydrogels. A higher cross-linking degree leads to an increase of mechanical strength. During polymerization different parameters can be varied (temperature, solvent, reaction time) which will affect the elastic behavior of hydrogels. Mechanical properties determine the swelling behavior and the possible application of hydrogels.

Ideal network structures are very rarely encountered[22]. In such a structure each junction is covalent and tetrafunctional. More often gels contain irregularities in the structure in form of multifunctional cross-links or entanglements which could be permanent or semipermanent (virtual cross-links). Defects which appear in the cross-linked network are dangling chain ends (unreacted functionalities) and chain loops. These structural defects (Fig. 2.5) do not participate in the retractive force of the network.

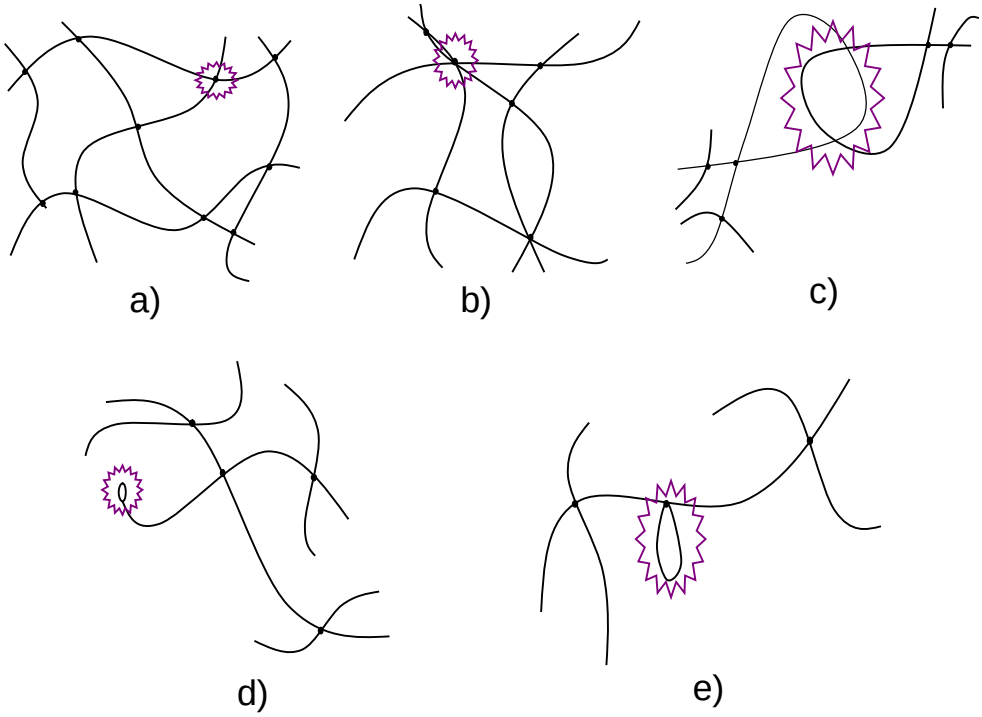

Fig. 2.5: Network structural defects: a) ideal network; b) multifunctional junctions; c) entanglements; d) free chain ends; e) chain loops

Due to the presence of cross-links gels cannot dissolve in water, but when they are placed in a water solution they expand by taking up the solvent. Diffusion of water into the gel causes stretching of polymer chains between junctions (Fig. 2.6).

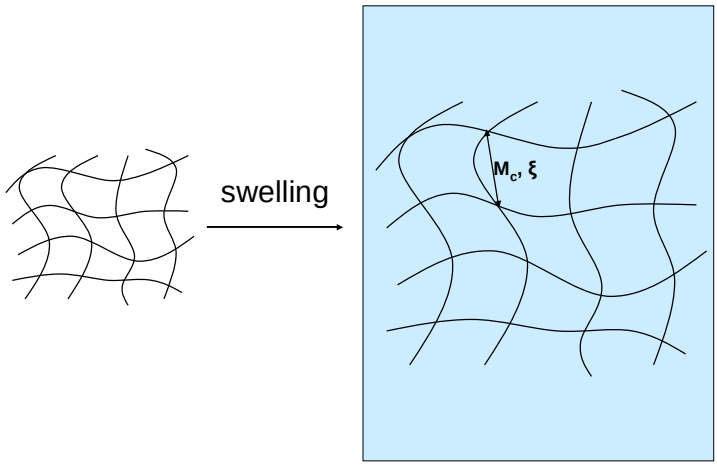

Fig. 2.6: Swelling of the gel in the presence of water.

Three important parameters for structural characterization of swollen gels are the swelling factor (Q), average molecular weight between cross-links (M_c) and network mesh-size (ξ). The swelling factor represents the ratio of the volume of swollen gel (V_s) and the polymer volume (V_p). It also equals the reciprocal of the polymer volume fraction in the swollen gel (υ_{2s}):

$$Q = \frac{V_s}{V_p} = \frac{1}{\upsilon_{2s}} \tag{2.7}$$

Highly cross-linked networks exhibit lower swelling than loosely cross-linked networks and thus have smaller swelling factors.

M_c represents the molecular weight of polymer chains between neighboring junctions. The network mesh or pore size ξ determines the average distance between cross-links points in the gel and thereby, the degree of gel porosity. With respect to their mesh-size hydrogels can be divided into macroporous, microporous or nonporous gels. The higher the cross-link density, the smaller M_c and mesh-size are (Fig. 2.8). The swelling factor can be determined experimentally by swelling measurements and allows the calculation of M_c and mesh-size.

According to the Flory-Rehner theory[23] absorption of the solvent by the network leads to stretching of chains between junctions. The chains will take less probable configurations, which leads to decrease of entropy. At the same time an increase of entropy occurs due to mixing of solvent with polymer. The Gibbs energy change of a system (ΔG) can be defined as the sum of two contributions[24]: Gibbs energy of mixing (ΔG_{mix}) and the elastic Gibbs energy (ΔG_{el}):

$$\Delta G = \Delta G_{mix} + \Delta G_{el} \tag{2.8}$$

The corresponding change of chemical potential is then:

$$\Delta \mu = \Delta \mu_{mix} + \Delta \mu_{el} \tag{2.9}$$

The Gibbs energy of mixing is:

$$\Delta G_{mix} = \Delta H_{mix} - T \cdot \Delta S_{mix} \ , \tag{2.10}$$

where ΔH_{mix} is the mixing enthalpy, ΔS_{mix} is the entropy of mixing and T is the temperature. The enthalpy of mixing is[24]:

$$\Delta H_{mix} = k_b \cdot T \cdot n_1 \cdot \chi \cdot \upsilon_2 \ , \tag{2.11}$$

where k_b is the Boltzmann constant, n_1 is the number of water molecules in the swollen gel, χ is the polymer-solvent interaction parameter and υ_2 is the polymer volume fraction in the swollen gel. The entropy of mixing is given[24]:

$$\Delta S_{mix} = -k_b \cdot \left(n_1 \cdot \ln \upsilon_1 + n_2 \cdot \ln \upsilon_2 \right) \ , \tag{2.12}$$

where again n_1 is the number of water molecules in the swollen gel and υ_1 is the volume fraction of water $\left(\upsilon_1 + \upsilon_2 = 1 \right)$. Assuming that in the gel the number of free polymer molecules (n_2) is zero, the Gibbs energy of mixing becomes:

$$\Delta G_{mix} = k_b \cdot T \cdot \left(n_1 \cdot \ln \upsilon_1 + \chi \cdot n_1 \cdot \upsilon_2\right) = k_b \cdot T \cdot \left\{n_1 \cdot \ln\left(1-\upsilon_2\right) + \chi \cdot n_1 \cdot \upsilon_2\right\} \tag{2.13}$$

The difference between the chemical potential of the solvent in the gel (μ) and in the free solution (μ^0) can be obtained by differentiation of ΔG_{mix} with respect to the number of solvent molecules:

$$\Delta\mu_{mix} = \mu - \mu_0 = k_b \cdot T \cdot \left[\ln\left(1-\upsilon_2\right) + \upsilon_2 + \chi \cdot \upsilon_2^2\right] \tag{2.14}$$

Multiplication with Avogadro's constant gives the chemical potential difference per mole:

$$\Delta\mu_{mix} = R \cdot T \cdot \left[\ln\left(1-\upsilon_2\right) + \upsilon_2 + \chi \cdot \upsilon_2^2\right] \tag{2.15}$$

The Gibbs elastic retracting energy per mole was determined by Flory[24]:

$$\Delta G_{el} = \frac{R \cdot T \cdot \nu_e}{2} \cdot \left(3\alpha^2 - 3 - \ln \alpha^3\right) \tag{2.16}$$

where ν_e is the number of effective chains (excluding free ends) and α is the linear expansion factor of the network. The change of chemical potential due to the elastic retractive force is:

$$\Delta\mu_{el} = \left(\frac{\partial G_{el}}{\partial n_1}\right)_{T,P} = R \cdot T \cdot V_1 \cdot \frac{\nu_e}{V_0} \cdot \left(\upsilon_2^{1/3} - \frac{\upsilon_2}{2}\right) \tag{2.17}$$

V_0 represents the volume of the unswollen polymer and V_1 the molar volume of the solvent. The total change of the chemical potential is the sum of two contributions and when the state of equilibrium swelling is reached, it equals zero:

$$\Delta\mu = \Delta\mu_{mix} + \Delta\mu_{el} = 0 \tag{2.18}$$

From this condition Flory derived an equation for calculation of the M_c value from the swelling ratio obtained in the equilibrium swelling experiment:

$$\frac{1}{M_c} = \frac{2}{M_n} - \frac{\frac{\bar{\nu}}{V_1}\cdot\left(\ln(1-\upsilon_2)+\upsilon_2+\chi\cdot\upsilon_2^2\right)}{\upsilon_2^{1/3}-\frac{\upsilon_2}{2}} \tag{2.19}$$

$\bar{\nu}$ is the specific volume of the polymer. This equation was later used, either in original form or in modified form by Bray and Merill[25], for evaluation of the average molecular weight between cross-links.

Once M_c is known, the network mesh-size (ξ) can be estimated according to the procedure derived by Canal and Peppas[26]. At first the average end-to-end distance of the polymer chains between cross-links in the absence of swelling water $\left(\sqrt{\left\langle \bar{r}_0^2 \right\rangle}\right)$ has to be calculated. It depends on the number average molecular mass of the chains between cross-links:

$$\sqrt{\left\langle \bar{r}_0^2 \right\rangle} = l\cdot\sqrt{2\cdot C_n\cdot\frac{M_c}{M_r}} \tag{2.20}$$

where l is the bond length of the polymer repeating unit, C_n is a ratio characteristic for the polymer and M_r is the molecular mass of the polymer repeating unit. The mesh-size of the network is related to the swelling factor of the polymer :

$$\xi = \sqrt{\left\langle \bar{r}_0^2 \right\rangle}\cdot\upsilon_2^{-1/3} = \sqrt{\left\langle \bar{r}_0^2 \right\rangle}\cdot\sqrt[3]{Q} \tag{2.21}$$

If a gel is swollen in water above the equilibrium condition (more water than the maximum amount the gel can take up), two phases will appear: a hydrogel phase and a water phase. The T-w_2 phase diagram of a hydrogel, where w_2 is the weight fraction of the polymer, represents various phases of the binary gel-water system and conditions under which these phases coexist. Hydrogel properties can be thus interpreted on the basis of a T-w_2 phase diagram. The line on the diagram which shows the maximum amount of the water that can be added to the polymer before a second phase (free water) appears is the swelling curve of the hydrogel. The schematic representation of a hydrogel phase diagram is shown in Fig. 2.7. As the water can exist in three different states of matter, liquid, vapor and crystal, there can be three different equilibria between a gel and a solvent[27]. Borchard et al.[27] investigated swelling of a cross-linked substance in equilibrium with a solvent. They found that in the cases where the temperature is between melting and boiling point of the solvent, the swelling curve will be almost parallel to the ordinate in the temperature-weight fraction diagram.

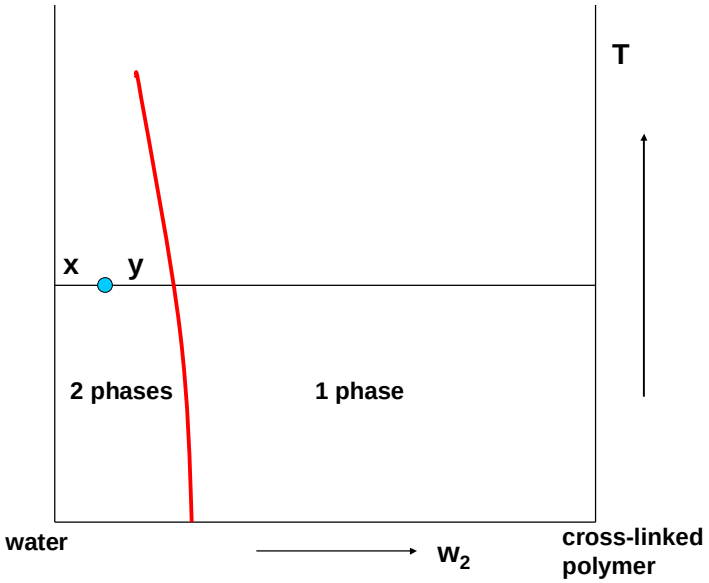

Fig. 2.7: Schematic representation of a binary phase diagram of hydrogel. The blue circle represents an overall composition in the two-phase area and the red line the swelling curve of a hydrogel.

An isothermal line intersecting the swelling curve is called a tie line. The ratio of two phases in a two-phase diagram at a given temperature can be obtained by the lever rule. From Fig. 2.7, the weight fraction of the gel in the binary mixture is:

$$f(gel) = \frac{x}{y + x} \tag{2.22}$$

According to this rule, the relative amount of a gel phase in the two-phase gel-water system is proportional to the fraction of tie line between the overall composition and the temperature axis of the diagram.

2.1.3 Polymeric hydrogels and drug release

In polymeric drug delivery systems different mechanisms can be applied to control the release of drugs[28]. Three different types of controlled devices are often encountered: diffusion-controlled systems, swelling-controlled systems and erosion-controlled systems. In diffusion-controlled and swelling-controlled devices the hydrogel matrices swell due to water penetration and the drug molecules can be released from the matrix via diffusion.

In **diffusion-controlled systems** the drug diffusion rate determines the drug release rate from the polymer. In a polymeric matrix the polymer represents an obstruction for drug diffusion and decreases the drug release rate. Swelling of the polymer lowers this diffusion barrier because big pores are formed through which drugs can easily diffuse out. Two kinds of diffusion-controlled systems are known: reservoir based devices and matrix based devices (Fig. 2.8). The reservoir devices possess a core filled with the drug, which is surrounded by a polymer membrane in order to slow down the drug release.

Matrix or monolithic devices contain a drug which is dispersed throughout the polymer structure and release occurs by diffusion through the polymer.

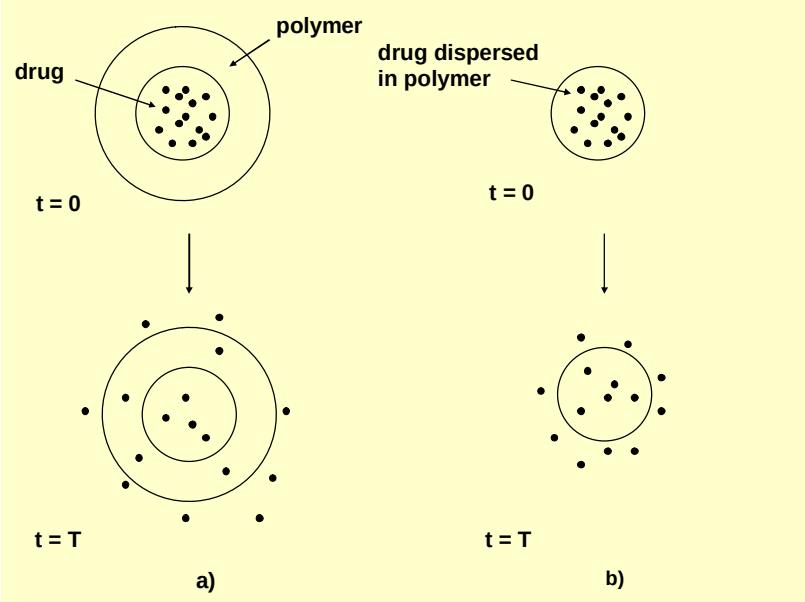

Fig. 2.8: Diffusion-controlled drug delivery systems: a) reservoir devices b) matrix formulations

In **swelling controlled systems** the drug is initially dispersed in a glassy polymer and is unable to diffuse (Fig. 2.9). During swelling the polymer undergoes a transition from the glassy to rubbery state. Only the drug in the swollen part of the polymer can diffuse out. In that process several fronts are formed, where a front represents a boundary between gel regions where the gel properties sharply change (Fig. 2.9). Colombo et al. described the movement of gel fronts and their influence on the drug release rate[29]. The swelling front divides the glassy polymer from the swollen region. The erosion front separates the matrix from the surrounding solvent. Between these two fronts a diffusion front can be observed which represents a boundary between a solid drug and a dissolved drug. Its position depends on the drug dissolution rate in the gel. If the swelling and erosion front move synchronously, the gel layer thickness will remain constant and zero-order release can be achieved. This means that drug will be released from a polymer at a constant rate.

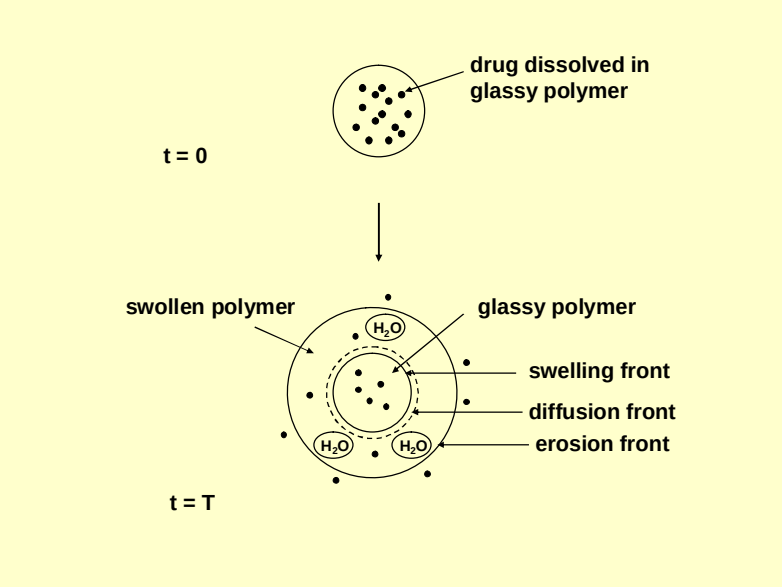

Fig. 2.9: Swelling-controlled drug delivery system

In the **erosion-controlled systems** a drug is dispersed in a polymer matrix and can only be released by erosion of the device itself (Fig. 2.10). The release rate is determined by the erosion rate and if it is constant, zero-order release can be obtained.

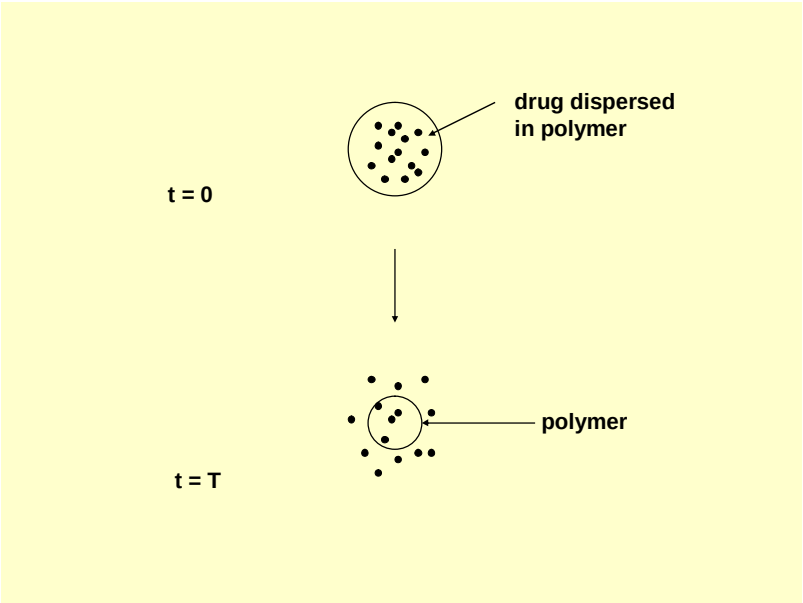

Fig. 2.10: Erosion-controlled drug delivery system

Ritger and Peppas developed an equation for description of the release kinetics from swellable polymeric devices[30]:

$$\frac{M_t}{M_\infty} = k \cdot t^n \tag{2.23}$$

where M_t is the amount of drug released at time t, M_∞ is the amount of drug released at infinite time, k is the kinetic constant and n is the diffusion exponent. When n equals one, the drug release will be zero-order. The drug release curve can be obtained by measuring the amount of released drug in certain time intervals (M_t = f (t)) and it represents an overall manifestation of the release properties of a matrix.

2.2 Diffusion

2.2.1 Principles of molecular diffusion

Molecular diffusion can be described as a random translational motion of molecules driven by their thermal energy. Thermal motion is random, which means that the molecules will tend to move down a local concentration gradient. A distinction can be made between two types of diffusional motion: transport diffusion and self-diffusion. Transport diffusion represents the net movement of molecules resulting from an overall concentration gradient. Self-diffusion relates to the motion when the chemical potential gradient equals zero and the quantity describing the migration rate in the macroscopic equilibrium is known as the self-diffusivity. Because it is more convenient to study systems under equilibrium conditions, most diffusion studies are related to the self-diffusion measurements.

Adolf Fick introduced two differential equations describing the Brownian motion under a concentration gradient. The first law relates the flux, J(r, t) (which is a vector), to the concentration gradient[31]:

$$J(r,t) = -D \cdot \nabla c(r,t) \,, \tag{2.23}$$

where D is the (transport) diffusion coefficient in units length^2/time and c(r, t) is the concentration. The negative sign indicates that the migration occurs in the direction of lower concentration. The diffusion coefficient increases with the temperature and is inversely proportional to the mass of the diffusive species. The second Fick law states that the change of concentration in time is equal to the local change of flux:

$$\frac{\partial c(r,t)}{\partial t} = -\nabla J(r,t) \tag{2.24}$$

Combining this equation with Fick's first law, the equation is obtained which describes the change of concentration gradient with time[31]:

$$\frac{\partial c(r,t)}{\partial t} = D \cdot \nabla^2 \cdot c(r,t) \tag{2.25}$$

Equation 2.25 can be applied only in the case of isotropic diffusion.

The diffusion process can be interpreted as a random walk, where the movement of each particle is represented by a sequence of steps or jumps, equal in size and with equal probability in any direction. The jump frequency is assumed to be constant. The property of random walk is the independence of individual steps whereby the movement of a certain particle does not depend on its history, but only on its position before the jump.

In order to determine the mean square displacement of such a molecule we can observe the propagation of a large number of molecules (an ensemble). The movement of a molecule i can be characterized by a time-dependent displacement vector $r_i(t)$. If a molecule i had a displacement r_i at t = 0, the function which gives a probability that a certain molecule j will be found at a position r_j' at time t, is known as the correlation function[32] $P(r_i | r_j', t)$. This function is sensitive to relative motions and it correlates the

displacements of $r_i(0)$ and $r'_j(t)$ both for i = j and i ≠ j. For this reason the self-correlation function[32] (i = j) has been introduced, $P_s(r|r',t)$, which gives the probability that a molecule at a position r at t = 0 will run a distance R in a time t and move to a new position r' (Fig. 2.11). This function is also called the propagator and contains the maximum information about the system. The total probability to find a particle at the position r' at the time t, $P(r',t)$, is given:

$$P(r',t) = \int P(r,0) \cdot P_s(r|r',t) \cdot dr \,, \tag{2.26}$$

where $P(r,0)$ represents the particle density ρ(r).

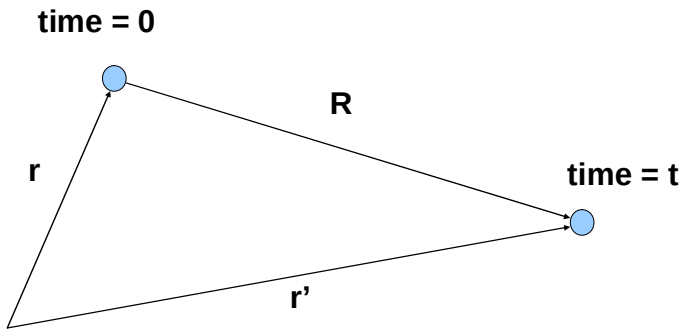

Fig. 2.11: Time dependence of a particle displacement

Fick's equation can be applied now for the case of self-diffusion if the concentration is replaced by the propagator $P_s(r|r',t)$:

$$J = -D \cdot \nabla' P_s \,,$$

$$\frac{\partial P_s}{\partial t} = D \cdot \nabla'^2 \cdot P_s \tag{2.27}$$

D is now the self-diffusion coefficient.

In the case of unrestricted isotropic three-dimensional diffusion ($P_s \rightarrow 0$ as $r' \rightarrow \infty$), the propagator, as the solution of eq. 2.27 shows, is a Gaussian function:

$$P_s\left(r|r',t\right) = \frac{1}{\left(4\pi Dt\right)^{\frac{3}{2}}} \cdot e^{-\frac{(r'-r)^2}{4Dt}} \tag{2.28}$$

In a similar way, the average propagator can be determined, $\overline{P_s}\left(R,t\right)$, giving the probability that a certain particle will have a net displacement R over a time t:

$$\overline{P_s}\left(R,t\right) = \frac{1}{\left(4\pi Dt\right)^{\frac{3}{2}}} \cdot e^{-\frac{R^2}{4Dt}} \tag{2.29}$$

In the case of one-dimensional diffusion along the z-axis, the mean square displacement can be now calculated by integration:

$$\left\langle z^2\left(t\right)\right\rangle = \int_{-\infty}^{+\infty} z^2 \cdot P\left(Z,t\right) \cdot dz = 2 \cdot D \cdot t \ , \tag{2.30}$$

where Z = z'(t) - z(0). For three-dimensional diffusion the mean square displacement becomes:

$$\left\langle R^2\left(t\right)\right\rangle = 6 \cdot D \cdot t \quad , \tag{2.31}$$

which is the Einstein-Smoluchowski equation.

2.2.2 Physical models for diffusion of small molecules in polymer gels

In order to be able to control the diffusion of drug molecules in polymers, a detailed understanding of the molecular diffusion process in polymer solutions and gels is needed. For this purpose it is necessary to determine how the molecular size and shape of

the solute molecule as well as the specific interactions between a matrix and a solute affect the diffusion behavior within the gel. It is known that the diffusion rates in gels are between those in solids and liquids. In order to relate diffusivity to structural properties of a swollen gel, various models for the description of diffusion of small molecules in polymer gels have been developed[33,34]. They have been divided into models based on obstruction effects, Free Volume Models and hydrodynamic models.

Models based on obstruction effects. These models are also known as lattice models because the gel is considered to form a polymer-solvent lattice. Here, the diffusion of small molecules in the gel is described to take place in the solvent of the swollen gel. The polymer chains act as obstructions for this diffusion because the lattice sites occupied by the polymer are not available to drug or water molecules. Increase of the polymer concentration in the gel leads to a decrease of the solute diffusion coefficient. Mackie and Meares[35] developed a concept for description of the diffusion of electrolytes in a resin membrane. According to them, the diffusion of a small molecule in a gel is a function of the volume fraction, υ_2, occupied by the polymer in the gel (in the absence of the diffusing molecule):

$$\frac{D}{D_0} = \left(\frac{1-\upsilon_2}{1+\upsilon_2} \right)^2 \tag{2.32}$$

D is the self-diffusion coefficient of the diffusing molecule in the gel phase and D_0 is the self-diffusion coefficient in the water phase without the polymer matrix. With increasing cross-link density, υ_2 increases due to the fact that a higher cross-linked network takes up less water upon swelling. The shortcoming of this approach is that it does not consider how the size and shape of the solute affect the diffusion coefficient.

The same lattice concept was improved by Ogston et al.[36], by taking into account the solute size. They assumed that the diffusion of variously sized molecules takes place in a solution of long molecular fibers with negligible width. The diffusion coefficient depends both on the size of solute and the size of molecular fiber:

$$\frac{D}{D_0} = \exp\left[-\frac{r_s + r_f}{r_f} \cdot \upsilon_2^{1/2} \right] \quad , \tag{2.33}$$

where r_s is the hydrodynamic radius of the molecule and r_f is the cylindrical radius of the fiber.

All these lattice models provided good results only for small-sized molecules in dilute polymer solutions and their main drawback is that the interaction between the diffusing molecule and the polymer matrix is described as between hard spheres.

Free Volume Models. These models assume that the molecular diffusion in the gel occurs due to random distribution of free volume voids in a polymer matrix. The diffusion process can be then interpreted as a sequence of jumps of a molecule into holes created by the thermal rearrangement of all species. The diffusion coefficient will be determined by the probability that there exists a hole larger than a critical size in which the molecule can move. Increase in polymer concentration reduces this probability, and therefore leads to decrease of the solute diffusion coefficient. The well-known concept was developed by Yasuda et al.[37]. Assuming that the free volume of the system arises mainly from the solvent contribution they developed the following equation:

$$\frac{D}{D_0} = \exp\left[\frac{B}{f_w} \cdot \left(1 - \frac{1}{1 - \upsilon_2} \right) \right] \quad , \tag{2.34}$$

where B is the minimum size of the hole necessary for the solute movement and f_w is the solvent free volume. These models were successfully applied in the cases of low concentrated drug solutions, but in general they also neglect the existence of interaction between the solute and the polymer matrix.

Hydrodynamic models. These concepts treat polymers as mobile species and also consider hydrodynamic interactions between all components in the system: the interactions of the solute with the polymer, solute with the solvent and the interactions of the solvent with the polymer. Philies developed an equation based on experimental results[38]:

$$D = D_0 \cdot e^{\left(-\alpha \cdot c^{\nu}\right)} , \tag{2.35}$$

where c is polymer concentration. α and ν are scaling parameters which depend on the size of solute molecule. This equation provided good results for polymer solutions of different concentrations and for solutes ranging from small-sized molecules to macromolecules, but the scaling parameters α and ν miss physical meaning and theoretical justification.

Many of the suggested diffusion models were not able to explain the temperature dependence of diffusion coefficient. Experiments have shown that often this dependence is exponential and can be described by the Arrhenius equation:

$$D = D_0 \cdot e^{-\frac{E_a}{R \cdot T}} , \tag{2.36}$$

here R is the universal gas constant, T the absolute temperature and E_a is the activation energy of diffusion. This equation is only valid in dilute polymer solutions. According to this equation a molecule can move from its surroundings into a neighboring hole only if it acquires sufficient energy to overcome the activation energy or the diffusion barrier. If the activation energy is known useful information about molecular motion in the gel can be obtained.

The diffusion of small molecules in polymers is a very complex process and that is why different theories exist trying to integrate the effects of molecular size and shape and specific interactions on the solute diffusion behavior. In many cases attempts to improve the existing theories are needed in order to accurately describe the drug diffusion in polymer gels.

2.3 Molecular rotation in liquids

The magnetic resonance method (will be discussed in Chapter 3) represents a valuable tool for the investigation of molecular rotational motion in liquids[39]. Basic

information about molecular mobilities can be provided by NMR relaxation measurements. The T_1 relaxation time is a time constant for the longitudinal (spin-lattice) relaxation process and T_2 is a time constant for the transverse (spin-spin) relaxation. The molecular correlation time for isotropic tumbling motion or rotation, τ_c, determines the frequency of molecular reorientation and represents the average time for one rotation to take place[39]. In the simplifying case of isotropic rotational motion and relaxation through dipolar interaction[40] the dependence of nuclear spin relaxation times on the correlation time τ_c can be easily described[41]. When the correlation time is short, T_1 and T_2 are long. This is the situation of small symmetric molecules in a low-viscosity solvent, where they undergo fast rotational motions and possess very short τ_c values. As the correlation time increases, T_1 decreases passing through a minimum value (Fig. 2.12). A further increase in τ_c leads to an increase in T_1, but T_2 remains small.

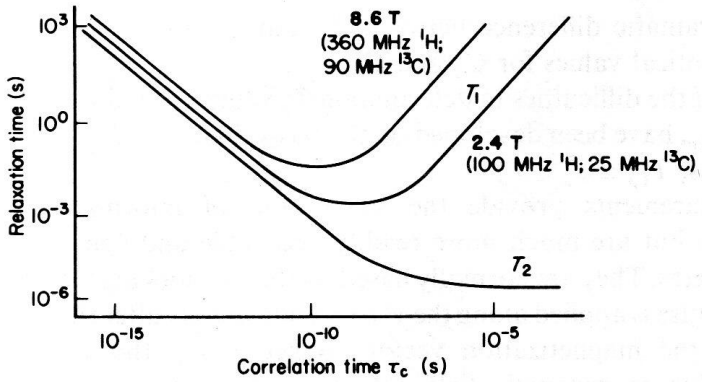

Fig. 2.12: Dependence of relaxation times T_1 and T_2 on rotational correlation time[41]

Tumbling motion of molecules larger in size occurs less freely in solution and the corresponding correlation times are longer. For those molecules which can fast and freely rotate, T_1=T_2. In most other situations differences between T_1 and T_2 are found.

In order to describe anisotropic molecular rotation in liquids it is necessary to introduce a model for the motion. Most molecules are asymmetric and their rotation is not isotropic, but preferred axes of rotation exist. In general the rotational motion about different axes occurs at different rates. For such a study the planar benzene molecule has been taken as an example[42]. Woessner et al. found that for such an axially symmetric

molecule which undergoes rapid anisotropic motion around the two rotational axes relaxation times will be nearly equal ($T_1 \approx T_2$), as for rapid isotropic motion. When the motion is strongly anisotropic T_2 is much smaller than T_1.

By measuring and comparing T_1 and T_2 it is immediately clear if the molecular rotation is isotropic or anisotropic. Relaxation measurements can therefore provide information about the effects of restricted geometries in which a molecule rotates. The motion in restricted geometries is encountered for small molecules in polymer solutions and in that way the influence of polymers on molecular rotation can be followed. Molecular dynamic simulations on the benzene molecule[43] show that the correlation time for reorientational motion around the symmetry axis (perpendicular to the plane) is shorter than the correlation time for the reorientation around the in-plane axes. That means that the rotation about the symmetry axis (spinning motion) is faster than the rotations about the in-plane axes (tumbling motion). By introducing benzene in a polymer matrix, it was found that the tumbling motion around the in-plane axes is further drastically slowed down, whereas the rotation around the symmetry axis is only slightly affected.

The molecular motion of a solute in a gel is also expected to be highly anisotropic. This is caused by the fact that for the tumbling motion around the in-plane axes molecules need more space and the energy barrier for such motion in the gel is higher. The sensitivity of NMR to molecular rotational diffusion makes it a useful tool to follow how the matrix affects the rotational mobility of drug molecules.

2.4 Molecular encapsulation

Inclusion compounds (complexes) are supramolecular structures formed by molecular encapsulation based on noncovalent interactions. These compounds represent complexes of host-guest type. They contain a molecular species with cavity or tunnels in its structure (the host) in which a second molecule (the guest) or some parts of it are located (Fig. 2.13). If in the host structure the space around the cavity is closed, the guest molecule will be entrapped like in a cage and such a complex is called a cage compound. The association between host and guest is not based on covalent bonding and the

molecular interaction is of the van der Waals type. Other forces like hydrogen bonding or hydrophobic interactions also play an important role in complex formation. One of the most common techniques to follow the formation of inclusion compound is NMR.

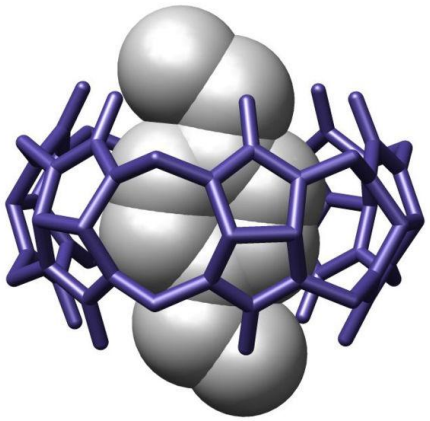

Fig. 2.13: Example of an inclusion compound between host and guest[44]

Cyclodextrins (CDs) are among the most widely used host molecules and are able to encapsulate drugs at a molecular level. Chemically they are cyclic oligosaccharides composed of glucopyranose units linked through α-1,4-linkages. α, β and γ CDs (with six, seven and eight glucose residues, respectively) are hollow molecules which enclose cavities of 5-8 Å in diameter. The outer surface of a CD molecule is hydrophilic while the inner cavity is hydrophobic. The lipophilic environment enables cyclodextrins to build inclusion complexes with many different drug molecules.

The most common way to prepare a CD-drug inclusion compound is by mixing an excess of the drug with cyclodextrin in solution and after equilibrium is reached to filter the mixture to obtain a clear drug-CD complex solution. Most frequently formed are 1:1 complexes, but also 2:1, 1:2 and other more complicated associations are encountered. Binding of a guest molecule to a CD in the case of 1:1 complex can be represented by the equilibrium reaction:

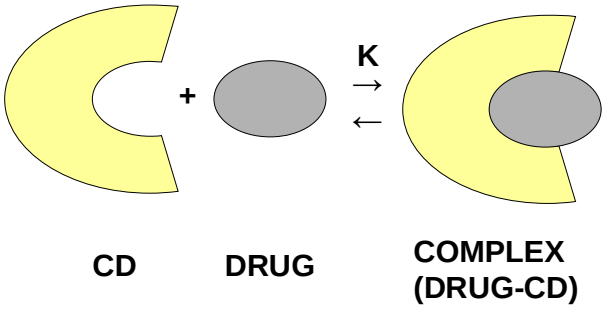

Fig. 2.14: Host-guest complexation

The above equilibrium usually is established very fast and the constant K is known as the complex stability constant. The complex usually possesses dynamic character which means that the associated drug molecules are constantly exchanging with the free drug species.

Molecular encapsulation reactions are thermodynamically driven. The driving force for the complexation is the substitution of enthalpy rich water molecules by a guest molecule. The cavity of CD is filled with water which is energetically unfavoured due to polar-nonpolar interactions. On the other side, unpolar drug molecules in bulk solution are surrounded by polar water. The energy of the system will be significantly lowered when the water molecules from the CD cavity are replaced by apolar drugs, which overcomes the lowering of the entropy. There are also other factors which influence inclusion complex formation[45]. Very important is that the guest is of appropriate size so that it can physically fit into the CD cavity. Very small or very large organic molecules will not be complexed. The complexation depends on the charges of drug and CD, temperature of the system, presence of other substances in solution and substitution of the parent CD molecule. The addition of polymers to a drug-CD complex solution can both enhance or reduce complexation[46,47]. In some cases polymers behave as competing host molecules for drug binding.

One of the most important applications of inclusion compounds in the pharmaceutical field is to enhance drug stability and drug solubility, both in liquids and

polymers[48]. The inclusion complex can also protect drugs from attack by various species. Such complexes are able to modulate drug release from polymer matrices which makes them very attractive for drug delivery. Due to the desirable properties of cyclodextrins, as nontoxicity and water solubility, efforts are made to develop CD-based hydrogels composed of cyclodextrins alone[49].

Chapter 3: Methods

3.1 Nuclear Magnetic Resonance (NMR) spectroscopy

NMR spectroscopy is based on the fact that most nuclei possess an angular momentum called spin. The angular momentum vector $\left(\vec{I}\right)$ is quantized[50]:

$$\left|\vec{I}\right| = \sqrt{I \cdot (I+1)} \cdot \hbar \ , \tag{3.1}$$

where $\hbar = h / 2\pi$, h is Planck's constant and I represents the spin quantum number which can have integral or half-integral values: 0, 1/2, 1, 3/2,…

A nucleus with spin quantum number I≠0 possesses besides the angular momentum also a magnetic moment μ[50]:

$$\vec{\mu} = \gamma \cdot \vec{I} \tag{3.2}$$

The proportionality factor γ is the gyromagnetic ratio and has a specific value for each nucleus. If the nucleus is placed in an external magnetic field B_0, the component of the angular moment along the direction of the field is quantized[50]:

$$I_z = m \cdot \hbar \quad , \tag{3.3}$$

where m is the magnetic quantum number and can have values m = -I, -I+1, …I-1,I. The spin in a magnetic field can therefore take only certain orientations and this is known as directional quantization (Fig. 3.1).

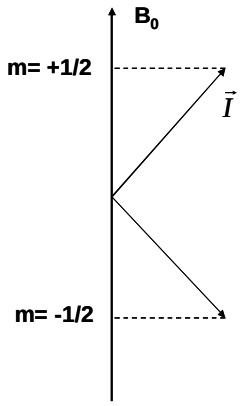

Fig. 3.1: Spin with the quantum number I = ½ in a magnetic field

The energy of a magnetic dipole in a magnetic field along the z-axis ($\vec{B} = B_0 \cdot \vec{k}$) is[50]:

$$E = -\vec{\mu} \cdot \vec{B} = -\mu_z B_0 = -m\gamma\hbar B_0 \tag{3.4}$$

That means that each orientation of a spin in a magnetic field will correspond to a different energy level (Fig. 3.2).

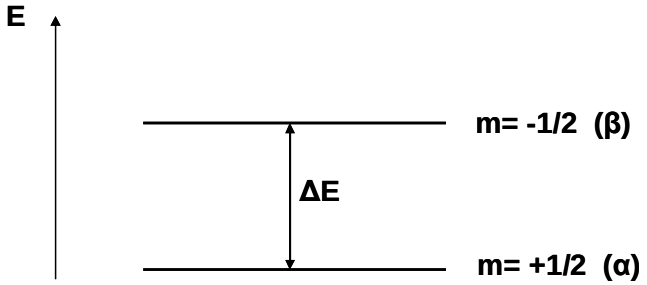

Fig. 3.2: Energy levels of a spin (I = ½) in the magnetic field

If m is positive the spin is oriented parallel to the field direction which is energetically favourable and its energy will be lower (assuming that γ is positive, there are a few nuclei that have negative gamma). The energy difference between two neighboring energy levels is:

$$\Delta E = \gamma \hbar B_0 \tag{3.5}$$

According to quantum mechanics only transitions between adjacent levels are allowed ($\Delta m = \pm 1$). Because this energy difference is much smaller than the thermal energy ($k_B T$), the populations of both levels are almost equal. At room temperature there is a slight excess in the lower energy level:

$$\frac{N_\beta}{N_\alpha} = e^{-\frac{\Delta E}{k_B \cdot T}} \approx 1 - \frac{\Delta E}{k_B \cdot T} = 1 - \varepsilon \quad ; \quad \varepsilon \approx 10^{-6} \tag{3.6}$$

In a system with N spins the sum of all magnetic moments forms a macroscopic magnetization and is represented by a vector oriented along the field direction.

Irradiation of spins with electromagnetic waves whose energy corresponds to the energy difference between two spin states leads to transitions between the levels. Absorption of photons can occur if the resonance condition is satisfied:

$$h\nu_1 = \Delta E = \gamma \hbar B_0 \tag{3.7}$$

This is the basis of the **continuous wave (CW)** NMR technique. The interaction between spins and radiation causes induced absorption, induced emission and spontaneous emission transitions. According to Einstein the two induced transitions have the same probability and spontaneous emission can be neglected for NMR. In the CW experiment there are two ways to achieve resonance, one is by keeping the frequency ν_1 constant and changing the magnetic field strength B_0 and the other is to vary the frequency of radiation at a constant value of B_0. The NMR spectrum is obtained when the absorbed energy ΔE is represented versus B_0 (at the constant ν_1) or versus ν_1 (at constant B_0) (Fig. 3.3).

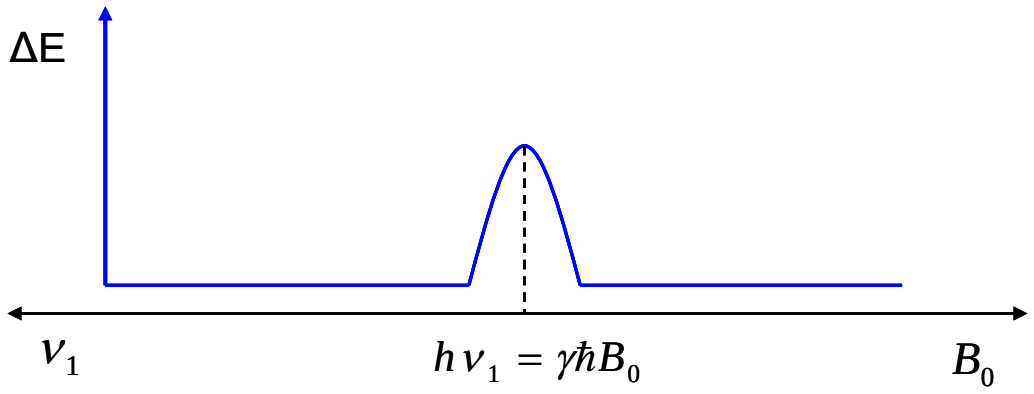

Fig. 3.3: The NMR spectrum

3.1.1 The pulsed NMR spectroscopy

In the continuous wave method the spectrum is measured by using only one frequency which is inefficient because most of the experiment time will be used for detecting the base line between resonances. A much more efficient way of exciting the spins is by using a pulsed radiation field. Fourier Transformation (FT) of such a pulse function has shown that the pulse contains a band of frequencies symmetrical about the central frequency ν_1[51]. The shorter the pulse, the larger the frequency range it includes. The frequency components located farther away from ν_1 possess lower intensities and in order to obtain a broad excitation spectrum very short and strong pulses are applied ("hard pulses").

In the classical interpretation each spin in the magnetic field precesses around the field axis with the Larmor frequency $\omega_0 = \gamma \cdot B_0$. The macroscopic magnetization under equilibrium conditions is along the field direction. In the NMR experiment a radio-frequency (rf) pulse is applied to the sample along the x axis. Quantummechanically this leads to transitions between spin states, but in the classical interpretation the rf excitation causes the magnetization to tip away from the equilibrium orientation along B_0. After the pulse the macroscopic magnetization will then also start to precess around B_0 with the frequency ω_0 (Fig. 3.4)

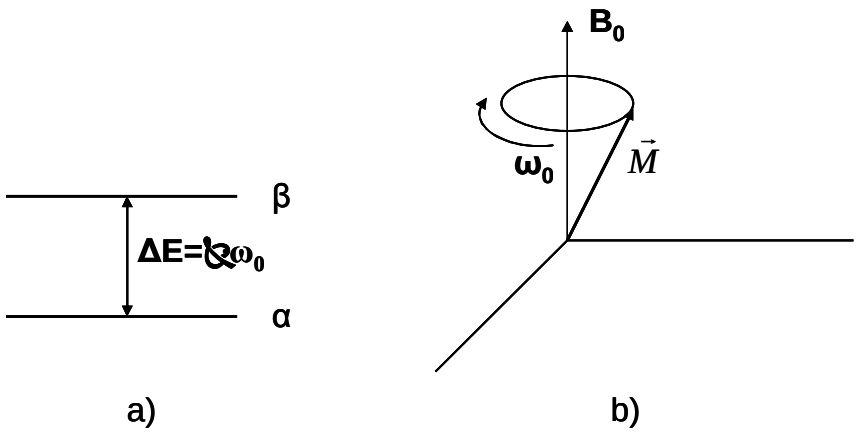

Fig. 3.4: Interaction of the spin system with the rf radiation in the quantum-mechanical interpretation (a) and classical interpretation (b)

In order to explain the interaction between spins and external magnetic field a rotating coordinate system has been introduced. This system with the axes x', y' and z' (z'|| z) rotates around the z axis with the frequency ω, the frequency of the excitation field, in the direction of precession. In this system a virtual field, B_{virt}, has to be introduced[51]. The linearly oscillating magnetic field produced by rf pulse, for instance along the x axis, can be represented as the sum of two vectors with magnitudes (B_1) rotating in the x-y plane in opposite directions. Only the component which rotates in the direction of precession, in first order interacts with the spin system. (Fig. 3.5).

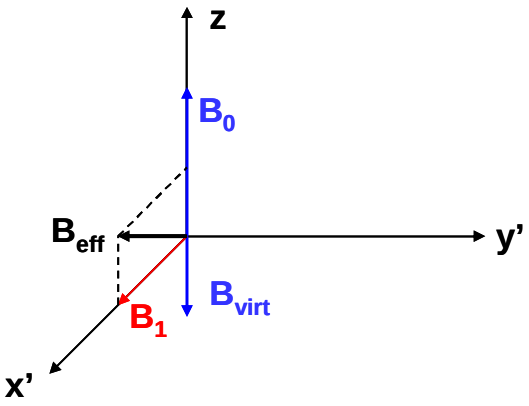

Fig. 3.5: Effective magnetic field in the rotating coordinate system

In the rotating coordinate system during the excitation rf pulse there are three magnetic fields: B_0, $B_{virt}=\omega/\gamma$ and B_1, which contribute to the total effective field B_{eff}. In the case when the photon frequency equals the resonance frequency ω_0, B_{eff} becomes equal B_1.
If the pulse with the time length τ and the frequency $\omega=\omega_0$ is applied to the system in equilibrium, the only field in the rotating coordinate system is B_1. The magnetization will start to precess around the field B_1. The effect of B_1 is to turn the magnetization vector around the x' axis in the y'-z plane over an angle θ. This angle is known as the **flip angle**. It depends on the pulse duration, applied field B_1 and the gyromagnetic ratio:

$$\theta = \gamma \cdot B_1 \cdot \tau \tag{3.8}$$

By varying the pulse length it is possible to adjust the value of the angle θ. Two important cases are 90^0_x and 180^0_x pulses, where the magnetization is turned through the angle $\pi/2$ and π, respectively, around the x' axis (Fig 3.6.).

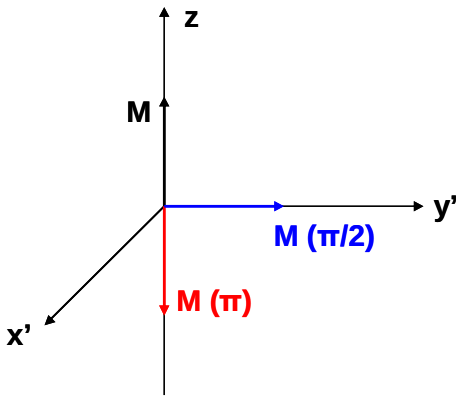

Fig. 3.6: Magnetization vector before pulse (black), after a 90^0_x pulse (blue) and after a 180^0_x pulse (red)

3.1.2 Relaxation

After applying rf radiation the spins absorb photons and undergo transitions between energy levels. These transitions tend to equalize the populations of the two involved levels (saturation). Further absorption of radiation would then be impossible if

there would not be relaxation phenomena[32]. When the pulse is turned off, the magnetization vector is turned over an angle θ and the system is not in equilibrium. The relaxation processes which try to restore the equilibrium state are spin-lattice and spin-spin relaxation. In the equilibrium state magnetization is parallel to the magnetic field. During these processes the magnetization component M_z will increase to its original value M_0, while M_x and M_y will decrease to zero.

Spin-lattice relaxation involves an exchange of energy between spins and their surrounding (lattice). Under the term lattice are assumed all degrees of freedom other than from the spins of a system. This relaxation pathway enables restoring of the M_z component of magnetization (longitudinal relaxation)[32]:

$$\frac{dM_z}{dt} = -\frac{M_z - M_0}{T_1} \quad , \tag{3.9}$$

where T_1 is the spin-lattice relaxation time.

The transverse relaxation process includes exchange of energy between spins and describes the decay of M_x and M_y magnetization components to zero[32]:

$$\frac{dM_{x,y}}{dt} = -\frac{M_{x,y}}{T_2} \quad , \tag{3.10}$$

where T_2 is the spin-spin relaxation time. Also this decay is exponential:

$$M_{x,y}(t) = M_{x,y}(0) \cdot e^{-\frac{t}{T_2}} \tag{3.11}$$

The exchange of energy between spins and lattice is always less probable than among the spins themselves and therefore T_2 cannot be longer than T_1 ($T_2 \leq T_1$). The T_2 time determines the width of the resonance line in the NMR spectrum. Usually the broader the line, the more rigid is the part of the sample where the spin is located.

3.1.3 Pulse techniques

Different combinations of applied pulses can be used for determination of T_1 and T_2 relaxation times, as well as for measurement of molecular self-diffusion coefficients[32]. The majority of methods are based on the application of combinations of 90^0 and 180^0 pulses.

a) Inversion recovery method

The inversion recovery method is used for determination of the spin-lattice relaxation time. The T_1 time is very important because it provides information about molecular mobilities. The pulse sequence is represented in Fig. 3.7.

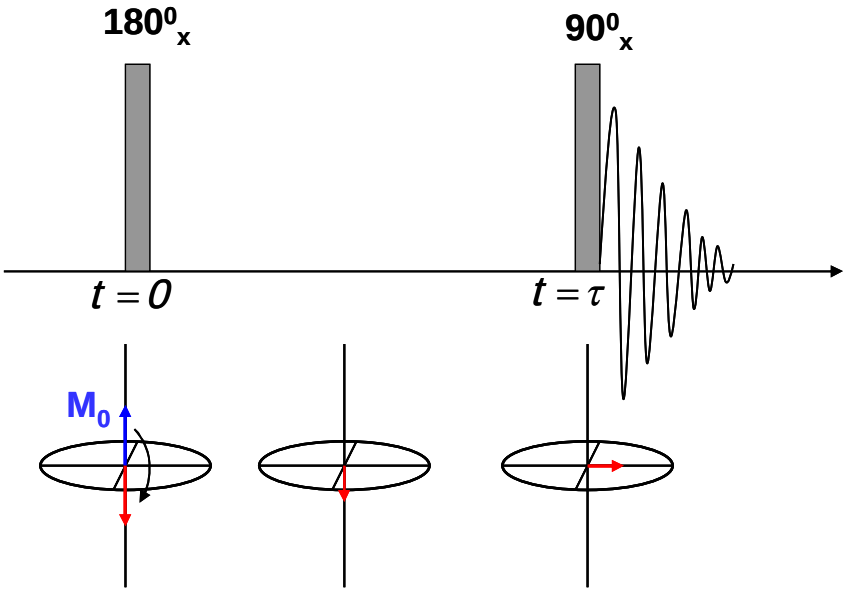

Fig. 3.7: Inversion recovery pulse sequence

The 180^0_x pulse inverts the magnetization vector M_0 and it becomes antiparallel to B_0. The longitudinal relaxation process proceeds for a time τ. The following 90^0_x pulse rotates the magnetization $M(\tau)$ into the x-y plane and the intensity of the NMR signal is proportional to $M(\tau)$. By measuring $M(\tau)$ for different time intervals the T_1 time can be calculated:

$$M(\tau) = M_0 \cdot \left(1 - 2 \cdot e^{-\frac{\tau}{T_1}} \right) \tag{3.12}$$

b) The Spin-Echo (Hahn-Echo) experiment

The Spin-Echo experiment is one of the basic and widely used NMR techniques for obtaining different kinds of information. The pulse sequence is shown in the Fig. 3.8.

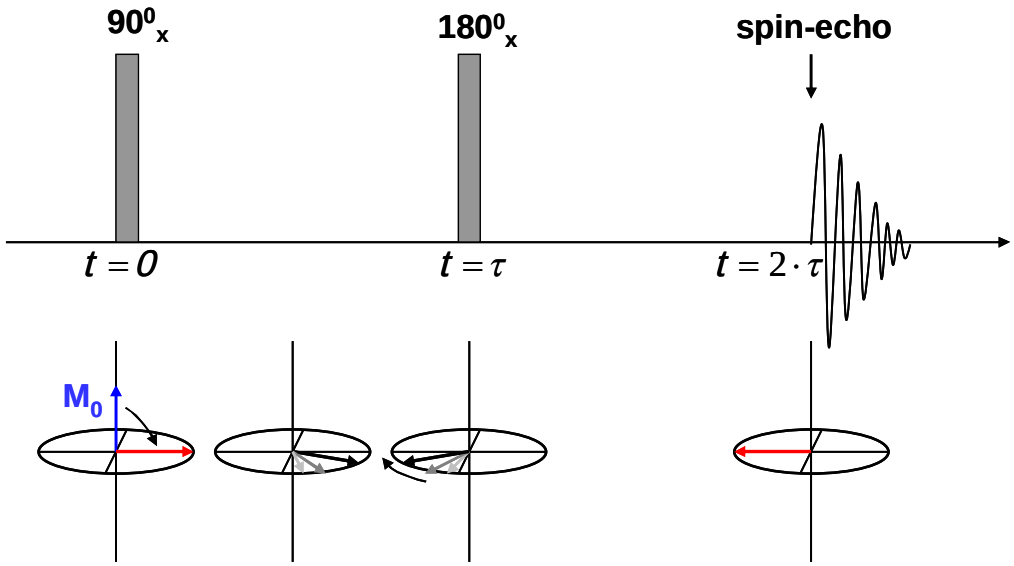

Fig.3.8: Spin-Echo pulse sequence

Due to inhomogeneity of the magnetic field or small differences in chemical shift, spins in a sample usually precess with different resonance frequencies. The 90^0_x pulse brings the total magnetization vector in the x-y plane. There, the magnetizations from different spins precess at different frequencies and that causes a dephasing of the transverse magnetization. After a time interval τ, a 180^0_x pulse is applied which deflects each vector through 180^0. The magnetizations remain in the x-y plane but after the pulse the vectors with lower precessing frequencies are in front of the vectors with higher frequencies. In that way the initial apparent loss of spin coherence is reversed and after the time τ (at t = 2τ) all spins independent of their frequency become phase coherent and build a spin-echo

signal. The echo attenuation is caused only by the spin-spin relaxation and this technique is therefore used to determine the T_2 relaxation time. With increasing time τ, the echo amplitude decreases:

$$E(2\tau) = M_0 \cdot e^{-\frac{2\cdot\tau}{T_2^*}} \tag{3.13}$$

The time constant T_2^* usually is longer than the T_2 time determined from the line width. Both relaxation times are influenced by molecular mobility and become shorter with increasing rigidity of a sample.

c) The Stimulated-Echo experiment

As already mentioned, in materials in which molecular motion is extremely slow, the T_2 relaxation time is significantly shorter than the T_1 time. That means that the transverse magnetization exists only over a short period of time. For diffusion experiments, one often needs to increase the observation time and this becomes possible if the transverse magnetization is stored for a certain time. This can be achieved by the stimulated-echo method whose pulse sequence is shown in the Fig. 3.9.

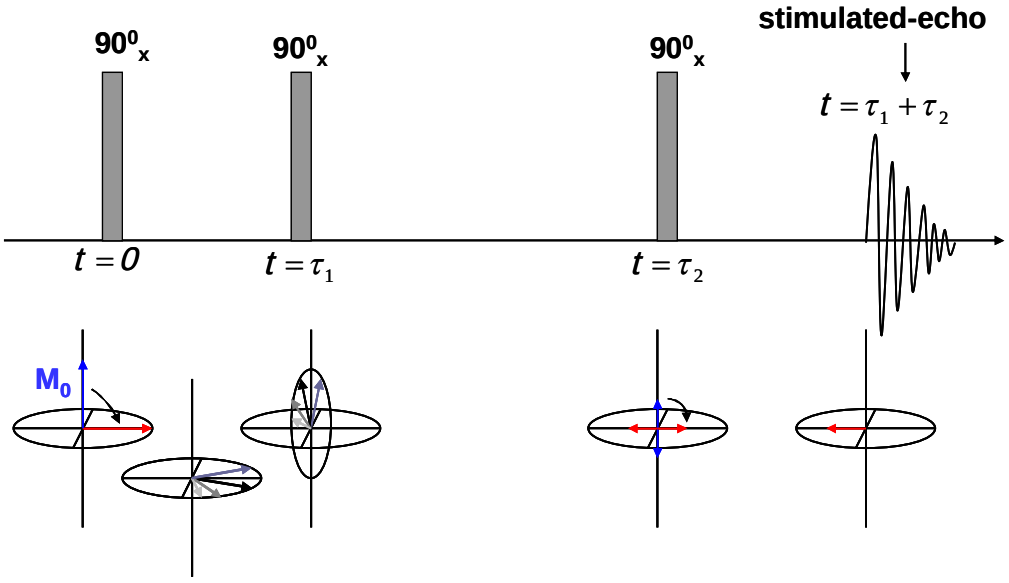

Fig. 3.9: Stimulated-Echo pulse sequence

By the first 90^0_x the equilibrium magnetization is transformed to transverse magnetization. During the τ_1 time the T_2 relaxation proceeds. The second 90^0_x pulse moves the magnetization vectors in the x-z plane. Here the component of the magnetization vector perpendicular to the field rapidly disappears (with time T_2). During the time interval between τ_1 and τ_2 time the former transverse magnetization is stored along the magnetic field B_0 and is affected by T_1 relaxation. Only half of the initial transverse magnetization can be stored because its x component has disappeared. At $t = \tau_2$ the third 90^0_x pulse is applied which inverts z-magnetization to the x-y plane. At the time $\tau_1+\tau_2$ a stimulated-echo signal is obtained. Although the signal is formed by only one half of magnetization this technique is very useful for overcoming limitations due to short T_2 values.

3.1.4 Parameters of the NMR spectrum

An isolated spin in a magnetic field possesses a resonance frequency:

$$\nu_0 = \frac{\omega_0}{2\pi} = \frac{\gamma}{2\pi} \cdot B_0 \qquad (3.14)$$

Interactions with electrons and other spins will cause a change of ν_0.

a) Chemical shift

Due to the presence of electrons the effective magnetic field (B_{eff}) at the position of the nucleus will be less than the applied field B_0. The nuclei are shielded by electrons:

$$B_{eff} = B_0 - \sigma \cdot B_0 = (1-\sigma) \cdot B_0 \quad , \qquad (3.15)$$

where σ is the shielding constant. The resonance frequency becomes then:

$$\nu_0 = \frac{\gamma}{2\pi} \cdot (1-\sigma) \cdot B_0 \tag{3.16}$$

The resonance frequency depends on the shielding constant and therefore chemically non-equivalent nuclei of a sample will have different resonance peaks in the spectrum. The chemical shift δ is a dimensionless quantity which describes the change of the resonance frequency with respect to a reference substance. As reference compound usually tetramethylsilane (TMS) is used for which it is assumed that δ(TMS) = 0.

$$\delta = \frac{\nu_{sample} - \nu_{ref}}{\nu_{ref}} \cdot 10^6 = \frac{\sigma_{ref} - \sigma_{sample}}{1-\sigma_{ref}} \cdot 10^6 \tag{3.17}$$

δ values are always given in parts per million (ppm). The chemical shift depends on the electronic structure of a molecule.

b) Spin-spin coupling

Nuclear spins are magnetic dipoles which can interact with each other. This interaction among the spins, the spin-spin coupling, also affects the magnetic field at the position of the observed nucleus.

One type of coupling mechanism is the dipolar or direct spin- spin coupling. It plays an important role in solid state NMR spectroscopy. The dipolar coupling represents the direct interaction between dipole moments. The strength of the interaction depends on the distance and relative orientations of the dipoles:

$$E = -\frac{\mu_1 \cdot \mu_2 \cdot (1-3\cos^2\theta)}{4\pi\varepsilon_0 \cdot r_{i,j}^3} \ , \tag{3.18}$$

where $r_{i,j}$ is the distance between spins i and j with dipole moments μ_i and μ_j and θ is the angle between internuclear vector $\vec{r}_{i,j}$ and the magnetic field $\vec{B}_0$. Depending on the orientation of the other spin, the resonance peak of the observed spin will be split into

two peaks. In liquids due to fast molecular motion this dipolar interaction is averaged to zero $\left(\left\langle 1-3\cos^2\theta\right\rangle = 0\right)$. In contrast, in solids it leads to very strong line broadening.

The other mechanism of coupling is J-coupling or indirect spin-spin coupling. It occurs only through chemical bonds and is always intramolecular. In high-resolution NMR of solutions it is responsible for the fine structure of the spectra. In solid state NMR it can usually be neglected because it is many orders of magnitude smaller than the dipolar coupling.

3.1.5 NMR self-diffusion measurements

For the measurement of molecular self-diffusion coefficients the pulsed field gradient echo (PFGE) techniques are important[31]. These techniques are composed of a sequence of rf pulses combined with field gradient pulses, which temporarily cause that the external magnetic field is no longer homogeneous. The precession frequency of the transverse magnetization of the spins during the gradient pulses will depend on their location. The gradient pulses therefore lead to a rapid dephasing of the transverse magnetization. In the case of the Hahn spin-echo sequence gradient pulses of duration δ are applied immediately after the first and second rf pulse (Fig.3.10).

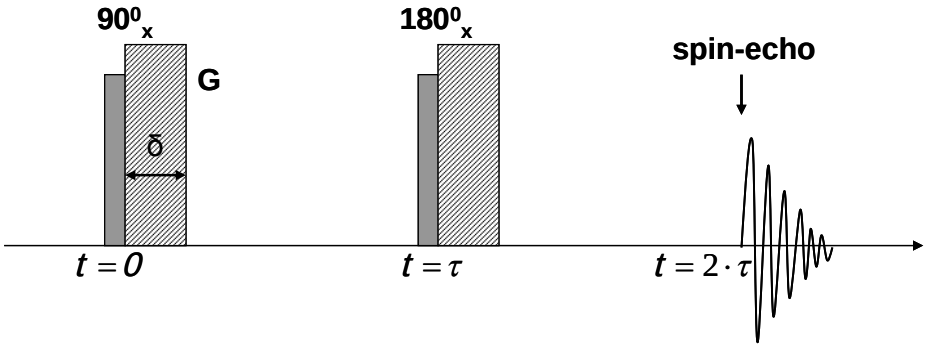

Fig. 3.10: Pulsed field gradient spin-echo technique

If the molecular species would not move in the time between gradient pulses, the dephasing of the transverse magnetization after the first gradient pulse would be completely reversed by the action of the second gradient pulse in combination with the

second rf pulse, as in the standard Hahn-echo experiment. But if the molecules during that time interval move, which causes an irreversible phase shift of the spins[52], the magnetization is not fully restored and this leads to an attenuation of the echo intensity. The time between two gradient pulses is denoted by Δ and represents the time over which the diffusion is followed, the diffusion time. In the case of stimulated echo (Fig. 3.11) the gradient pulses are applied after the first and third 90^0_x pulse. This enables an increase in the observation time for studying slower diffusion phenomena.

The spectrometer was equipped with a diffusion probe head which can impose magnetic field gradients up to 1200 G/cm. The temperature is changed using the variable temperature control unit. As temperature calibration an ethylene glycol sample was used, which possesses two proton NMR signals whose chemical shift difference is temperature dependent.

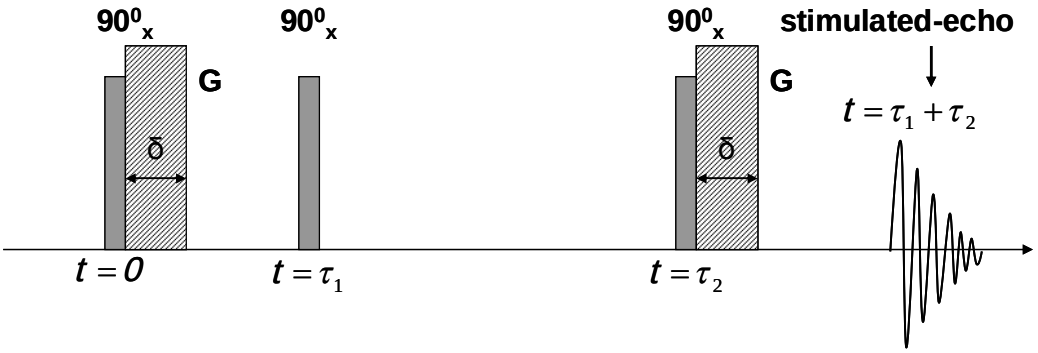

Fig. 3.11: Pulsed field gradient stimulated-echo technique

The Stejskal-Tanner equation[53] describes the attenuation of the echo intensity as a function of several parameters:

$$\frac{I(g)}{I(0)} = e^{-\gamma^2 \cdot G^2 \cdot \delta^2 \cdot D \cdot (\Delta - \delta/3)} \tag{3.19}$$

where I(g) and I(0) are the NMR spin echo intensities with and without magnetic field gradient and G is the magnetic field gradient strength. By increasing the gradient strength in steps and measuring the echo intensity it becomes possible to determine the diffusion

coefficient D of a molecule. The self-diffusion coefficient can be obtained either by exponential fitting of the data using eq. 3.19 or by calculating the negative slope of the logarithmic Stejskal-Tanner plot (Fig. 3.12).

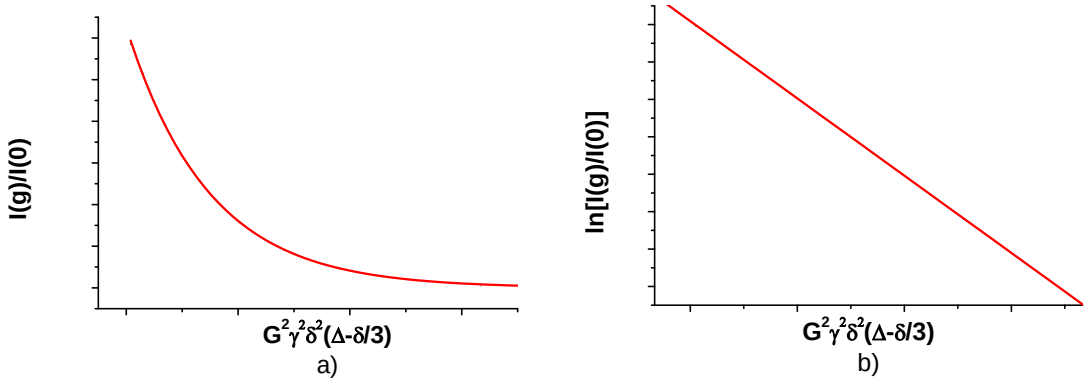

Fig. 3.12: Exponential (a) and logarithmic (b) Stejskal-Tanner plot for one diffusive species

The diffusion coefficient D for instance represents a valuable parameter to distinguish between a free molecule (A) and a molecule bound to a vehicle (B)[54]. The total echo intensity will then contain two contributions:

$$I = I_A + I_B = I_A(0) \cdot e^{-\gamma^2 \cdot G^2 \cdot \delta^2 \cdot D_A \cdot (\Delta - \delta/3))} + I_B(0) \cdot e^{-\gamma^2 \cdot G^2 \cdot \delta^2 \cdot D_B \cdot (\Delta - \delta/3)} \qquad (3.20)$$

If the two diffusion coefficients are significantly different, then it becomes possible to determine both diffusivities by applying a biexponential fit or a double linear fit (Fig. 3.13). The slope of the terminal part of the plot corresponds to the molecular species with the slowest diffusion. From the slope of the initial part of the plot the diffusivity of the faster molecular species can be obtained. The Stejskal-Tanner fitting procedure is done by using Microcal Origin software.

This shows that the use of magnetic gradient techniques provides information about molecular mobilities and opens the application for studying molecular association and interaction with different types of molecular carriers[55,56,57].

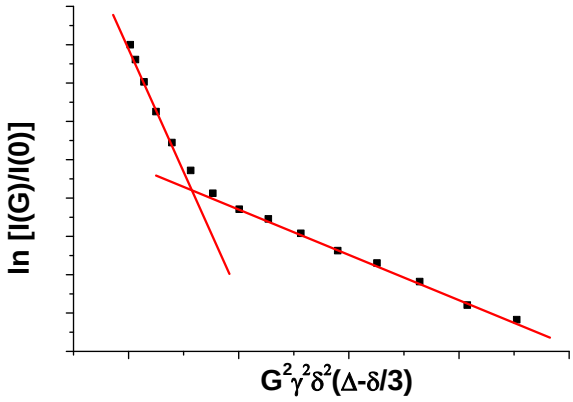

Fig. 3.13: Stejskal-Tanner plot for two diffusive species

3.1.6 Nuclear Overhauser Effect (NOE)

a) General

The NOE effect is related to the transfer of spin polarization from one spin to another via cross-relaxation[50]. The energy levels of a two-spin system with unlike spins A and B (same spins but different chemical shifts) are shown in Fig. 3.14. In good approximation only the transitions where one spin flips are NMR detectable. There are therefore two resonances, an A and a B resonance (in the absence of J-coupling). Relaxation transitions (spin-lattice relaxation) are possible between all spin energy levels when spin-lattice relaxation is caused by modulation of the A-B dipolar coupling through motion.

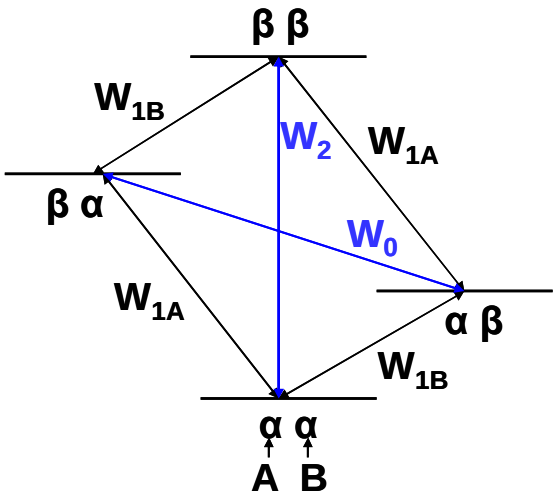

Fig. 3.14: Energy level diagram for a two-spin system (AB). With W are denoted spin-lattice relaxation probabilities for transitions between spin states

In Fig. 3.14 W_{1A} and W_{1B} then represent the relaxation probabilities for the single quantum transitions. There is also a relaxation transition, the double quantum transition, which includes a simultaneous flip of both spins ($\alpha\alpha \rightarrow \beta\beta$) with probability W_2. The transition with the probability W_0 ($\alpha\beta \rightarrow \beta\alpha$) is known as the zero quantum transition. If the A resonance is now saturated by rf excitation the populations of the levels $\alpha\alpha$ and $\beta\alpha$ and of $\alpha\beta$ and $\beta\beta$ become equal. In first instance, this has no effect on the intensity of the B signal. If now relaxation process W_2 occurs, it will lead to an increase of the population in the $\alpha\alpha$ state, thereby enhancing the intensity of the B resonance. W_0 relaxation in a similar way will lead to a decrease of the B intensity by saturation of the A resonance. These two competing mechanisms determine the observed amplification of the B resonance upon saturation of the A transitions. The NOE enhancement, $f_B(A)$, is defined by the relative change of B intensity by saturation of A:

$$f_B(A) = \frac{B - B_0}{B_0} \tag{3.21}$$

B_0 is the equilibrium intensity of B.

The importance of the NOE technique is due to the fact that the occurrence of a NOE enhancement implies that the two nuclear spins must be physically near (distance smaller than ca. 0.5nm), otherwise the dipolar coupling responsible for the W_0 and W_2 relaxation processes is ineffective.

b) Saturation Transfer Difference (STD) spectroscopy

The STD NMR technique is an one-dimensional NOE method for detection of weak interactions between low molecular weight compounds and large biomolecules[58,59]. The method is based on the transfer of magnetization from a spin A on a receptor to a spin B on a ligand molecule. The spin on the receptor is selectively saturated and the observation of an effect on one of the spins of a bound molecule enables to identify the ligand and to screen for direct ligand-receptor interaction (Fig. 3.15).

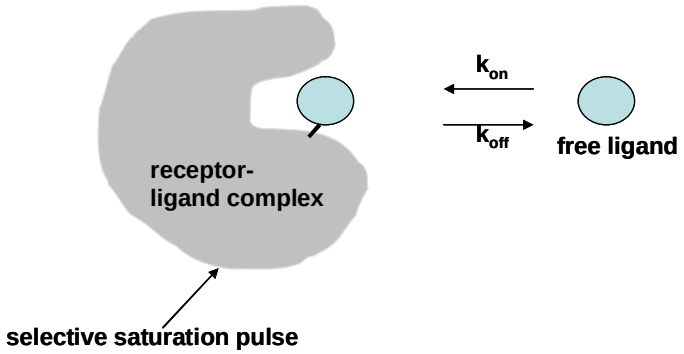

Fig. 3.15: Saturation transfer on a ligand in fast exchange between the free and the bound state

In practice the STD experiment goes as follows. The NMR spectrum of a macromolecule and ligand is measured, once with the saturation rf field off-resonance (reference spectrum) and the second time under on-resonance conditions. In the off-resonance experiment the sample is irradiated far away from the receptor, ligand or water resonances. In the on-resonance experiment the broad signal from a macromolecule is saturated in such a way that the ligand resonances remain unaffected. The difference

spectrum (ΔI) is obtained as a difference between off-resonance (I_{off}) and on-resonance (I_{on}) spectra.

$$\Delta I = I_{off} - I_{on} \tag{3.16}$$

If the ligand or drug interacts with the macromolecule, due to saturation transfer, its signal intensity in the on-resonance spectrum becomes lower. The longer the residence time of the ligand or drug on a receptor, the higher its intensity in the difference NMR spectrum. For these reasons, the STD NMR has been used as a tool for characterization of low affinity binding between drugs and biomacromolecules. In principle the STD NMR method is based on the NOE mechanism but is easier to execute when the NMR resonance of the macromolecule is very broad.

3.1.7 Two-dimensional (2D) NMR spectroscopy

A general two-dimensional NMR experiment can be represented by the following scheme[60]:

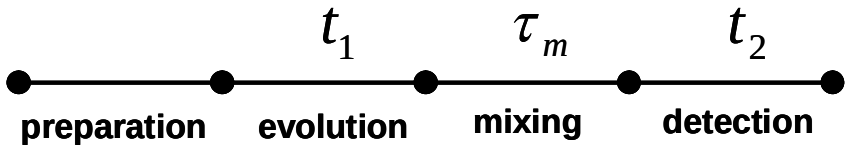

Fig.3.16: general pulse sequence of a 2D NMR experiment

The Free Induction Decay (FID) from such a 2D experiment depends on both the times t_1 and t_2 (τ_m is assumed to be constant). In a 2D experiment, a series of experiments are performed with increasing values of t_1. Each FID is then Fourier transformed (FT) first with respect to t_2 then with respect to t_1. Starting from a series of FIDs as a function of two time variables $S(t_1, t_2)$, the first FT converts it into a series of functions of one time and one frequency variable $S(t_1, \omega_2)$ (called interferogram). The second FT creates a

spectrum of two frequency variables $S(\omega_1, \omega_2)$. The 2D NMR spectrum can be represented in three dimensions where the intensity represents third parameter.

a) Nuclear Overhauser Enhancement Spectroscopy (NOESY)

The pulse sequence of the NOESY experiment is composed of three 90^0 pulses (Fig. 3.17).

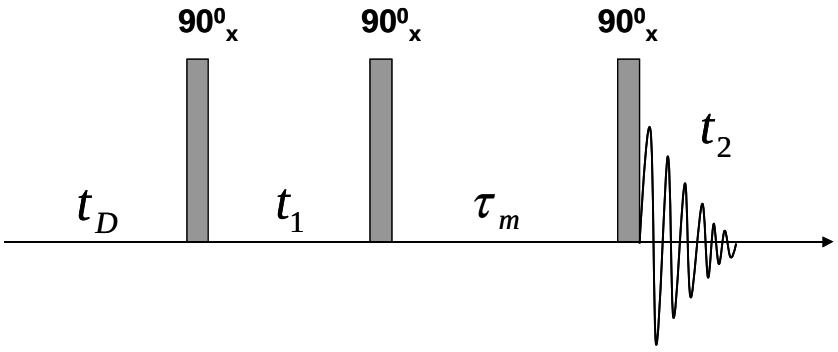

Fig. 3.17: NOESY pulse sequence

After the first pulse spins A and B precess in the x-y plane. The second pulse after the time t_1 puts the frequency labeled magnetizations in the x-z plane along the z-axis. The third 90^0 pulse is used to measure z magnetization that remained at the end of the mixing time. If no W_0 relaxation or chemical exchange occurs during this time in the 2D NOESY spectrum only diagonal peaks appear. Interesting information is obtained if during the mixing time spins exchange their magnetizations, either by W_0 relaxation through dipole-dipole interactions (cross-relaxation) or by chemical exchange. Fourier transformation with respect to t_1 then gives additional cross-peaks which connect A and B (Fig 3.18).

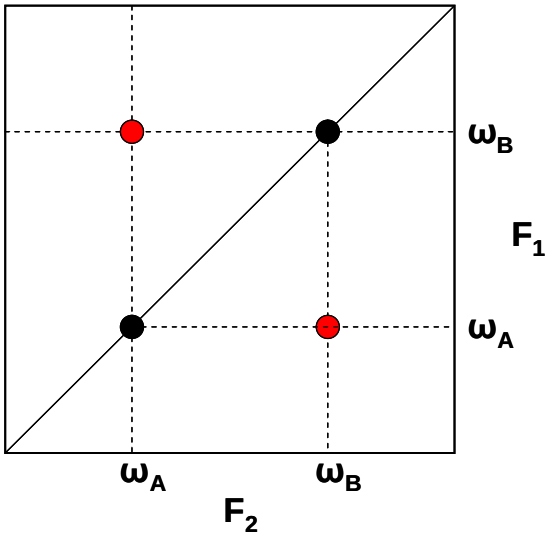

Fig. 3.18: Schematic plot of the 2D NOESY spectrum

The intensity of the cross-peaks depends on the NOE enhancement and the mixing time τ_m. This technique has important practical applications for the structure determination of large biomolecules, because the occurrence of a cross-peak implies that the two spins involved in the cross-relaxation process are physically near (0.5nm).

3.1.8 Solid-state NMR

The solid-state NMR technique differs significantly from high resolution NMR of liquids. The main reason is the much broader lines in the spectrum of a solid substance. This broadening appears due to interaction of a spin with other nuclear spins **(dipole-dipole coupling)** or with induced magnetic fields from electron motions in orbitals **(chemical shift anisotropy)**. These interactions are averaged for molecules in solution by fast, random molecular tumbling motion. The line broadening in the solid-state spectra causes also much lower signal-to-noise ratio. The additional difficulty for heteronuclei as ^{13}C, ^{15}N and ^{31}P is that the T_1 relaxation times in solids usually are longer than in solution and the experiments can not be repeated so fast. The latter problem can be partly solved by cross-polarization[61].

The chemical shift anisotropy (CAS)[62,63] arises because the electron clouds of a molecule are not spherically symmetric and the chemical shift depends on the relative

orientation of the external magnetic field with respect to the molecule. In a solution the orientation of the molecule changes very fast and only the isotropic part of the chemical shift remains. Magic Angle Spinning (MAS) of the sample is the well-known method to remove the anisotropy of the chemical shift and to obtain a spectrum governed by an apparent isotropic shift. For that purpose, the sample has to be rapidly rotated about an axis which makes an angle of 54.7^0 (magic angle) with respect to the magnetic field. If the rotational frequency is smaller than the line width, the spectrum will contain one line at the isotropic chemical shift (centerband) and sidebands separated by the rotational frequency. When the anisotropy is cancelled by fast rotation, the sidebands disappear.

The second source responsible for the line broadening is the **dipolar coupling**[62,63]. As eq. 3.18 shows, the dipolar coupling depends on the orientation of the spin pair with respect to the magnetic field. In a sample one spin feels a local magnetic field due to coupling with its neighbors. The strength of this field varies for each spin and is dependent on r and θ values. This causes a broad distribution of resonance frequencies. It is assumed that the spins A are abundant and the spins B to be observed are rare spins. That means that the homonuclear dipolar interaction between B spins is relatively small (large average distance r_{ij}). The dipolar coupling between B and A can be removed by decoupling, i.e. irradiation with a strong resonant rf field on the A spins. This field flips the magnetization from A nuclei from the +z axis to the –z axis and the B nuclei feel in average a zero local dipolar field[62].

The cross-polarization between A and B spins can be performed by applying first a 90^0 pulse along the x axis to the A spins, which turns the A spin magnetization to the y axis. Then a so-called spin-lock field along the rotating frame y axis is applied to the A spins, usually with the amplitude B_{1A}. This results in lowering of the A spin temperature. If during this lock-field a rf field, B_{1B}, is applied to the B spins which satisfies the Hartmann-Hahn condition:

$$\gamma_A \cdot B_{1A} = \gamma_B \cdot B_{1B} \quad , \tag{3.17}$$

the energy difference between spin states of spin A and spin B in the rotating frame becomes the same (Fig. 3.19).

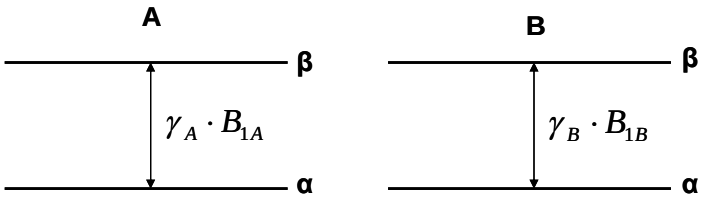

Fig. 3.19: Hartmann-Hahn condition for the spins A and B

Due to dipolar interactions between A and B spins, energy exchange can occur between the A and B spin reservoirs via flip-flop transitions. That means that a B spin flips from its β to α state and provides the energy for A spins to undergo a α→β transition. When after some time equilibrium is reached between the hot B spins and the cold A spins, the B spins have been cooled down and one can show that the intensity of the B signal is enhanced by a factor γ_A/γ_B. When the B spins are ^{13}C spins and A spins protons, the gain in intensity in the ^{13}C NMR spectrum is about a factor 4. The CP pulse sequence is shown in the Fig.3.20:

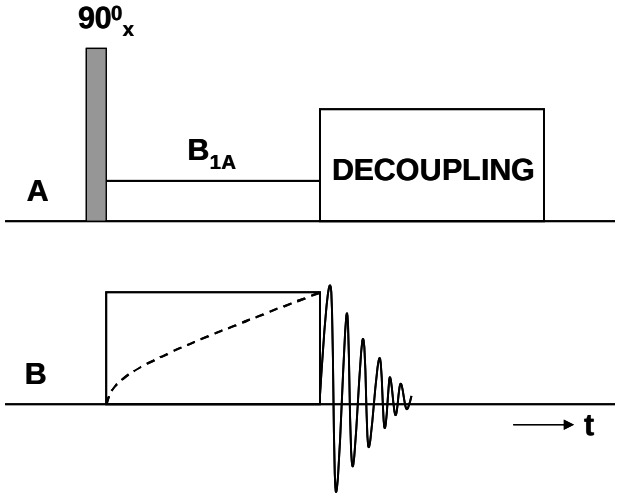

Fig. 3.20: CP pulse sequence

Cross polarization occurs due to dipolar interactions which decrease with the distance and by this method only those B nuclei which are located close to A spins can be detected. Another advantage of the CP method is that the repetition rate of the pulse sequence is

now determined by the spin-lattice time of the A spins, although the B spin spectrum is measured.

CP is often combined with the MAS method and this is known as a CPMAS NMR experiment. CPMAS is the most used solid state NMR technique and enables to obtain new information about the structure and dynamics of a solid substance.

3.2 Atomic Force Microscopy (AFM)

Atomic Force Microscopy is a mechanical imaging technique for characterization of the topography of a surface and of its physical properties. An atomic force microscope is able to monitor nanometer-sized features on a surface and to create three-dimensional surface images. The main part of the microscope is the cantilever which represents a string fixed at one end (Fig. 3.21). The free end of the cantilever contains a sharp pyramidal tip (nanoscopic needle). The tip is brought in the proximity of the sample and moved across its surface. By monitoring the motion of a tip across the surface, a 3D image of the specimen is obtained.

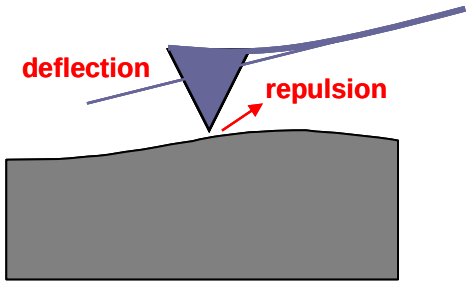

Fig. 3.21: AFM cantilever with the tip in the proximity of a surface

The working principle of AFM is based on the fact that the interaction between the tip and the surface depends on the intermolecular (interatomic) distance. When two atoms approach, they at first attract each other by a weak attractive force. When the distance between them becomes smaller than approximately the bond distance in a molecule, a strong repulsive force appears. The main idea is that the attraction or repulsion between

the tip and a sample surface causes a deflection of the cantilever, to the surface or away from it. The block diagram of an atomic force microscope is shown in the Fig. 3.22.

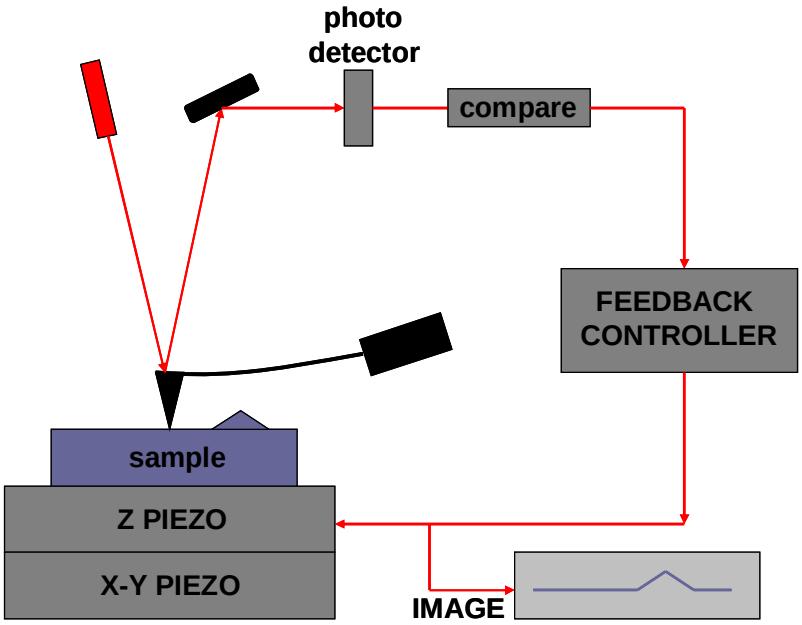

Fig. 3.22: Components of atomic force microscope

The principal components of the microscope are z motion generators, force sensors and feedback controllers[64].

As z motion generators piezoelectric materials are used. They possess a property to transform electrical energy into mechanical motion. When a potential is applied to a piezoelectric material, it will change its geometry depending on the shape and the field strength.

Force sensors are responsible for measuring the force between the tip and the surface. The deflection of the cantilever is proportional to the force according to Hook's law:

$$F = -k \cdot d \tag{3.18}$$

k is the string constant that depends on material and the shape of the cantilever and d is the deflection of cantilever. The motion of the cantilever is measured by the "light lever" method. A laser beam is focused on the cantilever opposite from the tip. Reflected light is

collected by two photo detectors or by a slit detector (Fig. 3.20). Bending of the cantilever causes a change of the position of the reflected spot and the measured differential voltage between the two detectors represents the AFM signal.

Feedback control is achieved via piezoelectric material which controls the cantilever position. Its function is to keep a constant force between the tip and the sample surface. A change of the force induces a voltage in the detector which further acts on the piezoelectric tube. That enables the establishment of the appropriate tip and surface relative positions. The x and y piezoelectric tubes allow scanning of the whole sample surface.

3.2.1 Imaging modes

In the AFM technique there are several imaging modes for characterization of surfaces[65]. The basic principle of moving the tip across the sample surface is common for all of them. The way of applying force between sample and tip can be different and one can distinguish between the contact mode, intermittent-contact mode and non-contact mode.

In the **contact mode**[65] a constant force is applied to the surface and deflection of the cantilever is a measure of this force. Changes of the sample height cause the cantilever to bend and the feedback system re-adjusts its position to keep the cantilever deflection and thus the force, constant (Fig. 3.23). Biomaterials such as polymers often have soft surfaces and dragging the tip across the sample can damage their surface.

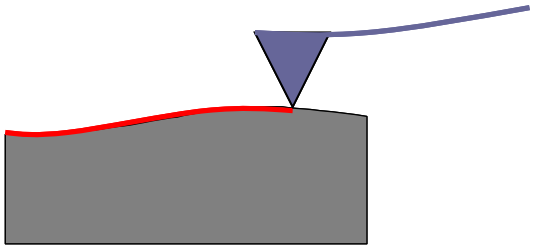

Fig. 3.23: AFM contact mode

The intermittent contact mode[65] (Fig. 3.24) is widely applied for analysis of soft materials. This is a dynamic mode where the cantilever vibrates and the amplitude of this vibration is kept constant

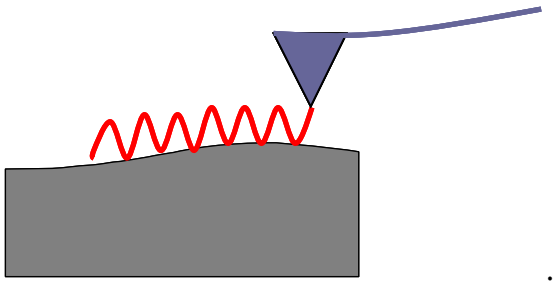

Fig. 3.24: AFM intermittent contact mode

During these oscillations the tip comes very close to the surface where strong repulsion occurs. If there are some features on the surface, this causes a loss of energy during contact and the amplitude is reduced. Then the feedback system re-adjusts the height to maintain the amplitude constant. In this mode the contact time between tip and sample is decreased and that reduces the possibility of sample damaging. By monitoring the phase shift between cantilever oscillation and the signal sent to piezo tube, information about changes of viscoelastic properties of the material can be obtained.

The non-contact mode[65] (Fig. 3.25) is also a dynamic mode where the cantilever vibrates, but there is no direct contact between the tip and the surface. This enables investigation of very soft and elastic materials because the force between cantilever and sample is much smaller.

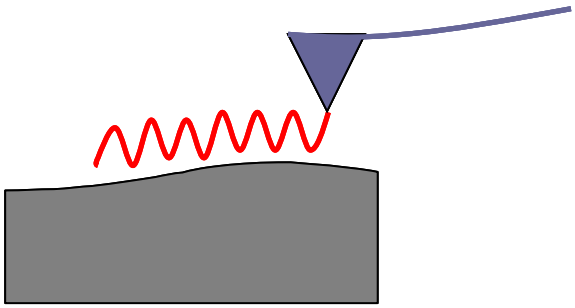

Fig. 3.25: AFM non-contact mode

Different imaging modes enable broad range of application of AFM, starting from observation of molecules, over analysis of membrane surfaces to imaging of living cells.

Chapter 4: Materials

4.1 PEG-based hydrogels

As matrix for the drug delivery system studied here a group of hydrogels based on photopolymerized poly(ethylene glycol) diacrylate (PEGDA) was used. By varying the molar mass of the PEGDA oligomers, networks can be prepared with varying average molecular mesh sizes and chemical composition, which will affect the matrix swelling, the drug-matrix interaction and consequently the drug diffusion and the drug release rate[66].

The initial substances were composed of acrylate derivatives of PEG, PEGDA 4000, PEGDA 2000 and PEGDA 450. The numbers represent the number-averaged molecular weight of the PEG chains before polymerization in g/mol. PEGDA oligomers possess two photo-reactive sites and thus represent photopolymerizable materials (Fig. 4.1). Hydrogel precursor solutions were formed by dissolving 5g of PEGDA in a 50/50 mixture of water and ethanol (10g) containing 50mg of photoinitiator 2-hydroxy-1-(4-(2-hydroxyethoxy)phenyl)-2-methyl-1-propanone (Irgacure 2959). Irgacure 2959 and PEGDA 450 were obtained from Sigma-Aldrich, PEGDA 2000 and PEGDA 4000 were provided by DSM.

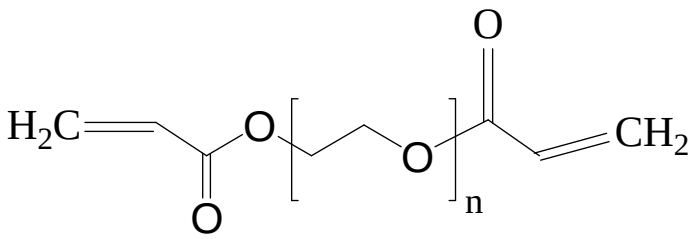

Fig. 4.1: Chemical structure of PEGDA oligomers

Photoplymerization was the method of choice to produce three-dimensional (3D) polymer networks. It offers several advantages like fast curing rates (in the range from seconds to minutes), low heat emission and in-situ applicability, which is important for many biomedical applications[67,68,69]. The photopolymerization technique for hydrogel formation assumes action of ultraviolet (UV) light on the precursor solution containing a

photoinitiator[70,71]. The photoinitiator is a substance which is able by absorption of light to undergo bond cleavage and create reactive free radical species. It is desirable that this substance is biocompatible, water soluble and non-toxic. Radicals attack acrylate double bonds and further promote photopolymerization reactions to create cross-linked hydrogels.

Films of 0.12mm thickness were produced at DSM by curing on glass plates at 22^0C on a conveyor belt fitted with a fusion BT13D D-bulb in an inert nitrogen atmosphere[66]. A UV dose of 3 J/cm^2 was determined using a UV Power Puck light meter. The chemical conversion was determined by Attenuated Total Reflection Fourier Transform Infrared (ATR FTIR) spectroscopy by measuring the peak intensity of the acrylate (C=O)-(CH) bend vibration at 1408 cm^{-1} and the acrylate C=O stretch vibration at 1193 cm^{-1}. It was shown that the conversion of the acrylate double bonds on both sides of the film (substrate and top) was above 98%.

The chemical structure of cross-linked PEGDA networks is shown in Fig. 4.2. The mechanical properties of the hydrogels as well as the permeability for molecules depend on the length of PEG segments between cross-links[18].

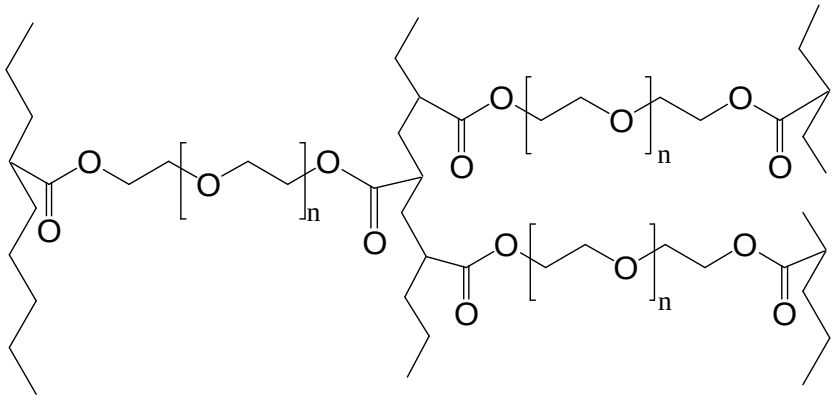

Fig. 4.2: Chemical structure of the cross-linked PEGDA networks

Gels were obtained by immersing polymers into water. The cross-linked PEGDA films were loaded with the drug according to the following procedure. Drug solutions in D_2O were prepared using 20mg of the drug and 1ml water. Then, the networks were loaded with drug by mixing 50mg of the dry polymer with 1ml of the drug solution. The

resulting mixtures were left to stand for two days in order to reach the state of equilibrium swelling. The samples always contained more water than required for the equilibrium swelling.

4.2 Drug molecules

The water soluble drugs employed were proxyphylline [7-(2-hydroxypropyl)-1,3-dimethylpurine-2,6 dione], flucloxacilline [sodium (2R, 5R, 6R)-6[[3-(2-chloro-6 fluorophenyl)-5methyl-oxaziole-4-carbonyl]amino]-3,3-dimethyl-7-oxo-4-thia-1-azabicyclo [3.2.0]heptane-2-carboxylate] and the pseudo drug fluoresceine [disodium 2-(3-oxido-6-oxo xanthan-9-yl)benzoate]. Flucloxacilline was obtained from DSM, fluoresceine and proxyphylline were obtained from Sigma-Aldrich.

Proxyphylline (Fig. 4.3) is a water soluble derivative (water solubility 1000 g/l, MW 238 g/mol) of theophylline, a vasodilator. It acts on passages which supply lungs with air, enables their relaxation and increased air flow. Therefore, this drug is very important in treatment and prevention of bronchial astma and chronic bronchitis.

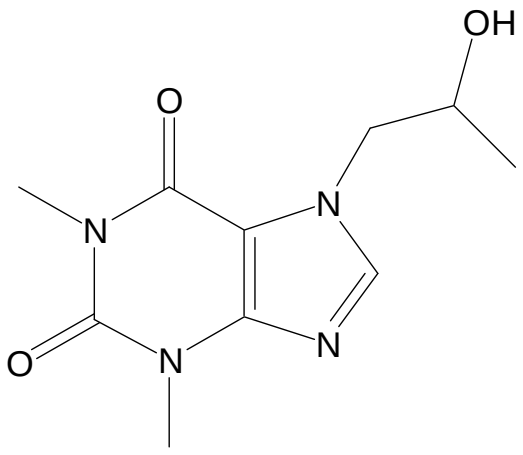

Fig. 4.3: Proxyphylline chemical structure

The antibiotic **flucloxacilline** (Fig. 4.4) (water solubility 100 g/l, MW 454 g/mol) is used in the treatment of bacterial infections. The bactericidal activity is based on its capability

to inhibit the formation of bacterial cell walls. This is mediated through the proteins located in the cell wall which have the affinity for penicillin binding.

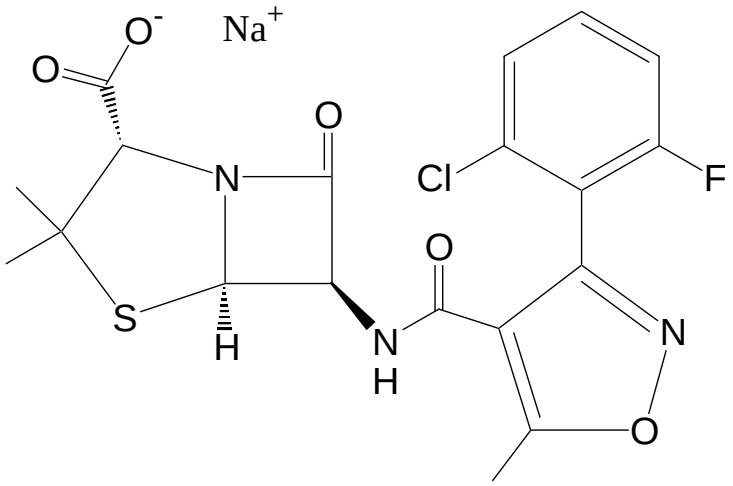

Fig. 4.4: Flucloxacilline chemical structure

The dye **fluoresceine** (Fig. 4.5) (water solubility 600 g/l, MW 376 g/mol) was chosen as a model drug of comparable size to the other two. The sodium salt of fluoresceine is called uranine and is used for dying materials and coloring agrochemicals and detergents. The important application in biology is as fluorescence detecting agent, for labeling and monitoring the molecules in various associations.

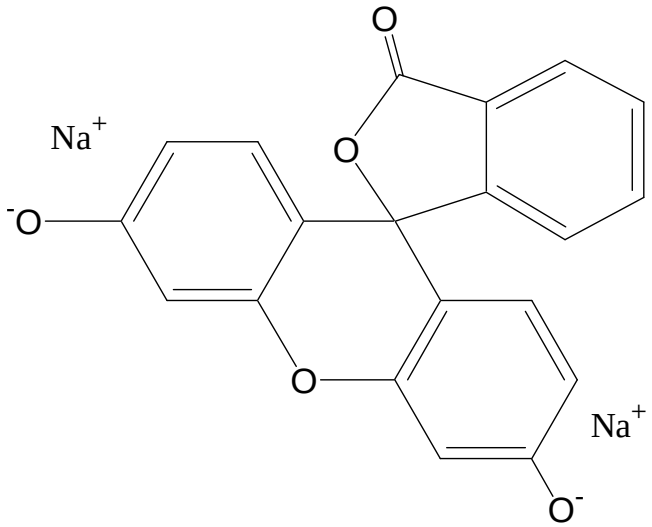

Fig. 4.5: Fluoresceine chemical structure

A water insoluble drug that was investigated is **ibuprofen** (Fig. 4.6) (MW 206 g/mol) [2-(4-isobutylphenol)propionic acid]. It is used for the relief of pain and fever and for the suppression and treatment of inflammatory diseases. The Ibuprofen was purchased from Sigma-Aldrich.

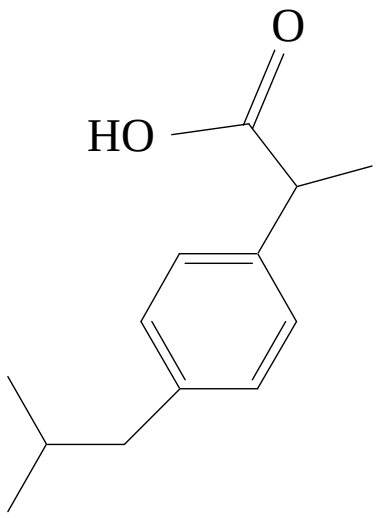

Fig. 4.6: Ibuprofen chemical structure

Another investigated drug with poor solubility in water is **amiodarone** (Fig. 4.7) (MW 682 g/mol) [(2-butylbenzofuran-3-yl)-[4-(2-diethylaminoethoxy)-3,5-diiodo-phenyl]-methanone]. It is used in the form of the hydrochloride salt which is a white to slightly yellow crystalline powder. Amiodarone is a very effective antiarrhythmic agent for various forms of irregular heart beat (tachyarrhythmias). It is used in cases of life-threatening heart rhythm disorders. Amiodarone was obtained from DSM.

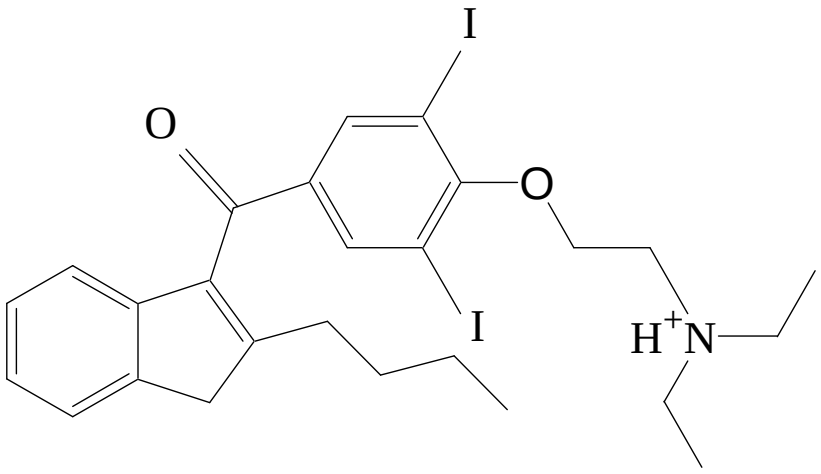

Fig. 4.7: Amiodarone chemical structure

All drugs were used as obtained and D_2O was the solvent.

4.3 Cyclodextrins

Cyclodextrins (CDs) are cyclic oligosaccharides composed of glucopyranose units linked through α-1,4-linkages. The α, β and γ CDs which contain six, seven and eight glucose units, respectively (Fig. 4.8), were obtained from Sigma-Aldrich.

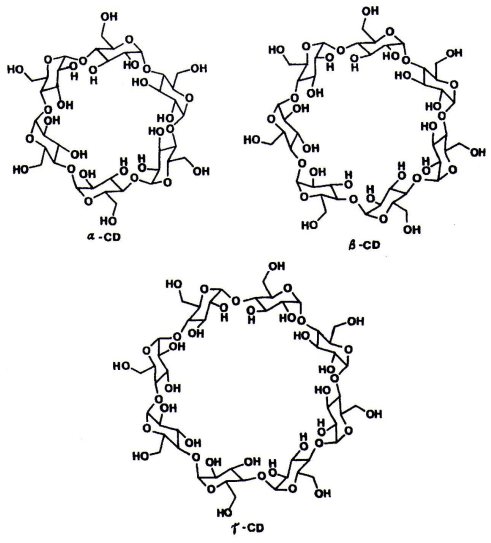

Fig. 4.8: Chemical structure of α, β and γ cyclodextrins[72]

Topologically cyclodextrins are hollow toroids with one larger and one smaller opening (Fig. 4.9). Such a structure enables them to build inclusion compounds with variously-sized drug molecules (Sec. 2.4)[73,74]. Table 4.1 shows some important properties of cyclodextrins[75].

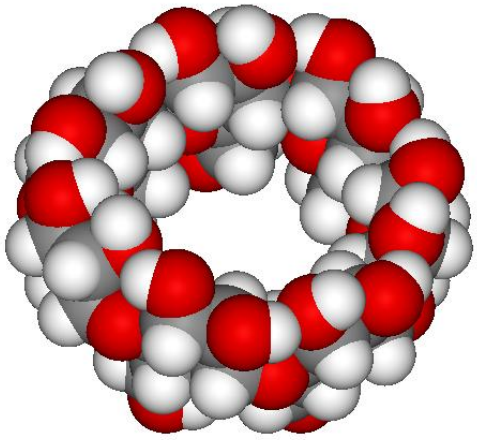

Fig. 4.9: Cone-shaped form of β cyclodextrin

All drug-CD complexes with water soluble drugs were formed by mixing equimolar amounts of drug and cyclodextrin. In the case of α and γ CD, 20mg of drugs was used. In the case of β CD, the amount of drug was decreased to 8mg because of the limited water solubility of β cyclodextrin. The mixture of guest/host molar ratio 1/1 was dissolved in 1ml D_2O.

	α CD	**β CD**	**γ CD**
MW [g/mol]	972	1135	1297
Glucose monomers	6	7	8
Internal cavity diameter [Å]	5.7	7.8	9.5
Water solubility [g/100ml; 25^{0}C]	14.2	1.85	23.2

Table 4.1: Physical properties of cyclodextrins

For the water insoluble drugs the molar fraction of the drug in the mixture with cyclodextrin was larger than that of CD (for ibuprofen drug:CD molar ratio was 6:1 and for amiodarone 2:1). The aim was to achieve high probability of drug encapsulation by CD for poorly soluble drug molecules. The drug/CD mixtures were dissolved in 1ml D_2O. In the case of the amiodarone/CD mixture, for the solid-state NMR measurements the amount of water was reduced to 0.3ml. After dissolution, the mixtures were strongly stirred and left to stand for three days to achieve equilibrium. Then, the suspensions were centrifuged and the clear drug-CD complex solutions were obtained.

The PEGDA matrices were also swollen in these complex solutions, according to the above described procedure.

Chapter 5: Experimental results and discussion

5.1 Properties of PEGDA matrices

5.1.1 AFM analysis of polymer surfaces

For coating applications of PEGDA polymers their surface properties will play an important role. Although the surface properties of the PEGDA matrices seem to have no direct relevance for the drug diffusion investigated in this thesis, the AFM results are reported here, because they provide visual information about the effect of cross-linking on the structure of the matrix. Cross-link density is a very important parameter which determines physical, chemical and mechanical properties of polymer films. By changing the cross-link density of PEGDA networks the morphological properties of surfaces are also changed. The change of the surfaces of PEGDA gels in response to the cross-linking degree was examined.

The surface topography and morphology of these polymer films, as they were polymerized on glass plates, were characterized by tapping mode atomic force microscopy. The measurements were conducted in air under ambient conditions with the AFM system provided by JPK Instruments. As cantilever a silicon tip with a spring constant of 42 N/m and a resonance frequency of 320 kHz was used for all experiments. Topographic (height mode) and viscoelastic (phase mode) images were recorded simultaneously.

Recorded phase images provide information about changes in material properties, i.e. the contrast in a phase image is related to the variation in sample surface stiffness[76]. Stiffer regions of a surface induce a positive phase shift and therefore appear brighter on the phase image. Darker regions of the phase image are assigned to the softer materials. The higher the cross-link density, the higher is the stiffness of the material. It can be also expected that at higher degrees of cross-linking, the domain structure will be reduced[77]. The polymer surfaces were examined on various length scales (< 10 μm).

The surface of the dry PEGDA 4000 matrix at room temperature is shown in the Fig. 5.1. Both height and phase images are shown with the scan size of 10x10 μm.

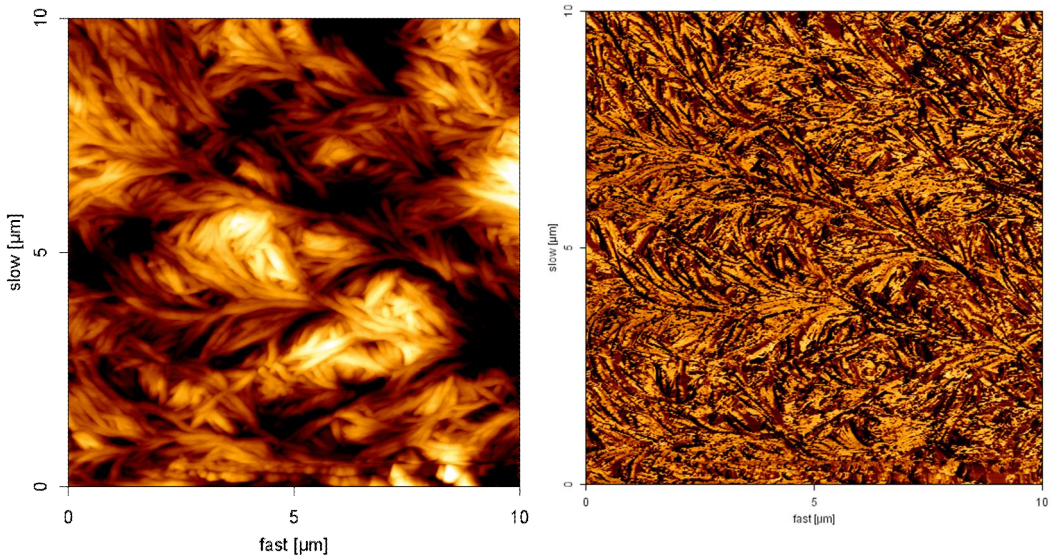

Fig. 5.1: Height (left) and phase (right) AFM image of PEGDA 4000 matrix. The scan size is 10x10 µm

The figure shows a branched morphology with a pronounced ordering. Finger-like patterns are observed revealing a fiber-like structure on the polymer surface. Fig. 5.2 represents the same sample on a smaller scale (2x2 µm).

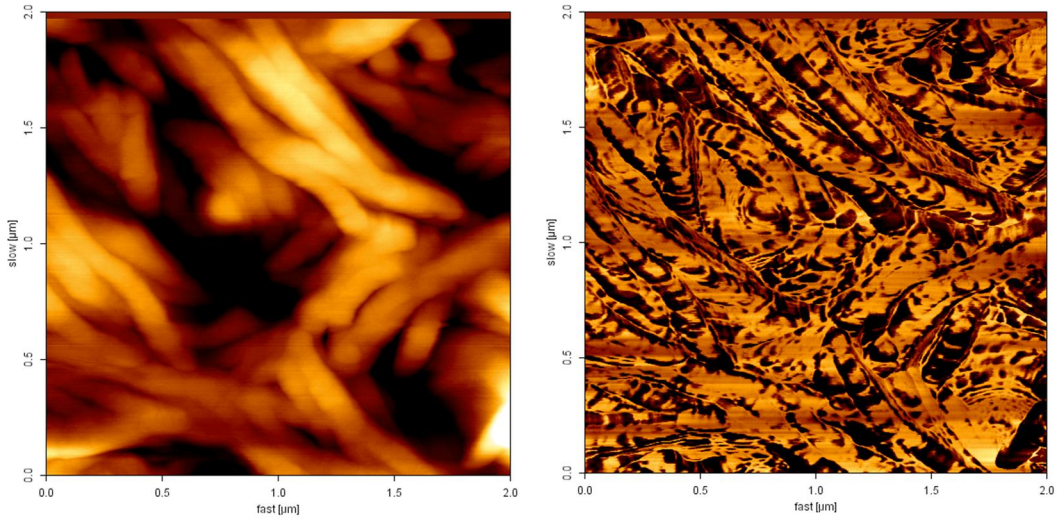

Fig. 5.2: Height (left) and phase (right) AFM image of PEGDA 4000 matrix. The scan size is 2x2 µm

It clearly shows bundles of locally oriented fibers. The corresponding phase image reveals stiffness variations even within a fiber. These images resemble morphological features of crystallized poly(ethylene oxide) (PEO) adsorbed on a substrate[78,79]. This phenomenon of molecular self-assembly in PEGDA 4000 polymer, resulting in finger-like branched patterns, can be explained by the relative large length of PEG chains between cross-links who tend to crystallize in thin films and close to interfaces. From the AFM pictures the average width of the fingers is about 100 nm which agrees with the width of PEO fingers at room temperature found by Reiter et al.[78].

When water is added, the polymer swells and this branched structure disappears. Fig. 5.3 shows the polymer gel surface of the same matrix after swelling in water. The image is obtained by contact mode AFM. The gel surface exhibits a sponge-like pattern with large holes among relative flat regions. Polymer swelling, therefore significantly changes surface morphology and nanostructure of PEGDA films.

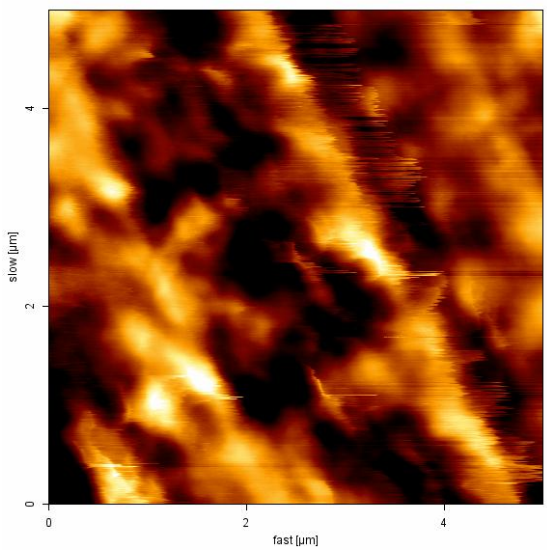

Fig. 5.3: Height image of swollen PEGDA 4000 polymer. The scan size is 5x5 µm

Fig. 5.4 represents the surface of the dry PEGDA 2000 matrix at 10x10 µm length scale. A problem that appears at higher cross-link densities is volume shrinkage during the curing process. As a consequence this leads to formation of voids and cracks in the polymer.

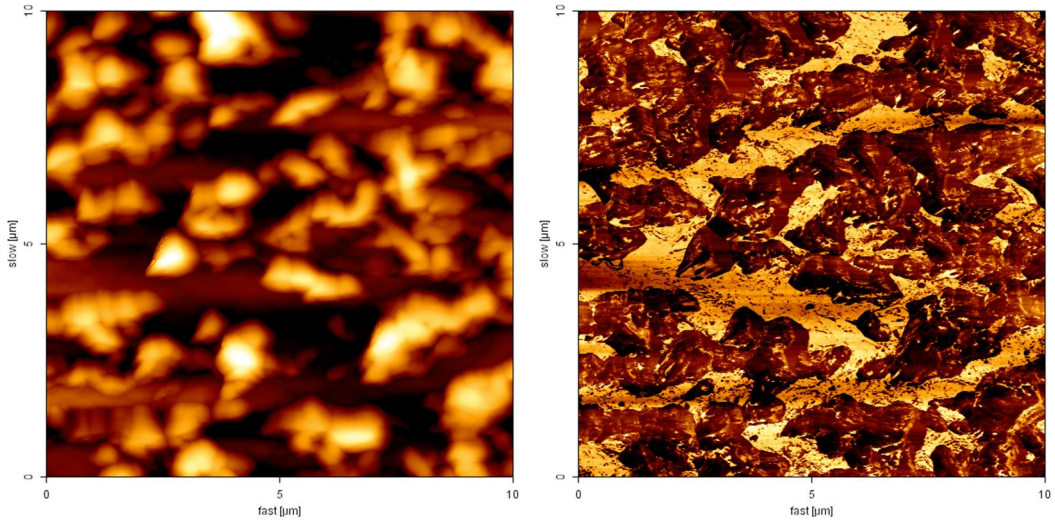

Fig. 5.4: Height (left) and phase (right) AFM image of PEGDA 2000 matrix. The scan size is 10x10 µm

The surface fractures in the case of PEGDA 2000 film are visible in the AFM images. The height variations are very large and the dark regions in the height image (lower in height) correspond to the stiffer domains in the phase image. They probably display the surface of the glass plate between the higher and softer polymer domains. Due to that it was not possible for this matrix to observe fine features on the polymer surface itself and to characterize its nanostructure.

The morphology of the PEGDA 450 surface is shown in the Fig. 5.5 at two different length scales. Shrinkage occurred also in this case, but it was possible to observe and characterize small parts of the polymer surface free of cracks. The surface morphology is flat and uniform in their viscoelastic properties, which is desirable for polymer coatings applications. Small bright particles in the height image at some parts of the polymer sample probably appear due to air between the polymer surface and the glass plate. In agreement with that is the finding from the phase image that these particles are softer than the rest of the polymer.

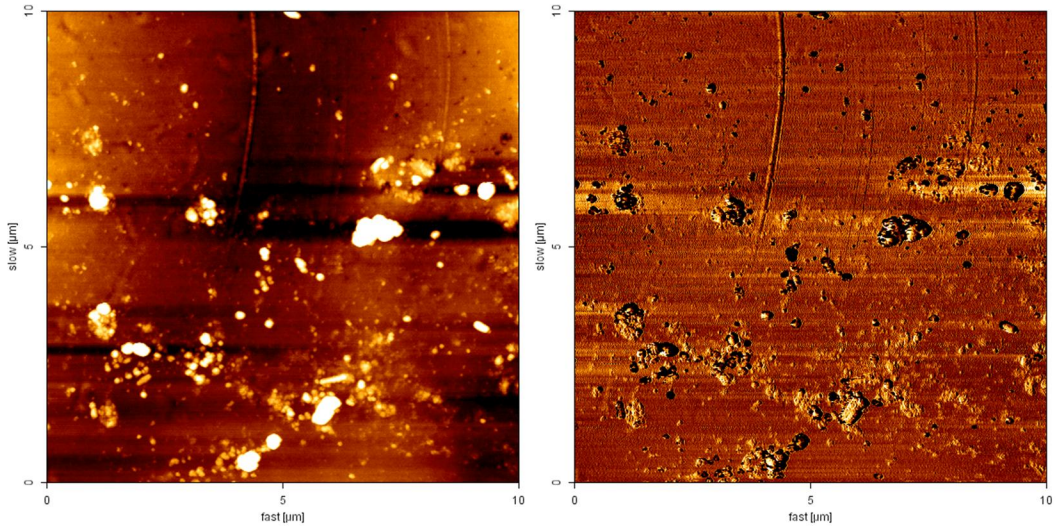

Fig. 5.5: Height (left) and phase (right) AFM images of PEGDA 450 matrix. The scan size is 10x10 µm

The AFM images of PEGDA polymers clearly show that the cross-link density significantly affects the topography and morphology of the polymer network surface. There is a tendency that with increasing cross-link density the domains on the surface become smaller in size. The PEGDA 2000 matrix represents an exception because its surface structure could not be characterized. A comparison between PEGDA 4000 and PEGDA 450 surfaces reveals that the higher the cross-link density the smoother the surface. The surface changes appreciably, when the polymer swells in the presence of a solvent.

The surface studies make clear that cross-linking and swelling are important factors for the designing of coatings.

5.1.2 Binary water/polymer systems – swelling behavior

The investigation of the drug delivery systems started with the two-component system consisting of water (D_2O) and cross-linked poly(ethylene glycol) diacrylate polymers of different cross-link densities: PEGDA 4000, PEGDA 2000 and PEGDA 450. For each network the swelling behavior was determined by measuring the proton NMR spectrum as a function of the water content. All NMR experiments are carried out

in 5 mm NMR tubes on a Bruker DRX 500 MHz spectrometer. To the dry cross-linked polymer D_2O was added in small steps. After every step the sample was left to stand for 48h in order to reach equilibrium and then the proton spectrum was recorded (Fig. 5.6). At first only a broad polymer line was observed. When the water-polymer equilibrium swelling composition was approached, the polymer line narrowed and a water peak (from HDO) at approximately 4.8 ppm showed up. When the amount of added water surpassed the amount given by the maximum water uptake of the network (maximum swelling), a second water peak, slightly narrower and downfield from the first peak showed up as shown for the case of PEGDA 450 in Fig. 5.6.

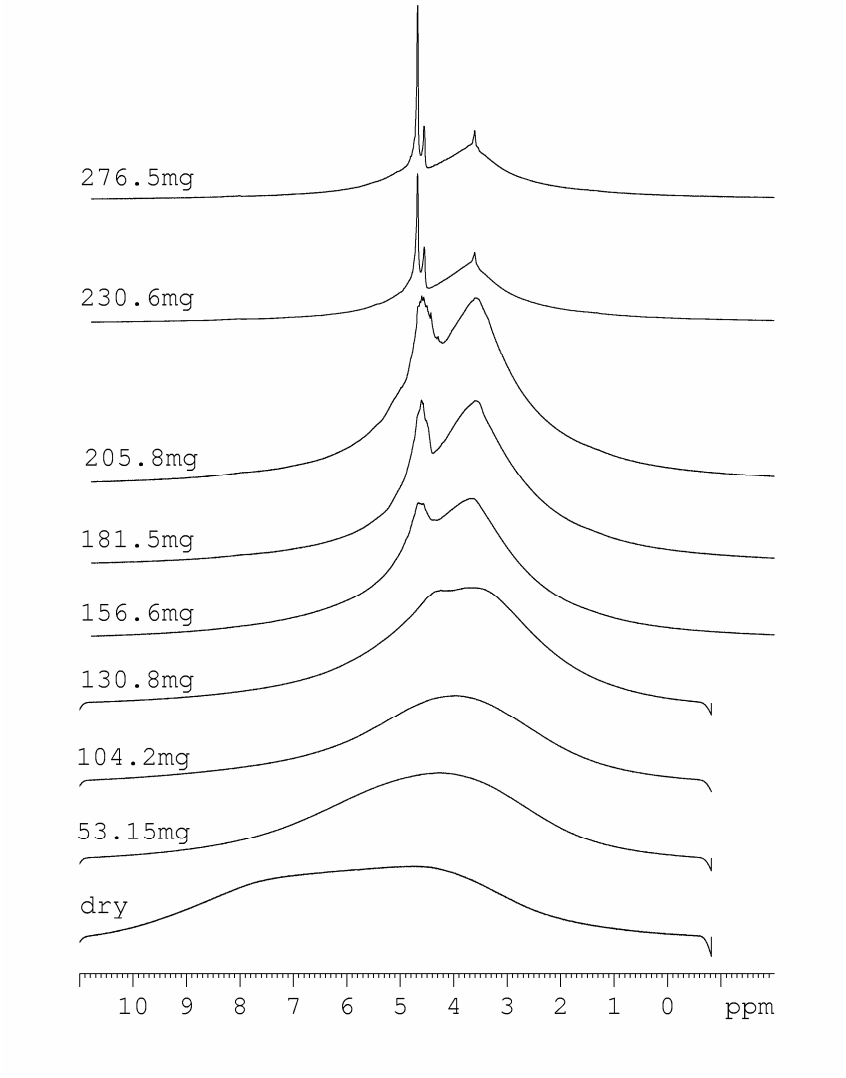

Fig. 5.6: NMR spectra of the PEGDA 450 matrix at different amounts of swelling water

The amount of water absorbed by the sample just before the second water peak appeared is the maximum swelling amount of the hydrogel. When we define a swelling factor, sw, as the ratio of the water weight at maximum swelling and the dry polymer weight, then the swelling factors are 4.0 (PEGDA 450), 6.0 (PEGDA 2000) and 10.0 (PEGDA 4000) (Table 1).

The average mesh size of a network, ξ, can be related to the swelling factor of the sample[26] as already shown in Chapter 2:

$$\xi = \sqrt{\langle r_0 \rangle^2} \cdot \sqrt[3]{sw} \quad , \tag{5.1}$$

where $\sqrt{\langle r_0 \rangle^2}$, representing the average end-to-end distance of the polymer chains between cross-links in the absence of swelling water, depends on the number-average molecular mass of the chains in the network between cross-links, M_c[26]:

$$\sqrt{\langle r_0 \rangle^2} = l \cdot \sqrt{2 \cdot C_n \cdot \frac{M_c}{M_r}} \quad , \tag{5.2}$$

where l is the bond length (taken as 1.5 Å), M_r is the molecular mass of the polymer repeating unit (44 g/mol) and C_n is the characteristic ratio for PEG (=4.0)[80]. The molecular weight between cross-links, M_c, was calculated using the Flory equation[24]. This equation was later applied by Lu and Anseth[81] for evaluation of M_c values in PEG-based networks:

$$\frac{1}{M_c} = \frac{2}{M_n} - \frac{(\bar{\upsilon}/V_1) \cdot \left(\ln(1-\upsilon_2) + \upsilon_2 + \chi \upsilon_2^2\right)}{\upsilon_2^{1/3} - (\upsilon_2/2)} \quad , \tag{5.3}$$

where M_n is the number-average molecular weight of the polymer before cross-linking, υ_2 the polymer volume fraction in the swollen gel, V_1 the molar volume of the water (18 cm^3/mol at room temperature), $\bar{\upsilon}$ the specific volume of the polymer, and χ the Flory-

Huggins polymer-solvent interaction parameter[82]. The calculated values of the M_c, average end-to-end distances and mesh-sizes are shown in the Table 5.1

Table 5.1 Calculated network parameters

network	M_c (g/mol)	$\sqrt{\langle r_0^2 \rangle}$ (Å)	sw= $\frac{weight\ water\ at\ \max.\ swelling}{weight\ dry\ polymer}$	ζ (Å)
PEGDA4000	1700	26.4	10.0	57
PEGDA2000	702	17.0	6.0	31
PEGDA 450	186	8.8	4.0	14

The accuracy of the average end-to-end distance for the PEGDA 450 network is not high, because it is questionable whether eq. 5.1 can be applied for a network with such a small M_c value[17]. The value of the mesh size ξ for this network should therefore be taken as an order of magnitude estimate, but it shows that in the PEGDA 450 network, the mesh size is of the same order of magnitude as the size of the largest drug molecule.

When the amount of added water surpasses the maximum swelling amount, a water phase coexists with a hydrogel phase. All samples investigated later always contained more water than the polymer can take up by swelling. Therefore, each sample was a two-phase system composed of a water phase and a gel phase in equilibrium. Fig. 5.7 shows the proton NMR spectra of the swollen networks. Beside the water peak at 4.8 ppm, there is an additional line somewhat broader and slightly shifted upfield. This line arises from the water in the gel phase of these systems. The two water peaks represent the two different populations of water molecules, “free water” in the water phase and “gel water”. A similar observation for hydrogels with high water contents was made by Calderara et al[83]. It can be observed that when the cross-link density of the matrix increases, the chemical shift difference between the two water populations also increases. The broad line at 3.7 ppm in the spectrum of Fig. 5.7 is the polymer line from PEG protons. The narrow line on the top of the broad polymer line arises from PEG chains which possess a higher mobility. They either are not part of the cross-linked network or arise from PEG dangling ends[18]. The acrylate CH_2 protons were not observed because

these parts of the network apparently have a higher rigidity and escape observation with the NMR spectrometer set up for high resolution liquid state NMR on static samples. As the cross-link density increases, the polymer network becomes more rigid and the PEG chains become less mobile which causes the broadening of the associated NMR polymer resonance peak.

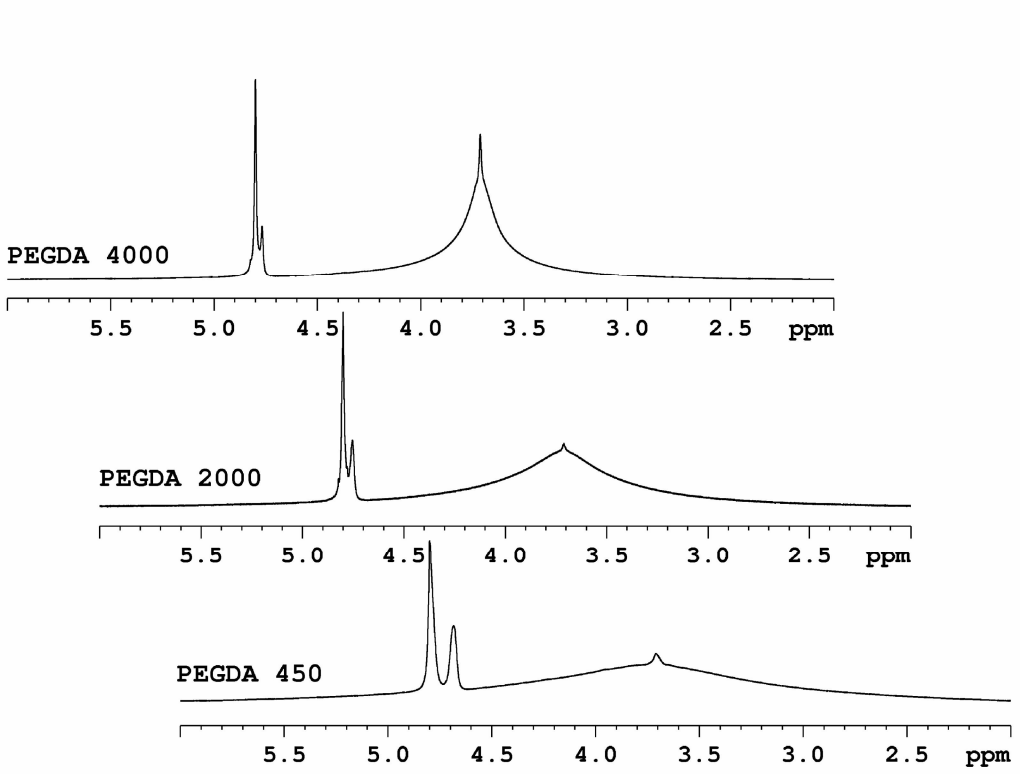

Fig. 5.7: ^{1}H NMR spectra of swollen PEGDA networks (50 mg polymer, 1 mL water)

5.2 Water/drug/polymer ternary systems

In order to study drug mobility in the gel as well as drug-matrix interaction, three-component systems (ternary systems) composed of polymer, drug and water were prepared. Composition of the mixture was the same for each type of the cross-linked network (1mL D_2O, 50 mg polymer and 20mg drug). The proton NMR spectra of the three (model) drug molecules, flucloxacilline, fluoresceine and proxyphylline were monitored in D_2O solution and in water-polymer mixtures. As an example Fig. 5.8 shows

the ^{1}H NMR spectra of flucloxacilline in water and in swollen matrices. The corresponding spectra of proxyphylline and fluoresceine are described in Appendix 9.1. Water and the polymer in these ternary systems exhibit the same behavior as in the binary polymer/water systems.

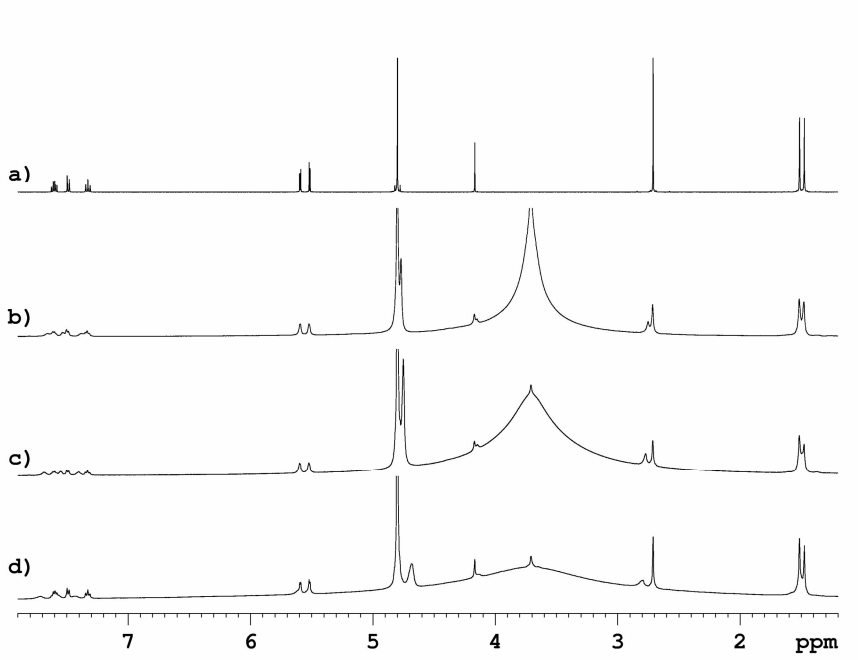

Fig. 5.8: ^{1}H NMR spectra of flucloxacilline in water solution (a), in PEGDA 4000 (b), in PEGDA 2000 (c), and in PEGDA 450 (d).

In order to extract more information about the drug behavior in the swollen gels, the ^{1}H NMR spectra of the aromatic protons of flucloxacilline at 7-8 ppm are shown in Fig. 5.9. The water solution spectrum of the drug is shown in Fig. 5.9 a, the spectra of the drug in the drug-polymer-D_2O mixtures in Fig. 5.9 b-d. In the spectra of the ternary system every drug line consists of two components, just as observed for water in Fig. 5.7. Beside the drug lines at the same chemical shift as for the drug in the water, there are additional lines. Fig. 5.9 indicates that, as expected for a water-hydrogel two-phase system, the drug molecules partition between the water phase and the hydrogel phase. In the water phase of such a system the NMR spectrum of the drug shows the same J-multiplets as in solution, but the lines are somewhat broader. To each J-multiplet in the spectrum belongs

a much broader line shifted to low-field of which the J-coupling multiplet structure is no longer visible. These broader lines represent the drug population in the hydrogel phase. With increasing cross-link density the chemical shift difference, $\delta_{drug}^{gel} - \delta_{drug}^{water}$, between these two populations increases (see also Table 5.2).

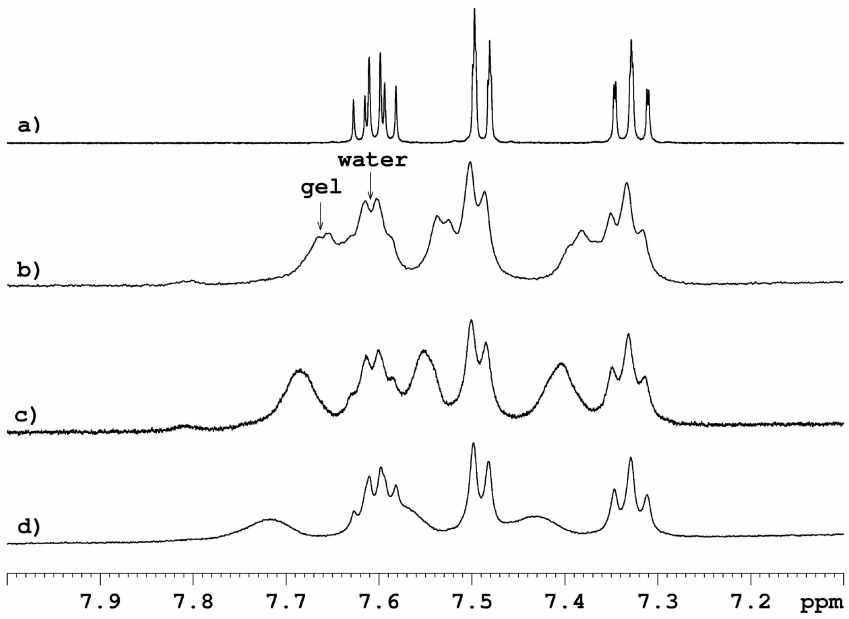

Fig. 5.9: ^{1}H NMR spectra of the aromatic region of flucloxacilline in water solution (a), in PEGDA 4000 (b), in PEGDA 2000 (c) and in PEGDA 450 (d).

The signals from the drug in the hydrogel phase become also broader with increasing cross-link density. A noteworthy observation is that the effect of the network on the chemical shift for water (upfield shift) is opposite to that of the drugs (downfield shift for most of the protons of the three drugs). For flucloxacilline the network effect differs even for different kinds of protons in the drug. That proves that the shifts are not due to magnetic susceptibility differences between the gel and the water phase.

For all drugs the shift, $\delta_{drug}^{gel} - \delta_{drug}^{water}$, doubles when going from PEGDA 4000 (calculated mesh size 57 Å) to PEGDA 450 (calculated mesh size 14 Å). Table 5.2 shows how the chemical shift difference changes for different drugs in different matrices.

Table 5.2 $\delta_{drug}^{gel} - \delta_{drug}^{water}$ for drug aromatic protons for all drug-polymer combinations; the accuracy of these values is approximately 0.004 ppm.

$\delta_{drug}^{gel} - \delta_{drug}^{water}$ in ppm	Proxyphilline (7.95 ppm)	Fluoresceine (7.8 ppm)	Flucloxacilline (7.8-7.2 ppm)
PEGDA 4000	0.020	0.081	0.046
PEGDA 2000	0.033	0.132	0.070
PEGDA 450	0.040	0.166	0.101

The fact that this shift depends on the network cross-link density, and that it is so small, means that the drug molecules in the gel are not simply permanently adhered to a polymer chain in the network. The situation must be very similar to that of the binding of a ligand to a macromolecule, where the ligand exchanges between free in solution and a position bound to the macromolecule[84].

Proton NMR spectra of fluoresceine and proxyphylline in the swollen matrices exhibit the same behavior, the lines of the drug in the water phase are accompanied by additional lines arising from drug molecules present in the gel phase of the two-phase systems.

5.3 Lateral mobility (self-diffusion)

The self-diffusion coefficients of the three drug molecules and of water are determined by ^{1}H PFGE NMR under the same equilibrium conditions as used for the spectra in Fig. 5.7-5.9, that is with so much water that the water-polymer system is a two-phase system and the gel is maximally swollen. As shown above, the resonances of drug (and water) in the water phase are shifted from the resonances of the drug (and water) in the gel phase. That allows the measurement of drug/water self-diffusion coefficients in both phases in the same experiment.

The self-diffusion coefficients were measured by the Pulsed Field Gradient Echo NMR technique and evaluated using the Stejskal-Tanner procedure[53]. The pulse sequences employed were the Hahn-echo for the proxyphylline and flucloxacilline self-diffusion measurements, and the stimulated-echo for fluoresceine. In the case of fluoresceine, the Hahn-echo technique could not be applied due to the short T_2 time of the aromatic protons of this drug. All measurements were performed by keeping the pulse duration time δ (1 ms) and diffusion time Δ (20 ms) constant during the experiment and by varying the magnitude of the field gradient (0-500 G/cm).

5.3.1 Deconvolution of the spectra

In some cases, especially with the PEGDA 4000 matrix, the NMR drug lines of the drug in the gel phase and in the water phase overlap. For these cases the WinFit software is used to deconvolute the composite line. Overlapping signals are fitted with two lines, each a mixture of Gaussian and Lorentzian line types. The Gaussian and Lorentzian contributions were varied for each line or group of lines until optimal agreement with the experimental data is achieved. Fig. 5.10 shows the lines of proxyphylline in the swollen PEGDA 4000 matrix at T= 22 ^{0}C. The green and the violet line represent two deconvoluted component lines whose sum (red line) corresponds to the shape of the proxyphylline overlapping peaks (blue spectrum). After deconvolution the separate lines could be integrated to obtain the spin-echo intensity. In the case of PEGDA 4000 matrix the deconvolution was necessarily performed for each investigated drug molecule.

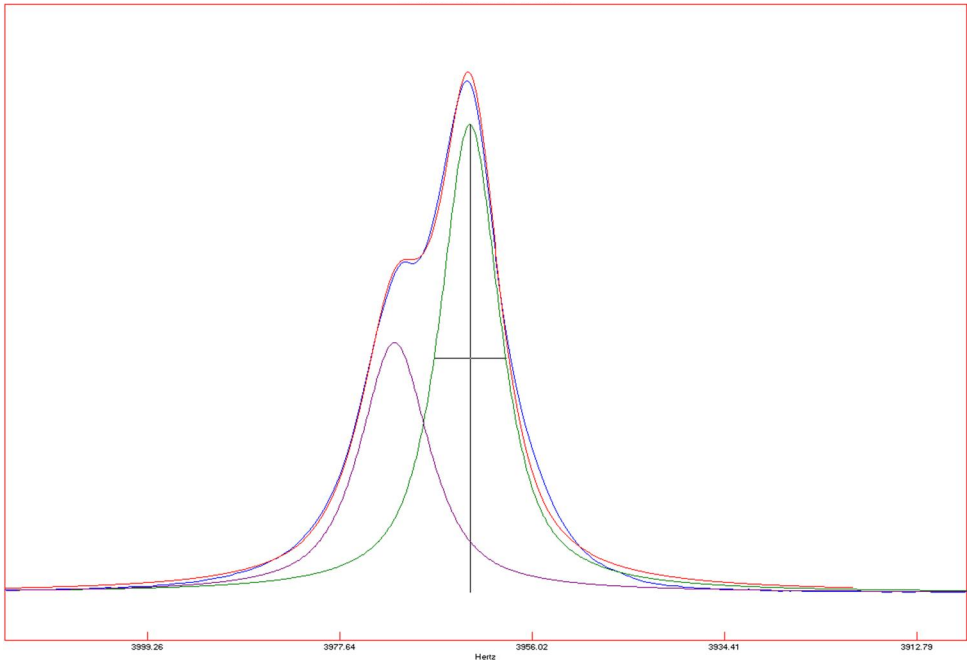

Fig. 5.10: Deconvolution of two proxyphylline lines in PEGDA 4000 matrix

For the determination of the drug and water self-diffusion coefficients two methods were used. In the first method the lines for the drug in the water and in the gel are first separated. The self-diffusion coefficient D for each of the two lines can be then obtained by exponential fitting of the data using eq. 3.19, or by calculating the negative slope of the logarithmic Stejskal-Tanner plot. In this study the average value of the diffusion coefficients obtained by these two fits is employed. Fig. 5.11 shows the PFGE decay curves for the proxyphylline/PEGDA 450 system at 22 ^{0}C when the behavior of the two lines (drug in gel and drug in water) is separately analyzed. The blue lines are related to the drug in the water phase and the red lines represent the drug in the gel phase. In the diagram a, the linear fits of both components are shown and the diagrams b and c represent the exponential decays for the two components. The average values for this system are for the drug in the water $D_{drug}^{water} = (4.84 \pm 0.06) \cdot 10^{-10} m^2 / s$, and for the drug in the gel $D_{drug}^{gel} = (0.54 \pm 0.02) \cdot 10^{-10} m^2 / s$.

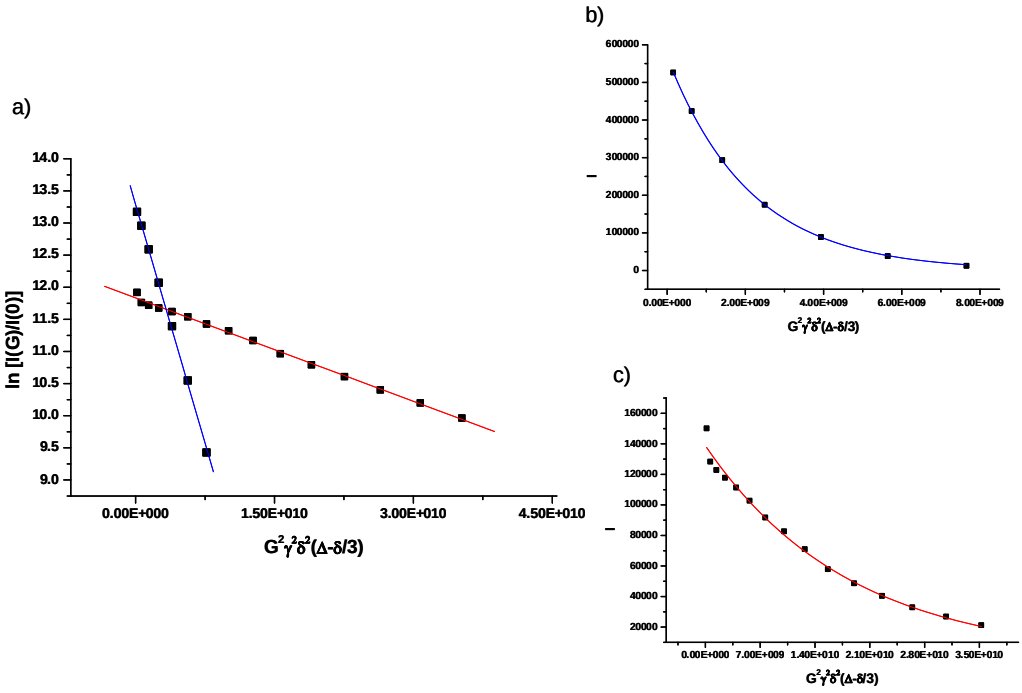

Fig. 5.11: PFGE decay curves for the proxyphylline/PEGDA 450 system at 22 ^{0}C after deconvolution of the two overlapping lines.

In the second method the intensity of both lines are integrated and plotted against G^2. Fig. 5.12 shows the biexponential fit of the same system as described above. This curve results when the integral of both lines is plotted and biexponentially fitted.

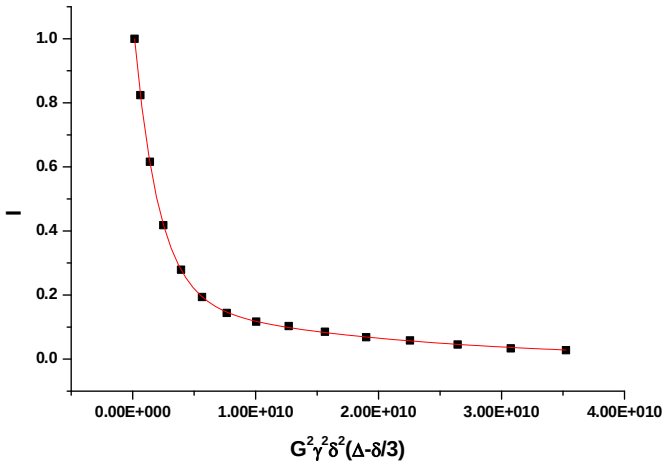

Fig. 5.12: PFGE decay curves for the proxyphylline/PEGDA 450 system at 22 ^{0}C when the behavior of the two components together is analyzed.

The diffusion coefficients obtained with this method are $D_{drug}^{water} = (4.99 \pm 0.06) \cdot 10^{-10} m^2 / s$ and $D_{drug}^{gel} = (0.54 \pm 0.02) \cdot 10^{-10} m^2 / s$. For this drug/matrix system there are no significant differences between these two methods. The second method is very accurate when the self-diffusion coefficients are sufficiently different. The first method is preferred when not. For all drugs in the PEGDA 4000 matrix the first method was applied. This is the lowest cross-linked network which affects the drug self-diffusion in the gel much less than the other matrices and therefore the differences between two drug components are not big enough that the biexponential fit can be applied. Also, proxyphylline was the only drug where the first method was preferred for all PEGDA matrices because this drug is smaller than the other ones and therefore is less influenced by the network.

5.3.2 Effect of the network on the self-diffusion

The self-diffusion coefficients of flucloxacilline, fluoresceine, and proxyphylline were measured using the signals at 2.7 ppm (CH_3), 7.6 ppm, and 8 ppm (aromatic protons), respectively at three different temperatures (12, 22, and 37 ^{0}C). The diffusivity data for every drug-polymer network combination at the three temperatures are shown in Table 5.3. The existence of different self-diffusion coefficients and chemical shifts for drug and water molecules in the water and gel phase proves that water and drug do not exchange fast between the water and gel phase during the time scale of the experiments. This implies that the water and gel phase domains have sizes far greater than the nanometer scale. This agrees with the system used, which consists of mm-sized polymer films separated by water/drug solution.

The drug diffusion in the water phase should be independent of the cross-link density of the gel phase. Table 5.3 shows that the drug-diffusion coefficient in the water phase of the PEGDA 4000 gel clearly deviates from the corresponding values for PEGDA 2000 and PEGDA 450 matrices. This is not due to a measurement error, but due to a slow exchange of the drug between the water and the gel phase of PEGDA 4000.

Table 5.3 The drug and water self-diffusion coefficients (in 10^{-10} m^2/s) at three different temperatures and the corresponding diffusion activation energies (in kJ/mol) for all three networks. The average experimental error of the diffusion values is estimated to be less than ±5%, for the activation energies the maximum error is ±10%.

Drug	**Proxyphilline**				**Fluoresceine**				**Flucloxacilline**			
T in ^oC	**12**	**22**	**37**	**E_A**	**12**	**22**	**37**	**E_A**	**12**	**22**	**37**	**E_A**
PEGDA 4000												
D_{drug}^{gel}	1.5	2.0	2.7	17	1.0	1.3	1.7	15	1.2	1.6	2.1	17
D_{drug}^{water}	2.7	4.0	5.8	23	1.8	2.7	3.8	21	2.6	3.8	5.3	21
D_{HDO}^{gel}	9.4	13.2	17.5	18.3					10.2	12.9	17.3	16
D_{HDO}^{water}	13.7	18.3	26.5	20					13.4	17.9	26.9	21
PEGDA 2000												
D_{drug}^{gel}	1.0	1.3	1.8	19	0.4	0.5	0.7	18	0.3	0.4	0.6	18
D_{drug}^{water}	3.4	4.5	6.7	20	2.2	3.2	4.6	21	2.6	3.6	5.3	21
D_{HDO}^{gel}	7.0	9.6	12.8	19	7.2	9.3	13.1	18	7.1	9.3	13.0	18
D_{HDO}^{water}	13.2	18.7	25.5	20	13.2	18.0	26.0	20	13.5	18.6	26.5	20
PEGDA 450												
D_{drug}^{gel}	0.4	0.5	0.7	15	0.1	0.1	0.2	14	0.1	0.1	0.1	14
D_{drug}^{water}	3.4	4.9	6.8	20	2.3	3.1	4.6	21	2.6	3.7	5.2	21
D_{HDO}^{gel}	4.3	6.0	8.1	19	4.5	6.0	8.6	19	4.3	5.9	8.0	18
D_{HDO}^{water}	13.2	19.1	25.7	20	12.8	17.7	24.9	20	13.4	18.3	25.7	19

The mobility of the drug in the other networks is lower and such exchange is not noticed for these cases. The water diffusion coefficient in the system composed of PEGDA 4000 and fluoresceine could not accurately be determined in the same experiment due to the large gradient strength that was needed for the fluoresceine diffusion.

The diffusivity of the drug molecules in the hydrogel changes when the cross-link density, or the average PEG chain length between cross-links, of the polymer matrix is changed. With increasing cross-link density, from PEGDA 4000 to PEGDA 450, the self-diffusion coefficients of the drugs in the hydrogel decrease and the difference between diffusion rates of the drugs in the water phase and in the gel phase becomes more pronounced. Some of the data of Table 5.3 can be represented in a different way. A good impression of the effect of the gel network density (mesh size) on the diffusivity is obtained when the relative diffusion coefficients $D_{drug}^{gel} / D_{drug}^{water}$ are calculated (Fig. 5.13).

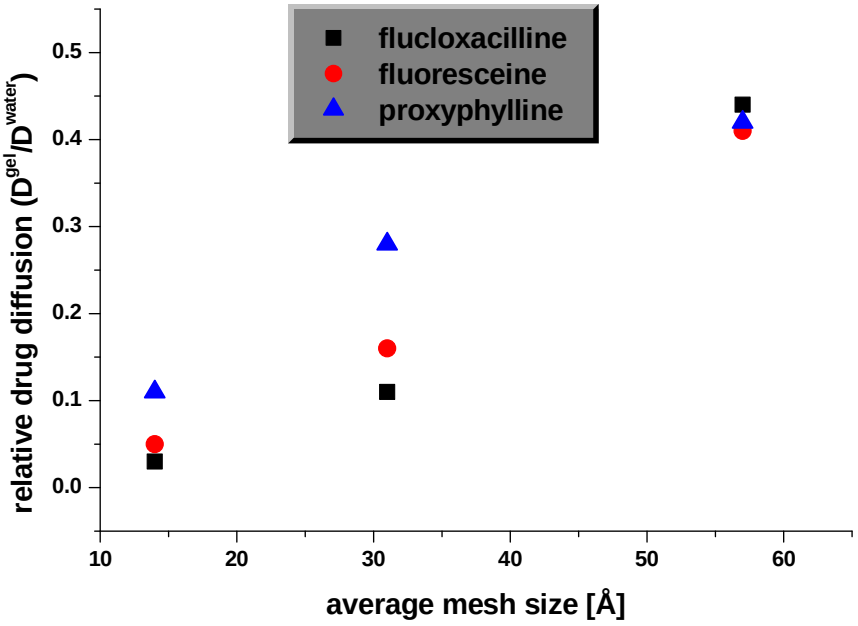

Fig. 5.13: Dependence of the relative drug diffusion coefficients on the polymer mesh size. The temperature averaged values are shown.

This representation shows that the polymer network has the greatest effect on the diffusion of the largest drug molecule (flucloxacilline with MW 494 g/mol) and the smallest effect on the smallest drug (proxyphylline with MW 238 g/mol). For the network with the largest mesh size (PEGDA 4000) the drug size has little or no effect on the relative drug diffusivity. At the intermediate cross-link density (PEGDA 2000) the effect of the network on the drug diffusion is dependent on the drug molecular size. The mesh size apparently becomes small enough to affect the diffusion of all three drugs in a considerable way. For PEGDA 450, where the mesh size is of the same order of magnitude as the drug size, the drug size does not play an important role any more.
The quantitative values representing the network effect on the drug and water diffusion are shown in the Table 5.4.

Table 5.4 Relative drug diffusion coefficients $D_{drug}^{gel} / D_{drug}^{water}$ for all drug/PEGDA combinations and $D_{HDO}^{gel} / D_{HDO}^{water}$ for HDO in the gel and water phase.

	$D_{drug}^{gel} / D_{drug}^{water}$			$D_{HDO}^{gel} / D_{HDO}^{water}$	$\left(\frac{1-\upsilon_2}{1+\upsilon_2}\right)^2$
PEGDA	Proxyphilline MW 238	Fluoresceine MW 376	Flucloxacilline MW494	HDO	
4000	0.42	0.41	0.44	0.70	0.67
2000	0.29	0.16	0.11	0.52	0.50
450	0.12	0.05	0.03	0.32	0.36

The effect of the temperature on these values is smaller than the error in the values, therefore the temperature averaged values are given. The values for HDO are independent of the dissolved drug. In the last column the calculated values of the factor of eq. 2.32 are shown where υ_2 is the volume fraction of the polymer in the hydrogel.

Table 5.4 shows that the network slows down the drug diffusion in the gel relative to the drug diffusion in water. The smaller the drug, the less hindered its diffusion in the hydrogel.

With increasing cross-link density, also the rate of water diffusion decreases. The effect of the network on the water self-diffusion is smaller than on the drug diffusion. Actually, as Table 5.4 shows, the effect of the matrix on the diffusion of the small water molecules can be well described by the lattice model of eq. 2.32. The measurements also show that the diffusion of water in the hydrogel is not affected by the type of drug in the hydrogel, at least at drug concentrations that are used here.

5.3.3 Temperature dependence of diffusion and activation energies

Drug and water self-diffusion measurements for each combination drug-polymer matrix were performed in the temperature range between 12 and 37 ^{0}C. As the temperature increases the drug diffusion becomes faster, both for the population in the polymer network (the hydrogel phase) and for the population in the water phase.

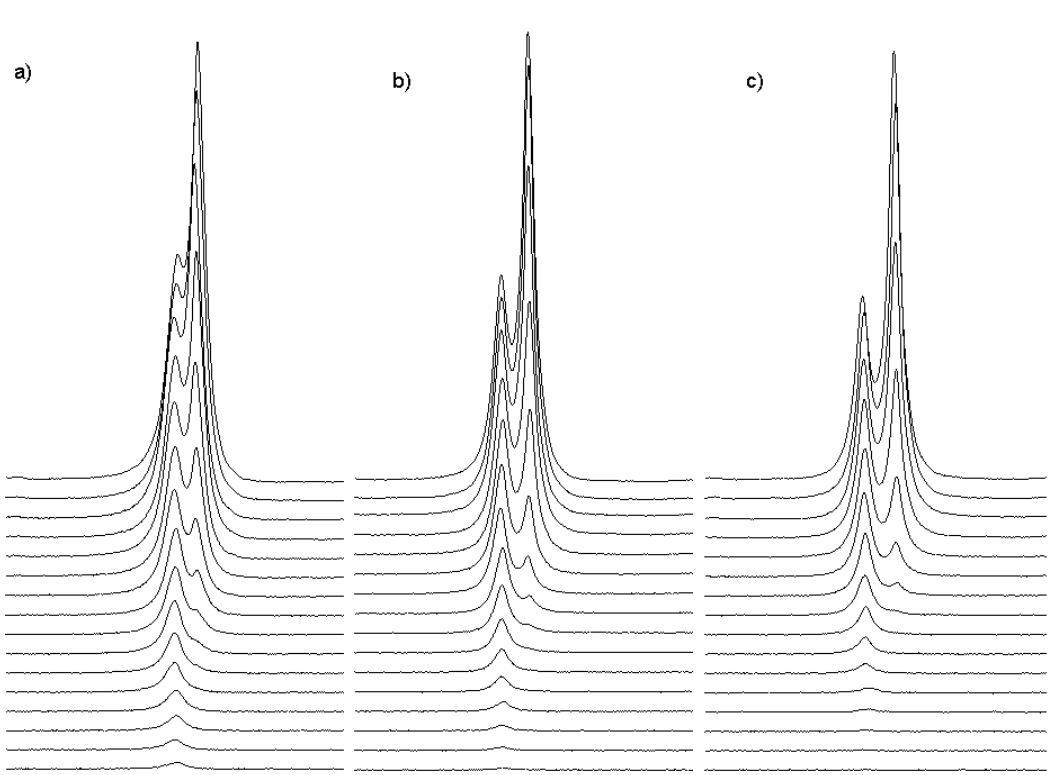

Fig. 5.14: The PFGE decay of proxyphylline peaks at 8 ppm in PEGDA 2000 matrix at 12 ^{0}C (a), 22 ^{0}C (b) and 37 ^{0}C (c). The gradient increases from the top to bottom spectrum

Fig. 5.14 shows the intensity decay of proxyphylline resonance peaks in the PEGDA 2000 matrix with increasing gradient strength at three different temperatures. In each of these three spectra a clear difference between the two components can be observed. The left peak whose decay is slower corresponds to the drug in the gel phase (with the lower diffusion coefficient). The right peak has a shorter decay and corresponds to the drug component in the water phase which diffuses faster. When the spectra at different temperatures are compared, it can be clearly seen that for each of the two components the decay becomes faster with increasing the temperature. This means that the diffusion becomes faster in both phases.

Diffusion through the polymer network can be interpreted as an activated process and the temperature dependence of the diffusion coefficient was fitted with an Arrhenius-type equation:

$$D = D_0 \cdot e^{-(E_a / RT)} \quad , \tag{5.4}$$

D_0 represents the diffusivity at infinite temperature, T the absolute temperature, and E_a the activation energy. Fig. 5.15 presents the Arrhenius plots for flucloxacilline in different cross-linked networks. The same plots for proxyphylline and fluoresceine are shown in Appendix 9.2. The Arrhenius plots of diffusivities are linear over the temperature range 12-37 ^{0}C and from the slopes of these plots activation energies both for the drug and water diffusion were determined. The values of activation energies are given in the Table 5.3. Because the curves in Fig. 5.15 are parallel, it can be concluded that the activation energies are independent of the phase in these two-phase systems and also independent of the polymer cross-link density. The values of E_a are comparable to the hydrogen bonding energy of water. This will be explained in more details in the next Chapter about diffusion model.

It is acknowledged that the temperature range is rather small and therefore the measured activation energies represent the value of $-R(\partial(\ln D)/\partial(1/T))$ in the middle of the studied temperature range.

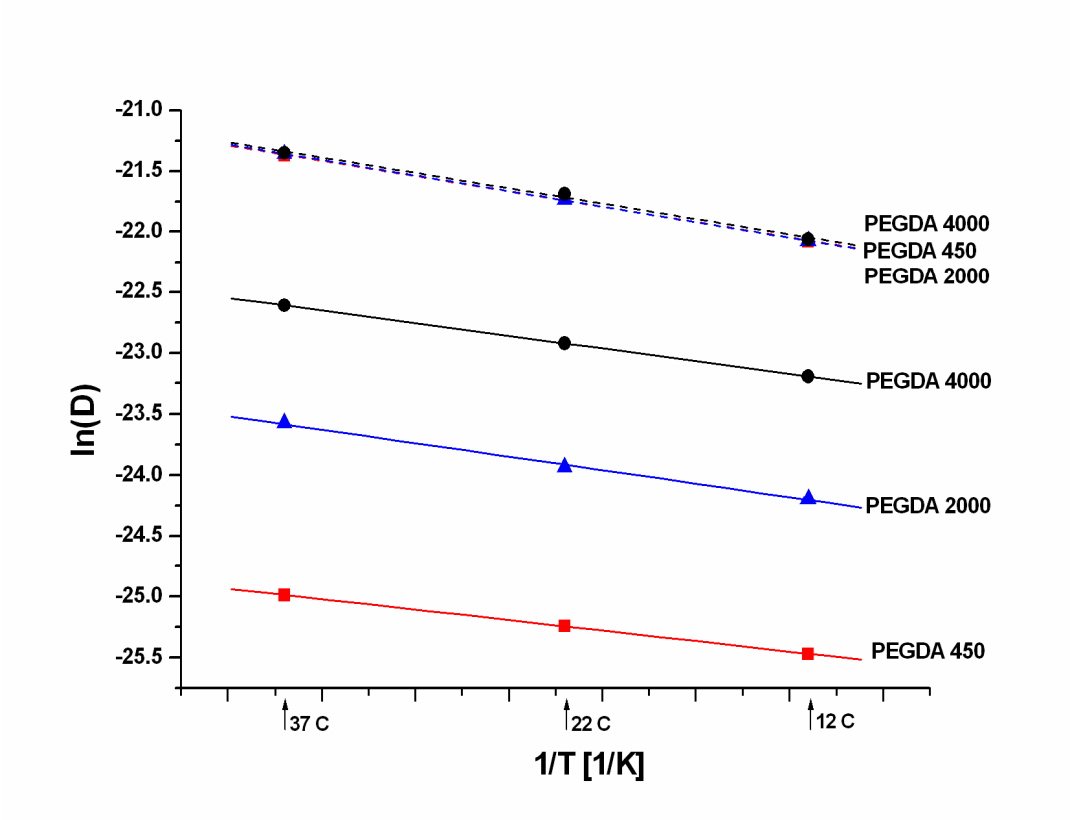

Fig. 5.15: Arrhenius plots of ln(D) of flucloxacilline versus the reciprocal of the absolute temperature in different matrices (PEGDA 4000-black lines, PEGDA 2000-blue lines and PEGDA 450-red lines). The three overlapping dashed lines represent the drug diffusion in the water phase, the solid lines in the gel phase.

5.4 Rotational mobility (rotational diffusion)

Self-diffusion coefficients give information about the translational diffusion motion of molecules. Rotational diffusion motions can be investigated by NMR relaxation measurements. The drug mobility in two different phases of the swollen polymer systems (free water and gel) can be specified by measuring T_1 and T_2 relaxation times. A molecular system for which the spin-lattice relaxation time T_1 approximately equals the spin-spin relaxation time T_2, executes an isotropic rotational motion. For a rigid molecular system or a system that exhibits strongly anisotropic rotational motions T_2 will be much shorter than T_1.

To investigate the rotational mobility of the drug molecules in the hydrogel matrices, the T_1 and T_2 relaxation times were measured for two drug molecules, proxyphylline and flucloxacilline, in the PEGDA matrices of different cross-link density. The spin-relaxation time (T_1) was measured by the inversion recovery method (Chapter 3). The intensity of the NMR signal is measured for different time intervals between the two pulses, and then fitted with the eq. 3.12. Fig. 5.16 presents the evaluation of the T_1 for flucloxacilline in PEGDA 2000 matrix at 25 ^{0}C.

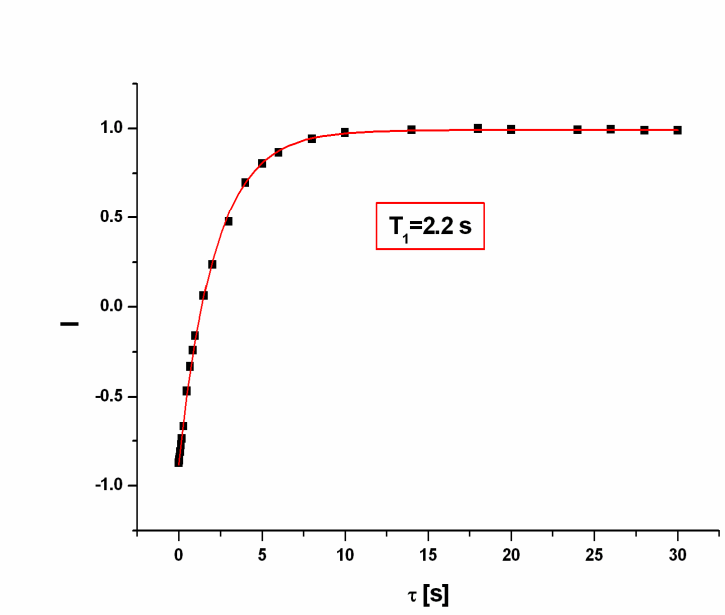

Fig. 5.16: Measurement of the T_1 time via the inversion recovery method for the flucloxacilline/PEGDA 2000 system at T=25 ^{0}C. The change of the peak intensity with the time τ between the pulses is shown and fitted with the single exponential.

The total signal intensity of both water and gel drug components is measured and as Fig. 5.16 shows there are no significant differences in T_1 times between the two drug populations. The average T_1 time for this system is 2.2 s. For the determination of the spin-spin relaxation time (T_2), the spin-echo technique is used (Chapter 3). In this case the echo attenuation is measured for different time intervals between the pulses and the results are fitted with eq. 3.13 (Fig. 5.17). Fig. 5.17 shows that two components with different T_2 relaxation times exist.

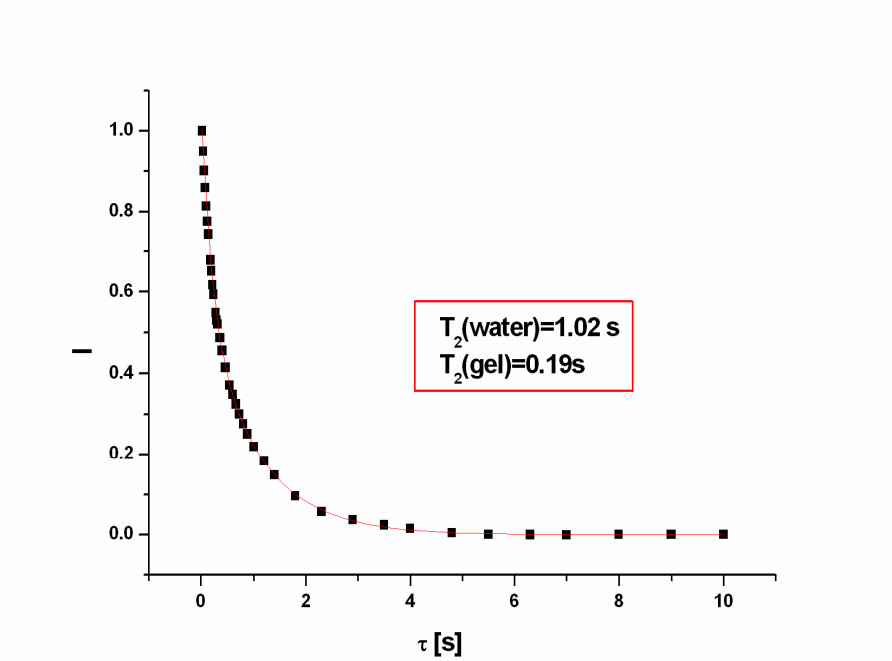

Fig. 5.17: Measurement of the T_2 time with the spin-echo technique for the flucloxacilline/PEGDA 2000 system at T=25 ^{0}C. The decrease of the signal intensity with the time τ between the pulses is shown and fitted with a double-exponential function.

The longer relaxation time (in this case 1.02 s) corresponds to the drug in the water phase and the shorter T_2 time (in this case 0.19 s) to the drug in the hydrogel. The measured relaxation times for all systems are shown in the Table 5.5. For the drugs in the water phase T_2 is only about 50% shorter than T_1, indicating that the rotational tumbling motion of the drug molecule in the water phase is almost isotropic. Changing from the water phase to the gel, the drug T_2 becomes 4-5 times smaller, whereas the T_1 is not significantly affected. For each drug molecule (with one exception) the relaxation times in the gel do not change by varying the cross-link density of the network. The exception is for the biggest drug molecule flucloxacilline (M=494 g/mol) for which in the highest cross-linked network, PEGDA 450, the T_2 time decreases by a factor 3 relative to T_2 in the other networks. This confirms that the drug size in this case approaches the pore size of the network and the tumbling motion becomes much more hindered.

Table 5.5 T_1 and T_2 relaxation times of drug molecules at 25 ^{0}C; the average error is about ± 10%.

	Proxyphylline		**Flucloxacilline**	
	T_1 [s]	T_2 [s]	T_1 [s]	T_2 [s]
PEGDA 4000				
water	2.2	0.98	1.8	0.9
hydrogel		0.22		0.23
PEGDA 2000				
water	2.6	1.3	2.2	1.02
hydrogel		0.29		0.19
PEGDA 450				
water	2.6	1.4	1.6	0.97
hydrogel		0.24		0.076

In order to develop a model for the anisotropic rotational motion of the drug molecules, the drug molecule is described as a rigid flat disc with axial symmetry (Fig. 5.18).

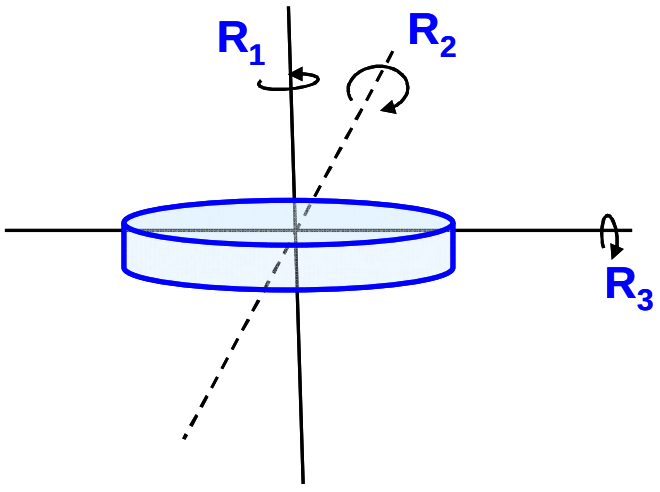

Fig. 5.18: The axially symmetric molecule with its axes of rotation

It can be expected that the rotational motion of such a disc about different axes occurs at different rates. R_1 is defined as the rotational diffusion rate around the symmetry axis

perpendicular to the plane and R_2 is the rotational diffusion rate around the in-plane axis. It is assumed that rotations around the two in-plane axes occur at equal rates (R_2=R_3). Thus, for a description of the rotation of axially symmetric molecules two rotational correlation times are sufficient.

The anisotropy effects can be better understood if the relaxation times for various ratios R_1/R_2 are known. By programming the equations developed by Woessner[42] in Mathematica 4.1, a qualitative picture of the relaxation rates for various ratios R_1/R_2 can be obtained (Fig. 5.19).

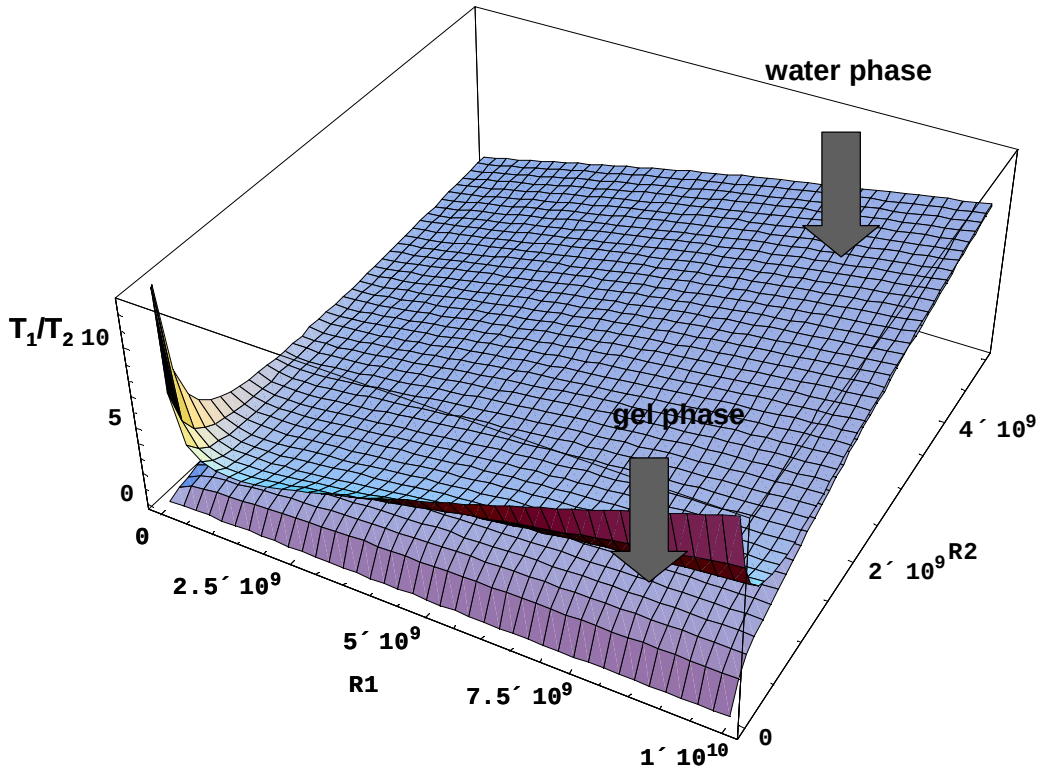

Fig. 5.19: T_1 and T_2 relaxation times with respect to the rotational diffusion rates about the two molecular axes, R_1 and R_2. Rotational rates are given in s^{-1}.

In this 3D plot the upper surface represents the T_1 values and the lower one the T_2. From this plot it can be concluded that the motion of the free drug molecules in the water phase of the PEGDA systems correspond to the situation in the upper right hand corner of the

surface (R_1 and R_2 both fast), where $T_2 \approx T_1$. The situation of drugs in the gel corresponds to the lower right hand corner of the figure 5.19 (R_1 still fast but R_2 much slower) where $T_2 << T_1$. This would mean that the rotational motion of the drug around the axis perpendicular to the plane (R_1) is not very much affected by the network, in contrast to the rotational motion around the in-plane axis (R_2).

The cross-section of the plot at the constant rotation rate R_1 about the symmetry axis (Fig. 5.20), corresponds to the transition of the drug from the water to the gel phase. Fig. 5.20 nicely shows how by changing to the hydrogel phase the tumbling motion (R_2) becomes significantly slower.

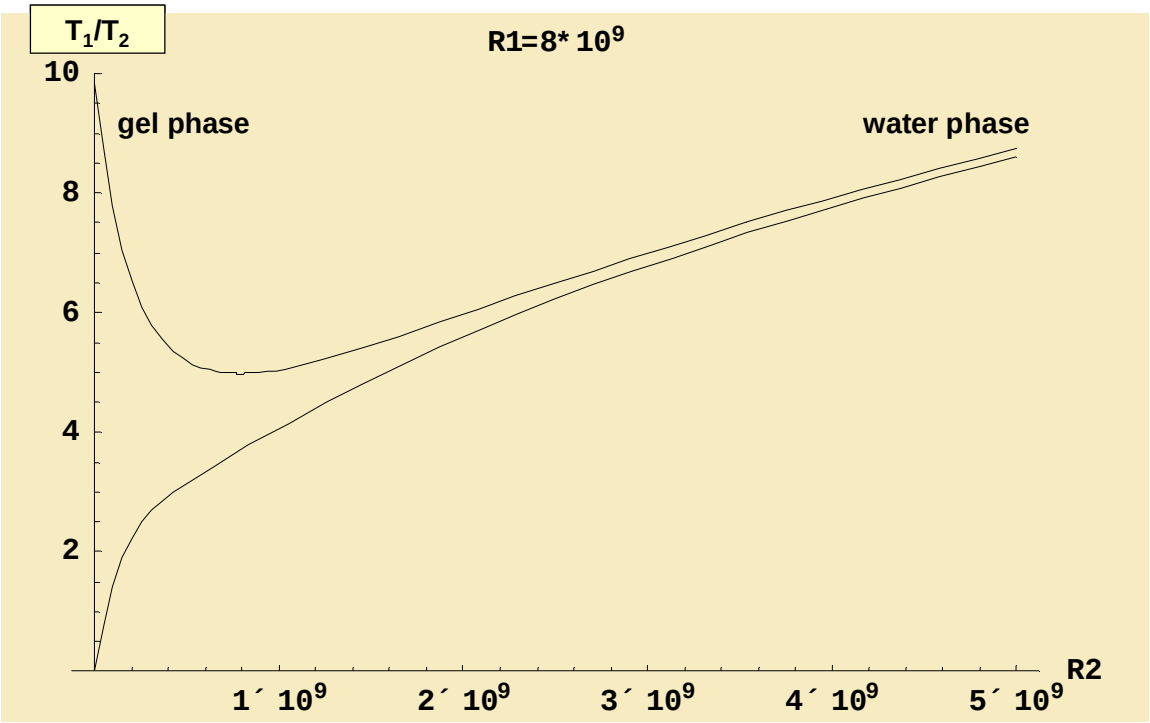

Fig. 5.20: Cross-section of the 3D plot at the constant rotation rate around the symmetry axis ($R_1 = 8 \cdot 10^9$). The upper curve corresponds to the T_1 and the lower curve to the T_2 relaxation time. Rotational rates are given in s^{-1}.

In the gel the motion of the drug molecules exhibits a large anisotropy, where the rotation around the in-plane axis is drastically slower than the rotation around the symmetry axis. This is caused by the fact that for the tumbling motion molecules need more energy and the energy barrier for such a motion in the gel is higher.

A similar phenomenon is found for benzene. Molecular dynamics simulations on the benzene molecule in benzene liquid[43] show that the rotation about the C_6 axis (spinning motion) is faster than the rotations about the in-plane axes (tumbling motion). By introducing the benzene in a polymeric matrix, the tumbling motion is drastically slowed down, whereas the rotation about the symmetry axis is only slightly affected.
The study of the drug rotational mobility shows that the rotational diffusion around the symmetry axis is not very much sensitive to the environment, but the rotational diffusion around the in-plane axis becomes strongly affected by changing from the water to the gel phase.

5.5 Drug-matrix interaction

As shown previously, for all three drugs the NMR resonances of the drug in the gel are shifted and broadened relative to the corresponding lines of the drug in the water phase. The higher the cross-link density, the higher the shift and the broadening are. Thus, also the shift and broadening (in addition to the self-diffusion and T_2 experiments) prove the existence of an interaction between the drug molecule and the network.

Not only the proton NMR chemical shifts serve as evidence that the drug molecules interact with the polymer network. Two NOE methods are used to confirm this finding. In the STD experiment, the on-resonance spectrum is obtained by saturation of polymer resonances in a region where no drug peaks are present (at 3.75 ppm). The off-resonance spectrum (reference spectrum) is obtained by saturation far away from both the drug and the polymer lines. Fig. 5.21 presents the STD NMR experiment on the proxyphylline/PEGDA 450 system. In Fig. 5.21a the black spectrum represents the reference spectrum and the red one is the on-resonance spectrum. By selective saturation of the polymer the signal intensity of the drug population in the gel phase decreases. The transfer of saturation from the polymer to the drug can only occur during the time the drug is very near (distance smaller than approximately 0.5nm) the polymer network. Therefore, the difference spectrum in the Fig. 5.21b contains only the peaks from the drug molecules which are that close to protons of the matrix. This shows that the drug molecules in the gel phase possess some binding affinity for the PEGDA matrix.

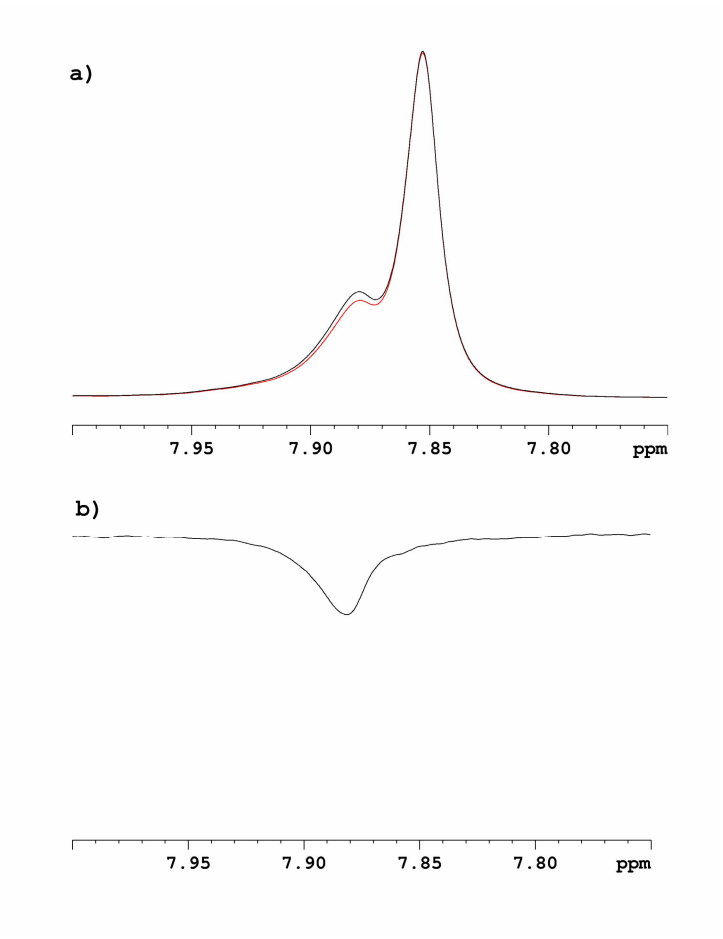

Fig. 5.21: STD NMR experiment for the proxyphylline/PEGDA 450 system. Off-resonance (black) and on-resonance (red) spectra (a) and the difference spectrum (b)

The second NOE method, also for detection of possible drug-matrix interactions is the 2D NOESY technique. The appearance of cross-peaks in the 2D NMR proton spectrum confirms the proximity between the corresponding protons. Fig. 5.22 presents NOESY spectra of the flucloxacilline/PEGDA 2000 and flucloxacilline/PEGDA 450 systems. Beside the cross-peaks arising from the protons in one molecule (intramolecular) or from interaction with water, there are additional cross-peaks. These are intermolecular cross-peaks which connect the drug protons with the polymer protons in the spectrum. This is also evidence for the existence of interaction between the drug molecules and the PEGDA matrices.

a)

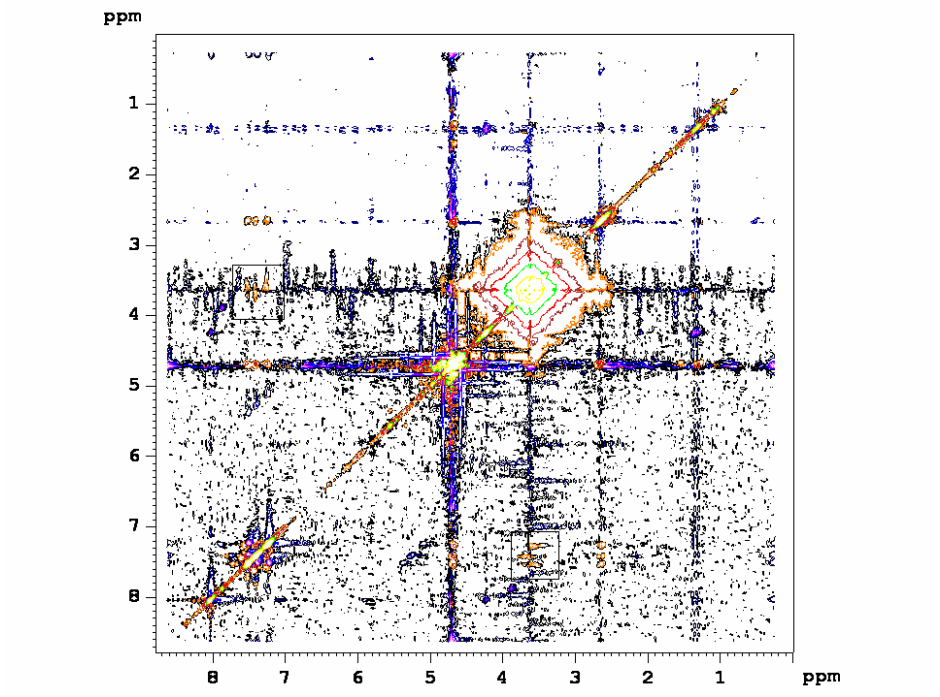

b)

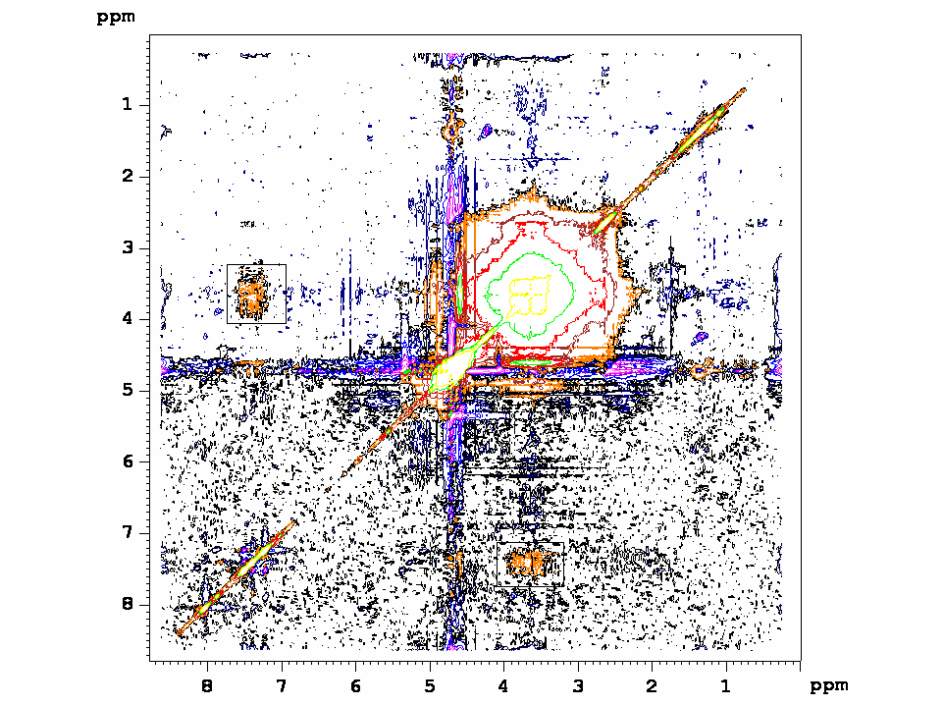

Fig. 5.22: 2D NOESY spectra of the flucloxacilline/PEGDA 2000 (a) and the flucloxacilline/PEGDA 450 (b) system. Mixing time was 2 s.

Although the drug molecules in the gel interact with the PEGDA polymers, the fact that the chemical shift in the gel phase depends on the network cross-link density, and that the shifts are so small implies that the drug molecules are not permanently attached to a polymer chain in the network. This is also confirmed by the non-zero diffusion coefficient in the gel D_{drug}^{gel}. Behavior of the drugs in the hydrogel resembles the behavior of a ligand that exchanges between bound to a receptor and the free in solution state. The exact model describing the drug-matrix interaction will be presented in the Chapter 6.

5.6 Drug-cyclodextrin complexation

Another type of drug carrying devices very important in drug delivery is represented by the class of cyclic oligosaccharides known as cyclodextrins. Cyclodextrins (CDs) are used as solubilizing agents to enhance drug solubility both in solutions and in swellable polymers, as well as to protect drugs from attack by various species[85]. Binding of drugs to cyclodextrins occurs via (partly) encapsulation of the drug in the inner hydrophobic cavity of a cyclodextrin.

NMR is a widely used approach to study inclusion complexation. As evidence of complex formation serve changes in the proton NMR chemical shifts of both species (drug and cyclodextrin) involved in the complexation. The magnitude of this change, $\Delta\delta$, is defined as a difference between the chemical shift of a proton in the pure compound and the chemical shift of that proton in the presence of the other substance. This change of the chemical shift $\Delta\delta$ depends on the location of the proton in the molecule, size of the CD cavity and the host/guest ratio[86]. The ^{1}H NMR chemical shift range of CDs is rather narrow, between 3.5 and 4.1 ppm. H-3 and H-5 CD protons are external protons and appear approximately in the region 3.8-4.1 ppm. H-2 and H-4 protons are located inside the cavity and their signals are expected between 3.6 and 3.7 ppm. The structural assignment of different cyclodextrin protons is given in the Appendix 9.3. Inclusion of the aromatic drug usually causes upfield shifts of the internal cyclodextrin protons. The resonances of the aromatic drug due to complexation are generally shifted downfield[87,88,89]. In this section, the interaction between some water soluble and water

insoluble drug molecules and different kinds of cyclodextrins (α, β, and γ) has been investigated.

5.6.1 Complexation of water soluble drugs

For the water soluble drugs the drug and CD concentrations were chosen in a way that the guest/host molar ratio was approximately 1:1. In the ^{1}H NMR spectrum of α CD in D_2O (Fig. 5.23a) the signals of external protons are found at ca. 3.65 ppm for H-2 and at ca. 3.60 ppm for H-4. The signals of protons attached to the interior of the cavity are found at ca. 4.0 ppm for H-3 and at ca 3.89 ppm for H-5 protons. After adding the flucloxacilline (Fig. 5.23) the complexation resulted in an upfield shift of the inner H-3 protons and at the same time in a slight downfield shift of the drug protons. The resonances of external protons (H-2, H-4) remained unchanged.

a)

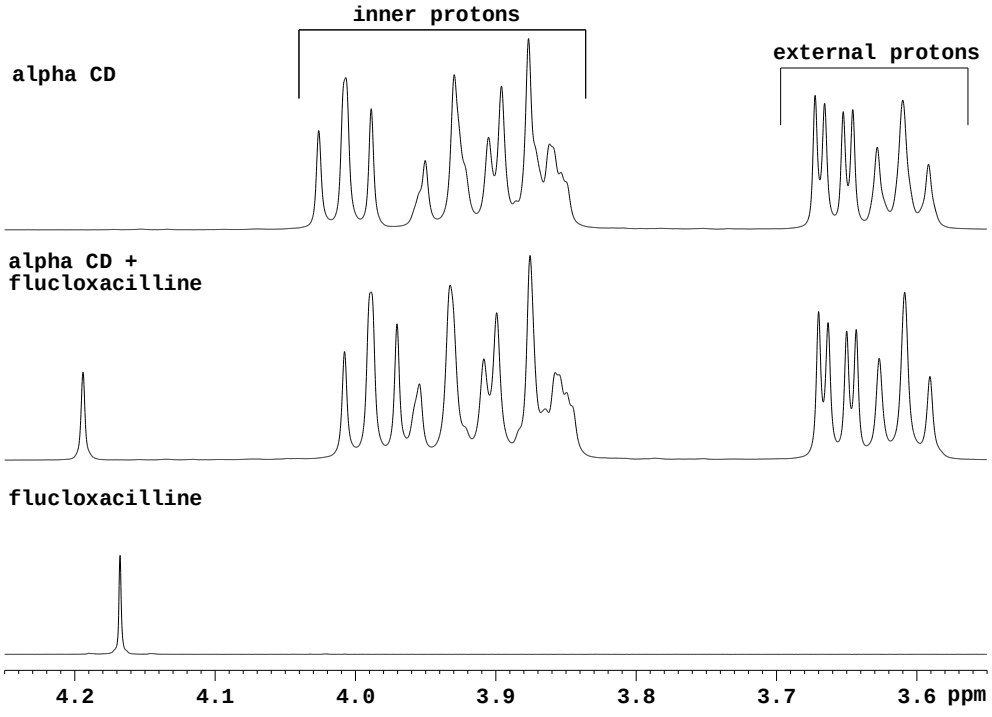

b)

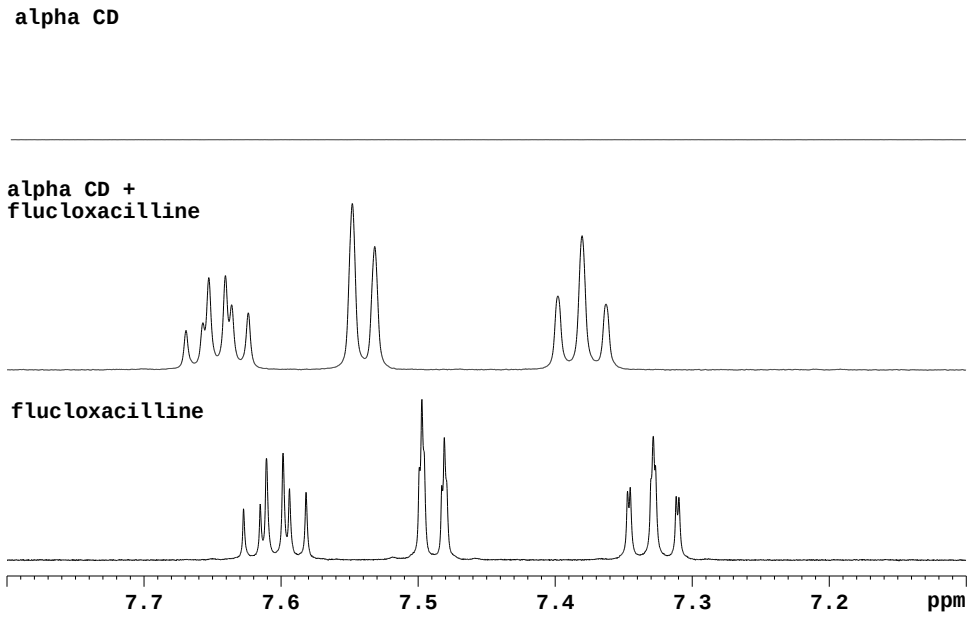

Fig. 5.23: ^{1}H NMR spectra of α CD and flucloxacilline in D_2O solution. Fig. 5.23a shows the CD spectral region and Fig 5.23b the aromatic spectral region.

Fluoresceine exhibits similar behavior except that the upfield shift of the H-3 and also H-5 protons is more pronounced. Additionally, an upfield shift of the external protons, H-2 and H-4, can be observed. (Fig. 5.24).

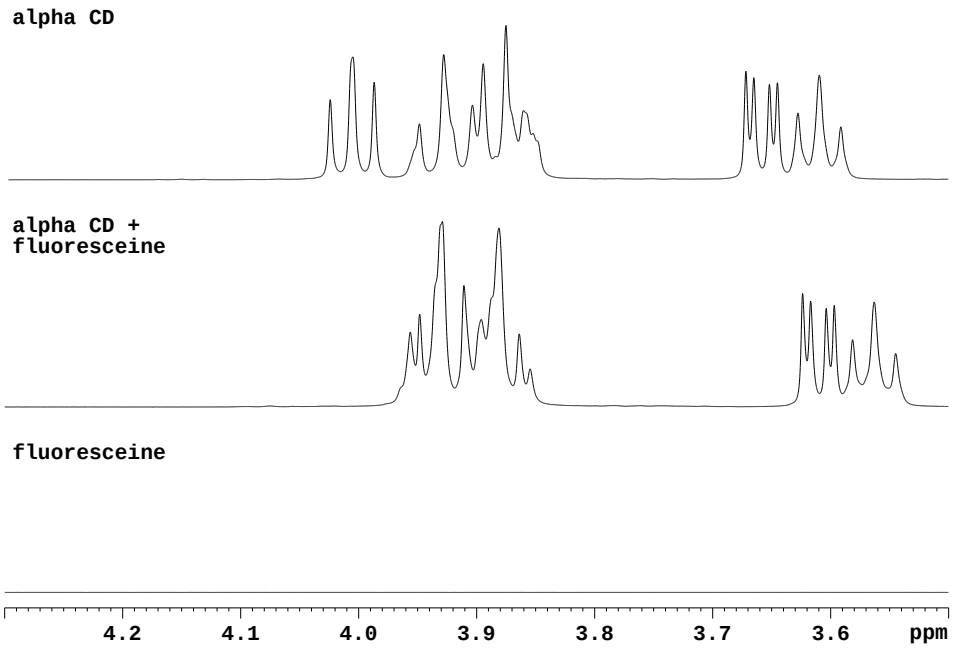

Fig. 5.24: ^{1}H NMR spectra of α CD and fluoresceine in D_2O solution.

This indicates that the fluoresceine molecule interacts not only with the protons inside the cavity, but also with the protons at the outer surface of the torus. Thus, in the case of this drug external complexation occurs as well. Fluoresceine protons were significantly shifted and also some new peaks appeared. These results confirmed formation of fluoresceine-CD complexes.

The similar analysis is repeated with β and γ cyclodextrin. Both flucloxacilline and fluoresceine exhibit the strongest changes of the ^{1}H NMR spectrum with γ-CD, then with β-CD and the spectrum changed least for the complexation with α-CD. This can be explained by deeper immersion of drugs in the wider cavity of β and γ cyclodextrin. Proxyphylline does not build inclusion complexes with cyclodextrins.

The 2D NOESY technique was also applied to confirm complexation between host and guest. For all experiments the mixing time was chosen to be 2s. Fig. 5.25 shows the 2D NOESY spectrum of the mixture of β-CD and fluoresceine in D_2O. Beside the intramolecular interactions, intermolecular cross-peaks were observed between aromatic protons of both drug molecules and H-3 and H-5 protons of α, β, and γ CD.

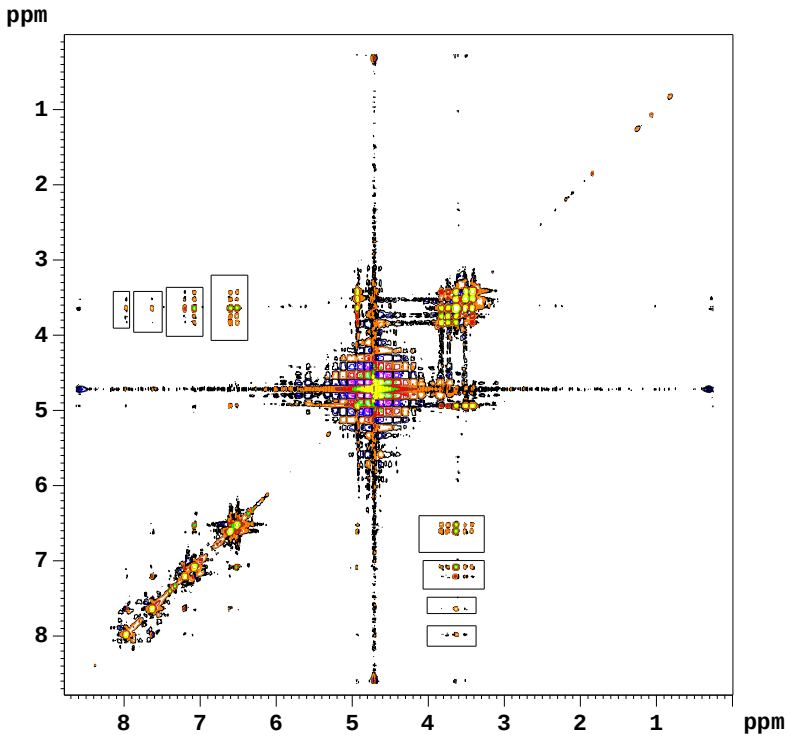

Fig. 5.25: 2D NOESY spectrum of β-CD and fluoresceine in D_2O

Cross-peaks between aromatic protons of fluoresceine and external protons (H-2, H-4) of cyclodextrins also confirm that this drug molecule interacts with the protons at the outer surface of the CD torus.

The PFGE NMR technique was employed to study drug and cyclodextrin diffusion in D_2O solution. The results are shown in Table 5.6. Drug and cyclodextrin diffusion coefficients were lower in comparison with the diffusion coefficients of the free drug in water and the free CD in water, respectively. It can be seen that the drug diffusion in the complex is faster than the CD diffusion in the complex. This must mean that the drug molecule exchanges fast between a state where it is bound in the complex and a state where it is free in the water solution. This is possible because these drugs are water soluble. The average diffusion coefficient of the complexed drug is then higher than that of cyclodextrin. The more time the drug spends in the complex, the smaller will be the difference between drug and CD diffusion coefficients. These changes of drug diffusion

in the presence of cyclodextrins served also as an evidence of formation of inclusion complex.

Table 5.6 Self-diffusion coefficients (in 10^{-10} m^2s^{-1}) of drug-cyclodextrin complexes

system	CD	Drug + CD in water	
		D_{drug}^{water} (3.6)	D_{CD}^{water}
flucloxacilline	α-CD	2.9	2.4
	β-CD	3.2	2.4
	γ-CD	2.2	2.0
system	CD	Drug + CD in water	
		D_{drug}^{water} (3.2)	D_{CD}^{water}
fluoresceine	α-CD	2.8	2.3
	β-CD	2.9	2.4
	γ-CD	2.1	1.9
system	CD	Drug + CD in water	
		D_{drug}^{water}	D_{CD}^{water}
ibuprofen	β-CD	2.8	2.7

For comparison the diffusion coefficients in the absence of CD are given in the headers in parantheses

5.6.1 Complexation of a water insoluble drug

All cases presented so far concern water soluble drug molecules. A very important application of cyclodextrins is as solubilizing agents to increase the water solubility and bioavailability of water insoluble drugs. This property of cyclodextrins is demonstrated on the example of ibuprofen which has a poor solubility in water. A formulation of 20 mg ibuprofen with 18 mg β cyclodextrin in D_2O has been prepared (drug:CD molar ratio ≈ 6:1). After filtration a clear solution is obtained and its NMR spectrum recorded. Fig. 5.26 presents the proton NMR spectra of β-CD alone and the

complex solution of β-CD and ibuprofen. After addition of cyclodextrin the drug lines are observed in the spectrum in D_2O solution which already shows that the drug solubility is enhanced.

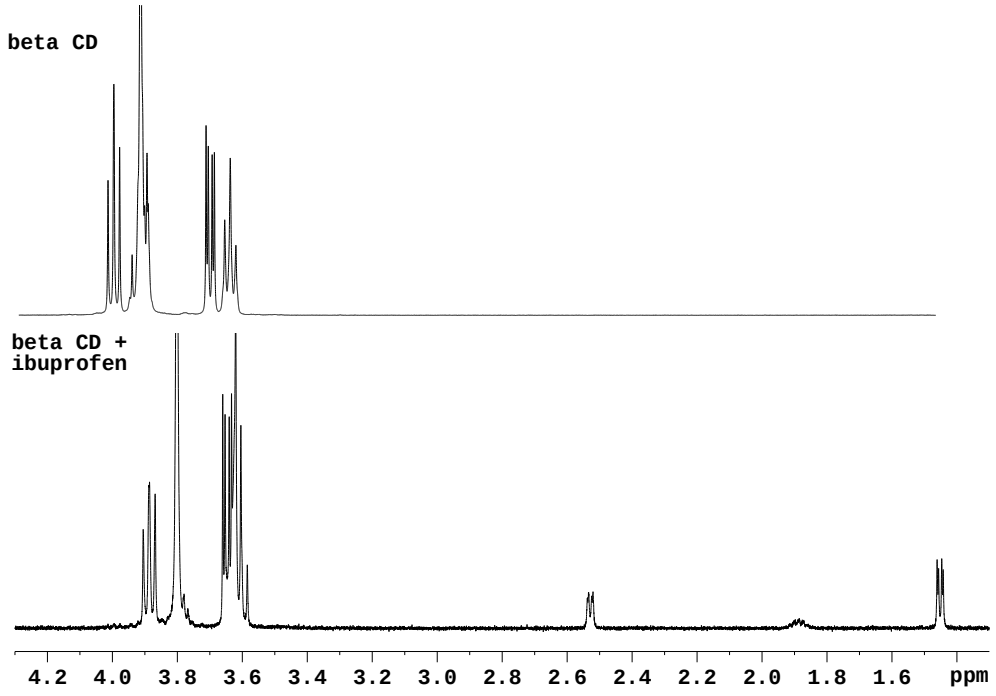

Fig. 5.26: ^{1}H NMR spectra of β-CD and ibuprofen in D_2O solution

Fig. 5.26 clearly shows that the inner protons of cyclodextrins are upfield shifted in the presence of the drug. This implies that the drug is located in the hydrophobic cavity of cyclodextrin. Although ibuprofen is a water insoluble drug, it is able to form an inclusion complex with β cyclodextrin in water. The diffusion of ibuprofen in the complex solution is measured with the PFGE method. The results are shown in the Table 5.6. In this case the drug and CD diffusivity in the complex are approximately equal. Because of the very low water solubility this drug spends almost 100% of the time in the complex with β-CD and that causes their diffusion coefficients to be the same. Encapsulation of ibuprofen by cyclodextrin opens a new possibility for CD applications for increasing the solubility of water insoluble drug in hydrogels.

5.7 Inclusion complexes in swollen polymer networks

The property of cyclodextrins to build inclusion complexes with different drug molecules led to the idea that the effective molecular mass of the drug thus will be increased. The hypothesis being investigated is that since the drug-CD complex will have a higher molecular mass than the drug molecule alone, the drug-CD complex once absorbed by the gel should exhibit a slower diffusion than a non-complexed drug molecule in the gel. For drug delivery this can be desirable and we therefore investigated the behavior of CD-complexed drugs in cross-linked polymer matrices, both for water soluble and water insoluble drugs.

5.7.1 Complexes of water soluble drugs in hydrogel

The investigated systems were composed of water soluble drug (flucloxacilline and fluoresceine), cyclodextrin (α, β and γ) and cross-linked polymer (PEGDA 2000 and PEGDA 450). The networks were let to swell in drug-CD complex solutions. The aim was to find out the effect of cyclodextrins on drug diffusion and therefore on drug release from a cross-linked polymer matrix.

The ^{1}H NMR spectra of a mixture PEGDA/CD/drug/D_2O (four-component system) are presented in Fig. 5.27 and 5.28. These figures show the effect on the proton spectra of flucloxacilline when α cyclodextrin is added to the PEGDA 2000 hydrogel. Figures 5.27a and 5.27c present the same spectra as in figures 5.9a and 5.9c, i.e. flucloxacilline in water and flucloxacilline in swollen PEGDA 2000 matrix, respectively. Comparison of the spectra 5.27b and 5.27d reveals that the peaks of the drug in the water phase of the two-phase systems after addition of cyclodextrin are at the same chemical shift as the corresponding resonances in the drug-CD complex solution. This indicates that the drug molecules which are present in the water phase in the four-component mixture are complexed with CD molecules. Upon comparison of the spectra in Fig. 5.27c (drug + PEGDA 2000) and in Fig. 5.27d (drug + CD + PEGDA 2000), the same pattern is

observed: each drug multiplet representing the drug in the water phase (Fig. 5.27c) or the drug-CD complex in the water phase (Fig. 5.27 d) is accompanied by a broadened line at the low field side.

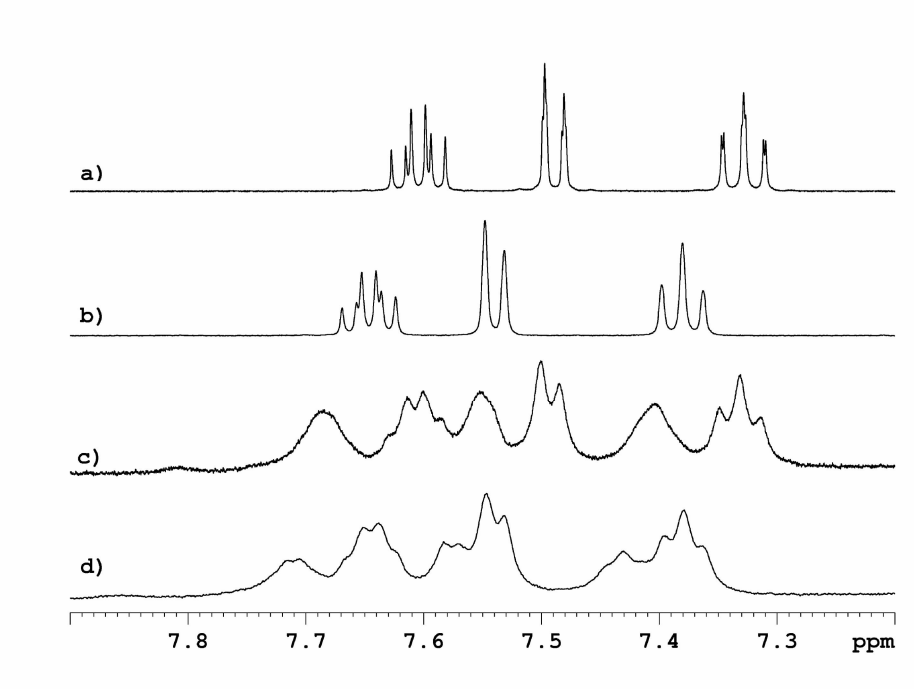

Fig. 5.27: The aromatic region of the ^{1}H spectrum of flucloxacilline in water (a), in water plus α-CD (b), in PEGDA 2000 plus water (c), and in the mixture water, α-CD and PEGDA 2000 (d).

It can be clearly seen that the corresponding broad lines in Fig. 5.27c and 5.27d do not have the same chemical shift. While chemical shift of the drug in the gel phase of swollen PEGDA matrix is affected by the presence of cyclodextrin, we conclude that the drug-CD complex in the case of Fig. 5.27d is (at least partly) absorbed in the PEGDA 2000 gel network. The complex is therefore found both in the water and in the gel phase and it is in a similar way as the drug alone, partitioned between the two phases of the four-component system.

In Fig. 5.28c and 5.28d the α-CD lines in the 2.6-4.1 ppm spectral region are presented, in addition to the broad polymer line and a flucloxacilline CH_3 resonance. The figure shows that the widths of the α-CD resonances are affected by the presence of the

network. The chemical shift of cyclodextrin resonances in the presence of polymer remained unchanged with respect to cyclodextrin resonances in D_2O solution. This is different for the drug, which has in the gel phase a chemical shift that differs from the drug shifts in the gel in the absence of CD. Therefore, the drug-CD complex is located in the gel, but the CD resonances are not affected by the gel. We will explain this in the next chapter. The fact that the resonances of flucloxacilline in the PEGDA network change when cyclodextrin is added is also shown in this figure by the high-field flucloxacilline line.

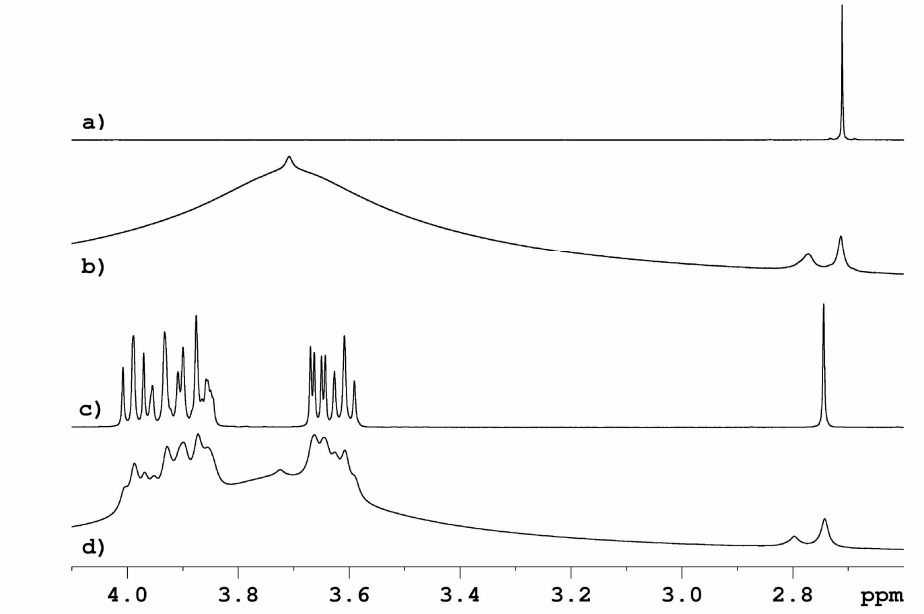

Fig. 5.28: The 2.6-4.1 ppm region of the ^1H spectrum of flucloxacilline in water (a), of the mixture flucloxacilline, PEGDA 2000 plus water (b), of flucloxacilline in water plus α-CD (c), and of mixture flucloxacilline, water, α-CD, and PEGDA 2000 (d).

In the same way as before the self-diffusion coefficients of drug and CD molecules in the PEGDA matrix can be determined. PFGE NMR diffusion measurements show that in the PEGDA 2000 matrix, α and β cyclodextrins have two components with different diffusivities. The component with higher diffusion coefficient corresponds to the complexed CD molecules in the water phase and the slower component corresponds

to the cyclodextrins in the hydrogel phase of a swollen polymer. In the systems with PEGDA 450 polymer only the fast cyclodextrin component is found. This can be explained by the small mesh size of the PEGDA 450 matrix which disables CD molecules to come into the gel phase. The drug-CD complexes due to their molecular size are not in all drug/cyclodextrin/PEGDA combinations absorbed by the gel. PEGDA 450 does not absorb any of the complexes. Also complexes with γ-CD are not absorbed by the PEGDA 2000 gel. The results of diffusion measurements in the swollen matrices are shown in the Table 5.7. Only those drug/CD/PEGDA combinations are shown for which the complexes are partitioned between the two phases.

Table 5.7 Drug self-diffusion coefficients (in 10^{-10} m^2s^{-1}) in the presence of cyclodextrins in the water phase and in the gel phase of PEGDA 2000.

system	CD	D_{drug}^{water}	D_{drug}^{gel}
Flucloxacilline	no CD	3.6	0.4
	with α-CD	2.9	0.5
	with β-CD	3.1	0.6
system	CD	D_{drug}^{water}	D_{drug}^{gel}
fluoresceine	no CD	3.2	0.5
	with α-CD		
	with β-CD	2.8	0.5

In the case when the polymer matrix is swollen in drug complex solution with γ cyclodextrin an interesting feature is observed. Fig. 5.29 shows the proton NMR spectra of PEGDA 2000 matrix, in one case swollen in flucloxacilline solution and in the other case swollen in the solution of γ-CD/flucloxacilline complex. From the figure it can be seen that in the presence of γ-CD the drug resonances in the gel phase become significantly smaller and hard to observe. Because of its big molecular size the drug complex with γ cyclodextrin can not be absorbed by the PEGDA 2000 gel. The chemical shift of the drug in the gel did not change by addition of cyclodextrin, which confirmed

that in this case complexes are not present in the hydrogel. The drug resonances from the water phase, as expected, are shifted due to complexation with γ-CD.

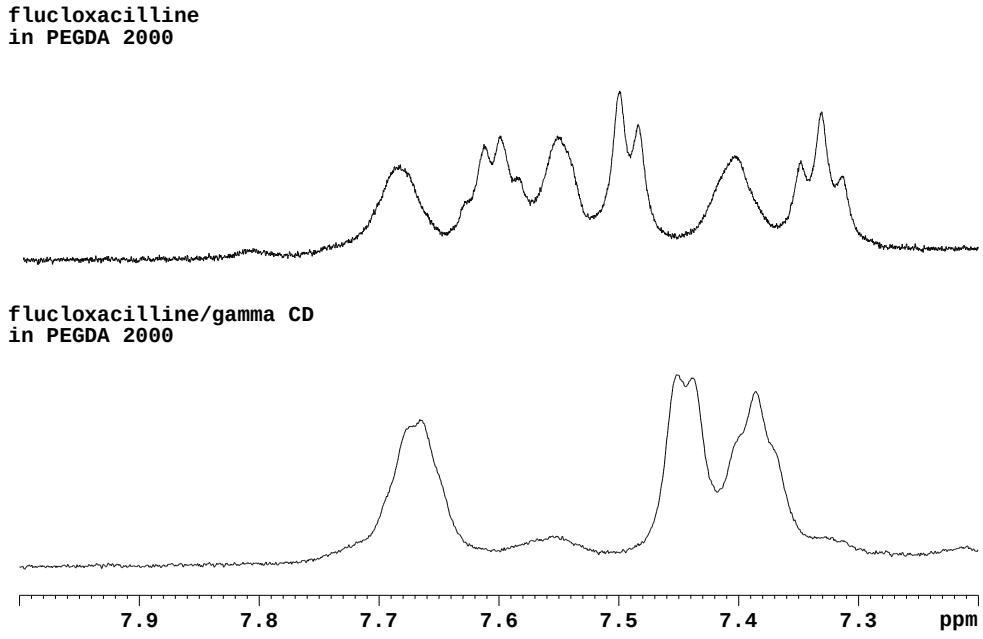

Fig. 5.29: Comparison of the ^{1}H NMR spectra of PEGDA 2000 matrix swollen in flucloxacilline solution and in flucloxacilline-gamma CD complex solution.

Diffusion measurements in water for this combination of drug and cyclodextrin in the complex (Table 5.6) have shown that drug and CD diffusion coefficients do not differ much. That means that the drug residence time in the complex with γ cyclodextrin is much longer than in the complex with α or β cyclodextrin. Because the drugs are for most of the time complexed in the gamma-CD complex and the complex is not taken up by the gel, much less amount of the drug is present in the gel phase. That explains the significant decrease of intensity of drug population in the gel in the presence of gamma cyclodextrin.

It was expected that the diffusion of a drug in a gel would slow down when the drug complexes with a host molecule, because of the bigger mass and size of the complex. However, inspection of Table 5.7 shows that this is not the case. In order to conclude what happens in the presence of cyclodextrins, the relative diffusion coefficients of flucloxacilline are calculated with and without CDs and presented versus

the polymer mesh size (Fig. 5.30). When the complex is not present in the hydrogel, the drug diffusion remained unchanged as for the PEGDA 450 polymer.

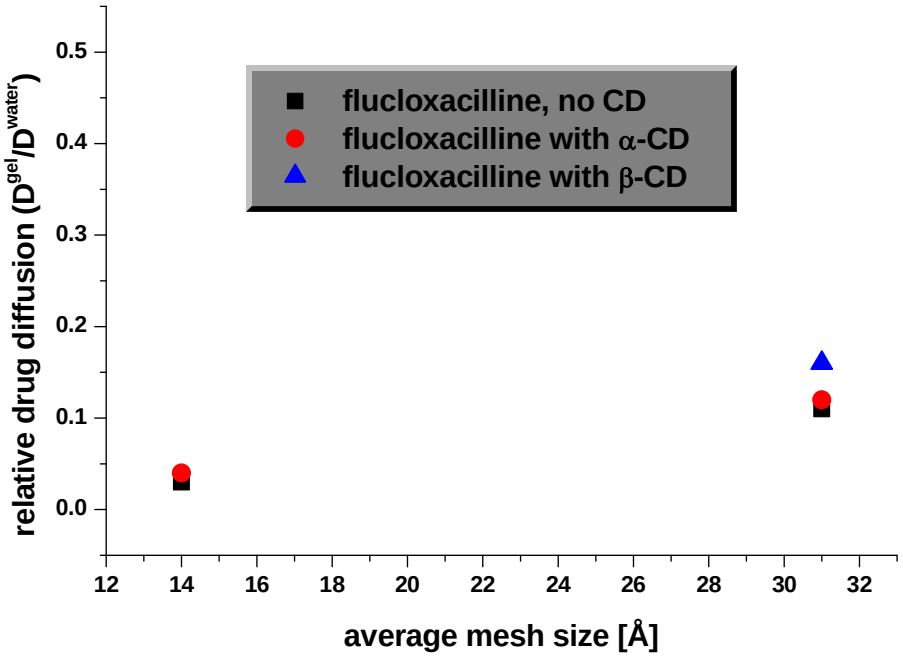

Fig. 5.30: Dependence of the relative flucloxacilline diffusion coefficients in the presence of cyclodextrins on the polymer mesh size. The temperature averaged values are shown.

When the complexes are partitioned between the two phases, in some cases drug diffusion is not significantly affected by cyclodextrins, but in some cases drug diffusion in the gel was even faster than without complexation. The explanation for this kind of behavior will be provided in Chapter 6, where the models for diffusion in the gel are presented.

5.7.2 Complex of water insoluble drug in hydrogel

The ability of cyclodextrins to complex water insoluble drug led to the idea that in this way a solution can be provided for introduction of drug molecules with poor water solubility into the hydrogel. Indeed, the complexation with β cyclodextrin enabled to

study the behavior of practically water insoluble ibuprofen in the swollen PEGDA 2000 network. The matrix was swollen in a D_2O solution of the drug complexed with β-CD. The proton NMR spectra shown in Fig. 5.31 present the complexation of ibuprofen with β-CD in D_2O (Fig. 5.31a) and the behavior of the complex in the polymer network (Fig. 5.31b).

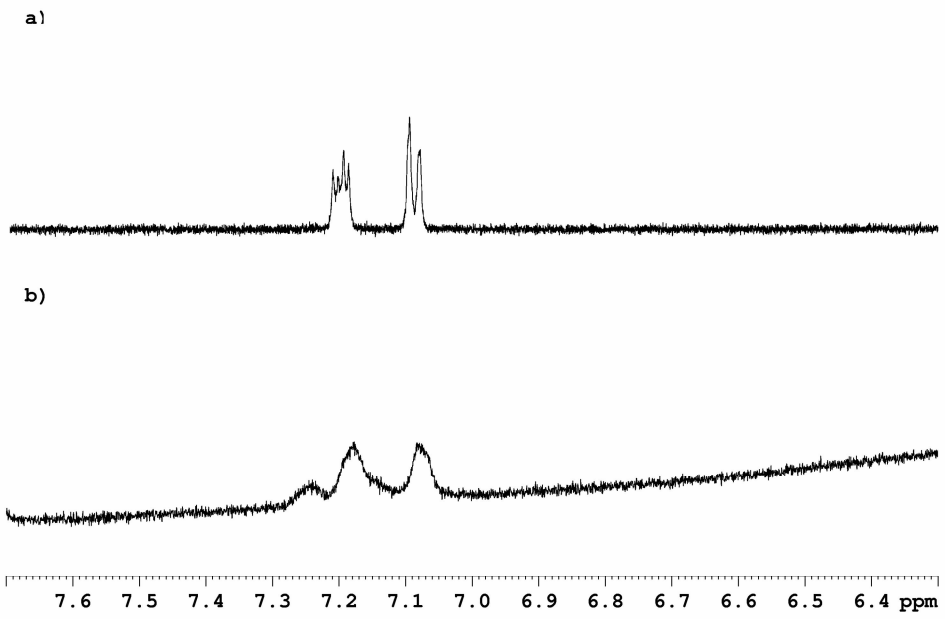

Fig. 5.31: The aromatic region of the ^1H spectrum of ibuprofen in the complex with β-CD in D_2O (a) and in the complex with β-CD in the swollen PEGDA 2000 matrix

In figure 5.31b it can be observed that beside the (broadened) resonances corresponding to the drug-CD complex in the water phase there are additional peaks, similarly as for the water soluble drugs. They arise from the drug population which is in the complexed form present in the hydrogel. The CD complexes of ibuprofen are also partitioned between the water and the gel phase.

Diffusion measurements on ibuprofen have shown that two components with different diffusivities exist. The faster component represents the drug population in the complex

with β-CD in the water phase and its diffusion coefficients is $D_{drug}^{water} = 2.61 \cdot 10^{-10} m^2 / s$. The second component represents ibuprofen population in the gel phase with the diffusion coefficient $D_{drug}^{gel} = 0.47 \cdot 10^{-10} m^2 / s$. The presence of the drug-CD complex in the gel creates the possibility to control the ibuprofen diffusion and the release of the drug from the gel. Also the chemical shift of ibuprofen is affected by the gel, which means that the drug is not 100% of the time bound to the CD.

Encapsulation by cyclodextrins opens a possibility to increase the solubility of insoluble drugs in hydrogel drug carriers. This is very important for practical applications because many important therapeutic drug molecules are poorly soluble in water. Just as in the case of soluble drugs, by changing the cross-link density of the polymer matrix the release rate from this matrix can be tuned. Such formulations could bring improvements in the delivery of drugs.

Chapter 6: Models describing the behavior of a drug in a gel matrix

In this section a model describing the drug mobility in the gel and the drug-matrix interaction is presented. The proposed model is primarily based on two sets of experimental data: chemical shift and self-diffusion data. Also, an explanation for the values of activation energies as well as for the drug interaction with the matrix in the presence of cyclodextrins is provided.

6.1 A model for the drug-matrix interaction

Various models for the description of diffusion of small molecules in polymer gels have been developed as explained in the Section 2.2.2[33]. In lattice models the diffusing molecule jumps between unoccupied lattice sites. The lattice sites which are occupied by the polymer chains represent obstructions for the drug diffusion and are not available for the diffusing molecules. Then, according to Mackie and Meares[35], the diffusion coefficient of a (small) molecule in a gel is a function of the volume fraction υ_2 occupied by the polymer in the gel (see eq. 2.32).

Higher cross-linked polymer networks absorb less water and thus the polymer volume fraction, υ_2, becomes larger. The polymer volume fraction in the gel υ_2 has been estimated for the three networks studied here, using the swelling factors reported in the previous section. The value of $((1-\upsilon_2)/(1+\upsilon_2))^2$ (eq. 2.32) is shown in the last column of Table 5.4. Comparison of this lattice model factor with the experimental diffusion coefficients shows the expected trend, the larger the volume fraction υ_2, the smaller the diffusion coefficients of the drugs and of water molecules. However, this lattice model description can not be entirely correct because it predicts for the same network an equal decrease of the diffusion coefficient for drug molecules and for water, which is clearly not the case (Tab. 5.4). Also we know from the chemical shifts $\delta_{drug}^{gel} - \delta_{drug}^{water}$ of Table 5.2 that the drug molecules (and water) must interact in some way with the network. In all lattice models the interaction between the diffusing molecule and the polymer matrix is described as between hard spheres.

The model proposed here is completely analogous to the ligand-macromolecule situation encountered so often for biomacromolecules[84]. It assumes that in the hydrogel phase the drug molecules are on average for a certain fraction of the time λ “bound” to

the polymer network and immobilized in the bound state. For the rest of the time drug molecules diffuse more or less freely in the water of the hydrogel phase, although hindered by the fact that part of the space in the gel is taken up by the polymer chains (Fig. 6.1).

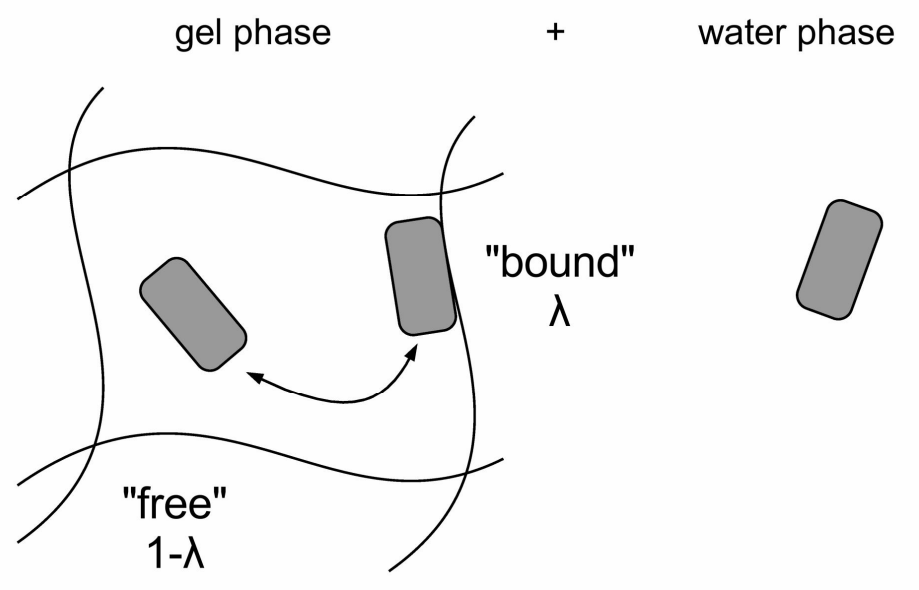

Fig. 6.1: Schematic representation of the drug diffusion model with two separated phases: (left) the hydrogel phase, (right) the water phase. The drug molecules are shown as rounded rectangles. In the gel phase the drug and water molecules (not shown) both exchange between a “bound” and a “free” state.

The meaning of “bound” should not be taken too literally. The model simply assumes that the gel water volume can be divided in a volume in which the drug molecule does not interact with the polymer and a volume in which the drug is under the influence of the polymer chains. The exchange between these two states of the solute molecules must be fast on the NMR time scale because one NMR signal and one diffusion coefficient for the drug population in the hydrogel phase is observed. The self-diffusion coefficient and chemical shift of the drug molecule in the hydrogel are then weighed averages of two diffusion coefficients, respectively, two chemical shifts:

$$D_{drug}^{gel} = \lambda \cdot D_{drug}^{bound} + (1-\lambda) \cdot D_{drug}^{free} \quad (6.2)$$

$$\delta_{drug}^{gel} = \lambda \cdot \delta_{drug}^{bound} + (1-\lambda) \cdot \delta_{drug}^{free} \quad (6.3)$$

where λ represents the fraction of the time (0<λ<1) the drug molecule is bound to the network, D_{drug}^{bound} and D_{drug}^{free} the drug diffusion coefficients of the drug in the bound state and moving in the gel water, respectively. In the same way δ_{drug}^{bound} and δ_{drug}^{free} are defined. The two equations (6.2) and (6.3) can be solved for λ and δ_{drug}^{bound}, if we make the following logical assumptions:

(a) $D_{drug}^{bound} = 0$ (the drug is immobilized during the time it is bound to the network)

(b) $D_{drug}^{free} = D_{drug}^{water} \cdot \left((1-\upsilon_2)/(1+\upsilon_2)\right)^2$ (due to obstruction by the network the diffusion is slower than in water, eq. 6.1)

(c) $\delta_{drug}^{free} = \delta_{drug}^{water}$

The values for D_{drug}^{water}, D_{drug}^{gel}, and $\delta_{drug}^{gel} - \delta_{drug}^{water}$ were measured. The results of the calculations are shown in Table 6.1. The parameter λ is found to be practically independent of the temperature for the investigated temperature range (vide infra) but clearly increases with the network density. In the PEGDA 450 matrix, λ approaches 1 for all three drugs. Unfortunately the $\delta_{drug}^{bound} - \delta_{drug}^{free}$ values can not be compared between different drugs, therefore from these data it can not be concluded that flucloxacilline interacts stronger with the network than proxyphylline.

It should be emphasized here that λ, the fraction of the time the drug molecule is bound to the polymer network, mainly depends on the amount of water absorbed by the hydrogel phase. The larger the amount of hydrogel water, the larger the water volume in which the drug moves independent of the network chains and the smaller the λ. Therefore λ increases with the cross-link density of the network. When λ only depends on the swelling factor, this also explains why λ is practically independent of the temperature over the temperature range 12-37 ^{0}C for all investigated drug-polymer combinations. The

swelling curve in the phase diagram for such systems (see figure 2.7) is almost parallel to the temperature axis[27].

Table 6.1 Experimental and calculated parameters for the exchange model of drug binding to the matrix; for all three drugs chemical shift values refer to aromatic protons.

System	$\delta_{drug}^{gel} - \delta_{drug}^{free}$ in ppm from experiment	λ	$\delta_{drug}^{bound} - \delta_{drug}^{free}$ in ppm calculated from eq.(6.3)
Proxyphylline			
PEGDA 4000	0.020	0.30	0.067
PEGDA 2000	0.033	0.51	0.065
PEGDA 450	0.040	0.77	0.052
Fluoresceine			
PEGDA 4000	0.081	0.30	0.27
PEGDA 2000	0.132	0.66	0.20
PEGDA 450	0.166	0.92	0.18
Flucloxacilline			
PEGDA 4000	0.046	0.40	0.11
PEGDA 2000	0.070	0.81	0.09
PEGDA 450	0.101	0.94	0.11

For the highest cross-link density, in sample PEGDA 450 with approximate mesh size of 14 Å, the drug molecules can be considered to be almost always within the water volume near the network chains. It should be realized however, that the relatively narrow line width (compared to the "rigid" line width) of the NMR lines of the drug in the gel shows that in the gel the drug molecules are still free to rotate, even in the highest cross-linked system, PEGDA 450. The interaction between drug and polymer network must be very weak, as is also shown by the value of $\delta_{drug}^{bound} - \delta_{drug}^{free}$ in Table 6.1, which is of the order of 0.1 ppm only. The drug molecules must be bound to the polymer by weak Van der Waals interactions.

6.2 Activation energies

The activation energies for diffusion of water and of drugs are all of the same order of magnitude (15-20 kJ/mol), both for the diffusion in the hydrogel phase as for the

diffusion in water phase. Their values are comparable to the hydrogen bonding energy of water. It seems that the barrier for diffusion for a molecule in water-rich systems is mainly determined by the interaction with water molecules. The similar conclusion was reached by Gao and Fagerness[90] for drug diffusion in hydroxypropyl methylcellulose gels.

The fact that the activation energies for the drug diffusion in the gel phase are so close to those of the drug in the water phase can be explained with equation 6.2. Taking into account that we find that λ is practically temperature independent (steep swelling curve in the phase diagram of fig. 2.7), the temperature dependence of the drug diffusivity in the gel is determined solely by the dependence of the diffusivity of the drug in the water. This explains also the independence of the activation energy on the polymer cross-link density.

6.3 Extension of the model in the presence of cyclodextrin

It was expected that the diffusion of a drug in a gel would slow down when the drug complexes with a host molecule, because of the bigger mass and size of the complex. Quaglia et al.[91], for instance, have found that complexation of nicardipine with β-CD decreases the drug diffusivity in a cross-linked PEG matrix. Inspection of Table 5.7 shows that in our case the complexation with cyclodextrins does not slow down the drug diffusion in the gel. For instance, for flucloxacilline $D_{drug}^{gel} = 0.4 \cdot 10^{-10} m^2 s^{-1}$ in the absence of CD and $D_{drug}^{gel} = 0.5 \cdot 10^{-10} m^2 s^{-1}$ with α-CD.

This surprising result can be explained by extending our model. It was mentioned in Chapter 5 that the CD resonances do not change when the polymer swells in the solution of a drug-CD complex. On the other hand, the drug resonances in the gel are affected by the presence of cyclodextrins which means that the drug-CD complex is located in the gel phase. That is also confirmed by the existence of two CD fractions with different diffusivities. Therefore, the cyclodextrins are present in the hydrogel in the complexed form, but they themselves do not interact with the polymer matrix and that is why their resonances are not shifted.

We can now extend our previous model in that we assume that flucloxacilline in the PEGDA gel network can exchange between *three* sites, flucloxacilline free in the gel water, flucloxacilline in the complex with α-CD in the gel water and flucloxacilline bound to the network chains. The flucloxacilline self-diffusion coefficient can then be written as:

$$D_{drug}^{gel} = \lambda \cdot D_{drug}^{bound} + \mu \cdot D_{drug}^{complex} + (1 - \lambda - \mu) \cdot D_{drug}^{free} \qquad (6.4)$$

where λ and μ are the fractions of time the drug spends in the bound state and in the complex, respectively. This equation contains too many unknowns to solve for coefficients λ and μ, as we did before with equation 6.2. But it is easy to see from eq. 6.4 that depending on the values of λ and μ, there can be situations where complexation with a host molecule even increases the drug diffusion rate, for instance when due to presence of the diffusing complex the fraction of the time the drug is "bound" to the polymer (coefficient λ) is decreased. The behavior of the drug when drug-CD complex is present in the gel phase is shown in Fig. 6.2. Instead of being immobilized by the network for a sizable fraction of the time the drug is then able to move for a larger fraction of the time. Complexation of a drug molecule to CD therefore does not necessarily slow down the drug diffusion in the matrix.

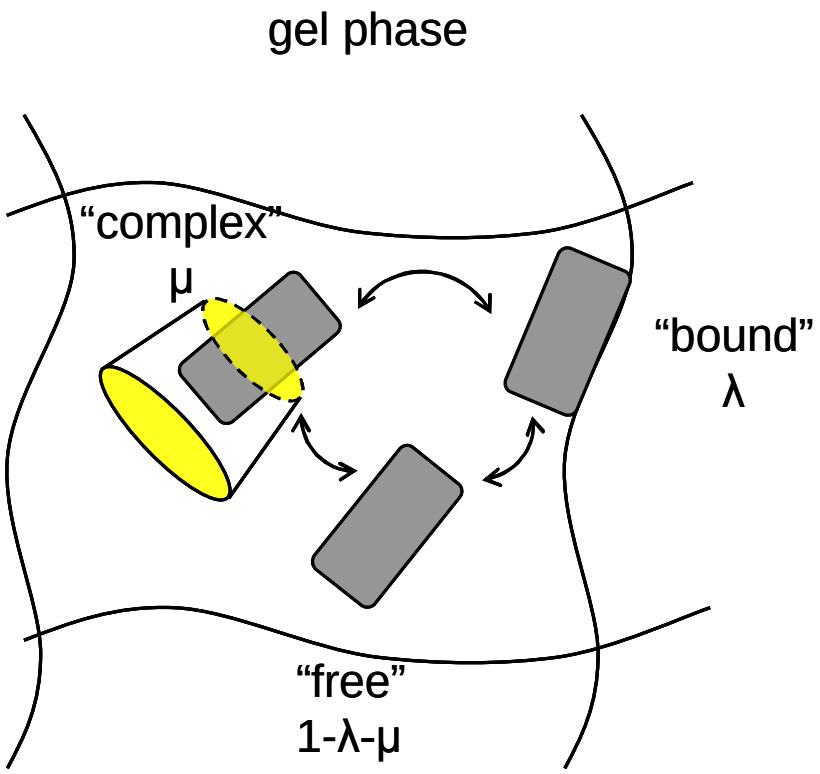

Fig. 6.2: Schematic representation of the drug diffusion model in the presence of cyclodextrins. The gel phase is shown with drug molecules presented as rounded rectangles. In the gel phase the drug molecules exchange between three sites.

Chapter 7: A novel drug delivery system for the drug amiodarone without polymer matrix

7.1 Introduction

Amiodarone is a very important drug molecule for the treatment of heart diseases such as arrhythmia and hypertension. Due to its poor solubility in water it is very difficult to make a water-based delivery system with a sufficient concentration of this drug. It is of great importance to overcome these limitations and to increase the availability of amiodarone to the human body. Our idea was to increase the water solubility of this drug by complexation to cyclodextrin. In that way the water solubility of the drug would be increased. Because drug-CD complexes can be absorbed by PEGDA matrices (as shown previously) in this way amiodarone would be introduced into a hydrogel drug delivery system. By changing the cross-link density of the polymer matrix, it would be possible to control the drug diffusion in the gel and to tune the drug release rate from the matrix. The same procedure was applied to the water insoluble drug ibuprofen and allowed to introduce ibuprofen in the PEGDA hydrogel (Chapter 5).

However during preparation of the amiodarone complex with γ-cyclodextrin, a completely different behavior of this drug is observed than in the case of ibuprofen. When mixing certain amounts of amiodarone and γ-CD at room temperature it was found that the viscosity of the solution is significantly increased, as can visually be detected from the mixture in the glass tube. The drug-CD mixture (in the absence of the polymer matrix) exhibits a behavior which seems to be not liquid-like. This striking feature of the amiodarone/γ-CD formulation has driven us to further investigate this system.

7.2 Experimental results

When the proton NMR spectrum of the amiodarone/γ-CD mixture in water is measured at room temperature (Fig. 7.1), it can be observed that the drug lines of the water insoluble amiodarone are present in the spectrum which shows that the drug solubility in the water has been increased via complexation with CD. Otherwise the drug resonances would not be detectable. Inspection of the spectrum also reveals that the CD lines (proton lines in the range between 3-4.5 ppm as well as the OH group of

cyclodextrin at ca 5.1 ppm) become strongly broadened. The narrow lines on the top of the broad CD lines arise from overlapping drug lines in the same spectral region.

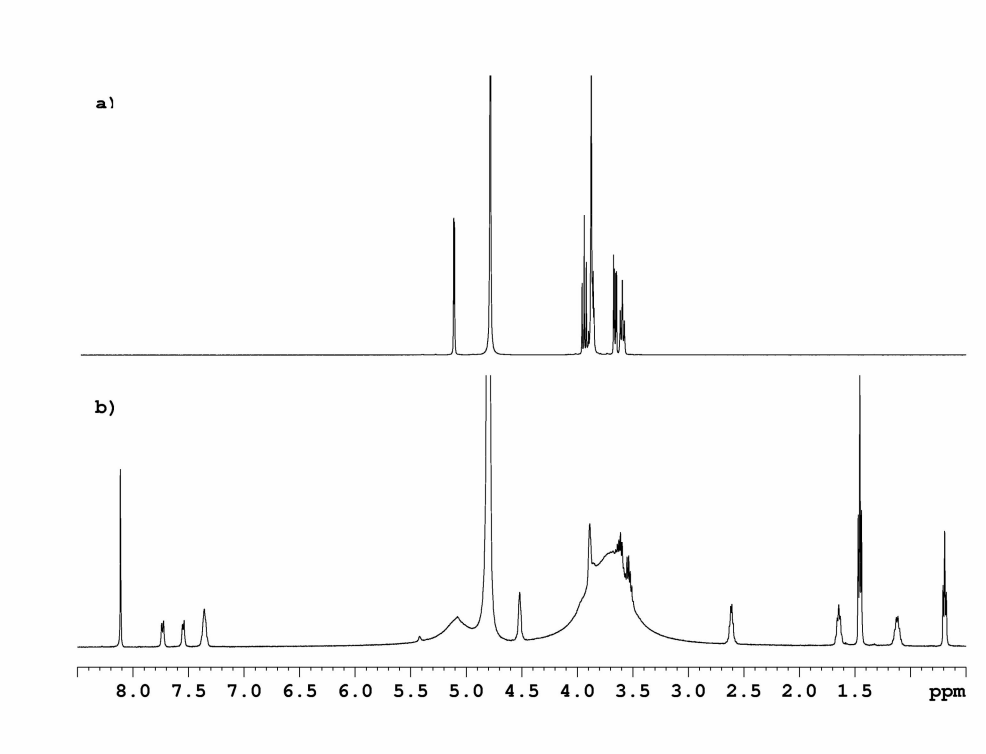

Fig. 7.1: The proton NMR spectra of γ-CD in D_2O (a) and amiodarone/γ-CD mixture in D_2O (b).

Fig. 7.2 shows the ^1H NMR spectra of the amiodarone/γ-CD system at different temperatures in the temperature range between 25 and 75 ^0C. With increasing temperature both the broad lines of cyclodextrin and the drug lines become narrower. Above ca 45 ^0C the lines are as narrow as from a solution of small molecules. Also it was observed that this narrowing of the lines with increasing temperature is reversible. When the sample is cooled down to the room temperature, the resonances get broad again.

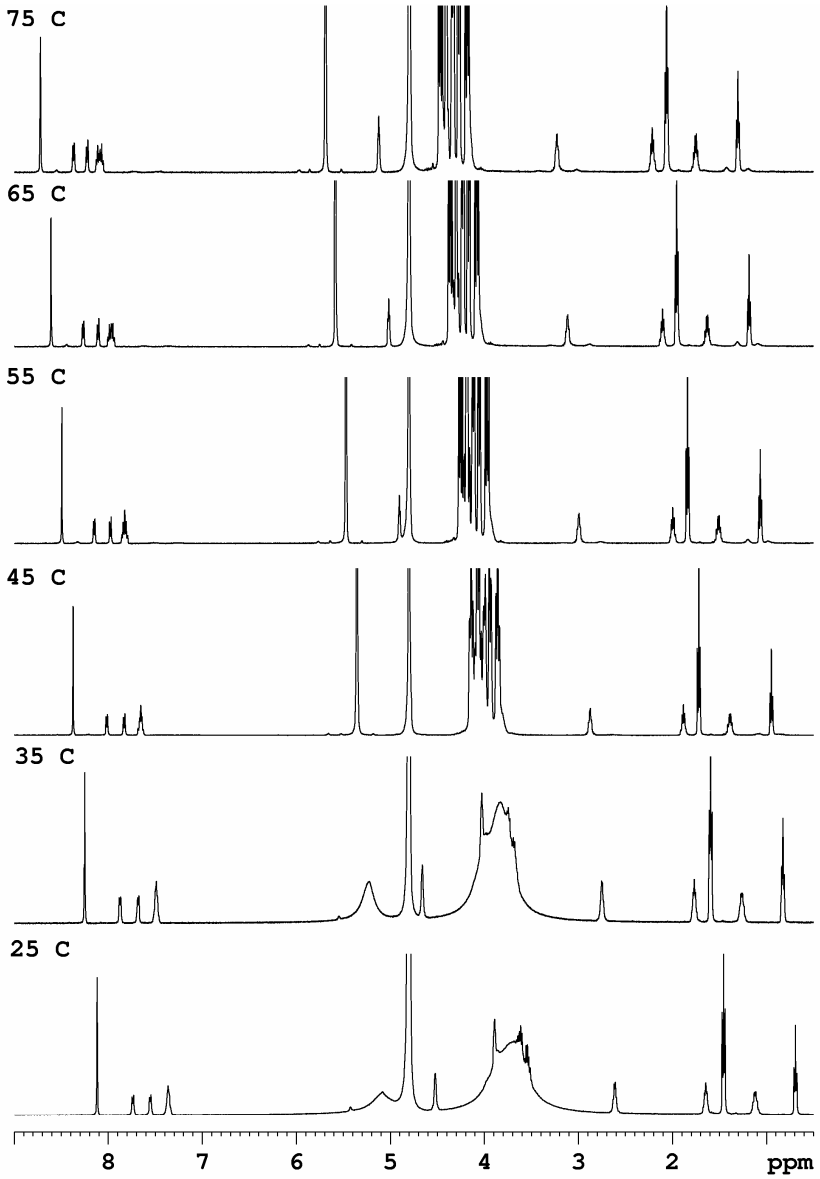

Fig. 7.2: Temperature dependence of the ^{1}H NMR spectrum of the amiodarone/γ-CD mixture in D_2O. The temperature was varied from 25 to 75 ^{0}C.

When the spectrum of the amiodarone and γ-CD mixture is compared to the spectrum of γ-CD alone at temperatures above 45 ^{0}C, it can be clearly seen that the CD lines in the mixture are significantly shifted upfield relative to the solution of the CD alone in water (Fig. 7.3). That means that although the sample is liquid-like at 65 ^{0}C, the amiodarone and the CD still form an inclusion complex.

Integration of the drug lines as well as the CD lines at different temperatures shows that the intensities of both the drug and CD lines increase significantly with the temperature in the range 25-70 ^{0}C. This means that at room temperature part of the drug and CD is NMR invisible. Therefore there must be at least two fractions of amiodarone/CD complexes. One fraction at room temperature is so rigid, that it can not be observed by our high resolution ("liquid" NMR) experiment. The other fraction with broad CD lines also has a limited rotational mobility but not so much that it escapes NMR detection.

The self-diffusion measurements at room temperature, when the CD lines of the fraction with limited mobility are broad, reveal that the diffusion of the visible drug fraction is extremely slow. The diffusion coefficient of amiodarone at room temperature is $9.55 \cdot 10^{-12}$ m^2s^{-1}, which is even slower than the diffusion of the biggest water soluble drug (flucloxacilline) in the highest cross-linked polymer network (PEGDA 450). The diffusion of the invisible drug fraction can not be determined and is expected to be even slower.

Fig. 7.3 shows the ^{1}H NMR spectra of the drug and γ-CD mixture for different molar fractions of the amiodarone in the system. By increasing the drug concentration in the amiodarone/γ-CD mixture, starting from zero concentration, the cyclodextrin lines become broader up to the point where the molar ratio of the drug and CD is between 1:2 and 1:1. Then the CD line widths remain constant.

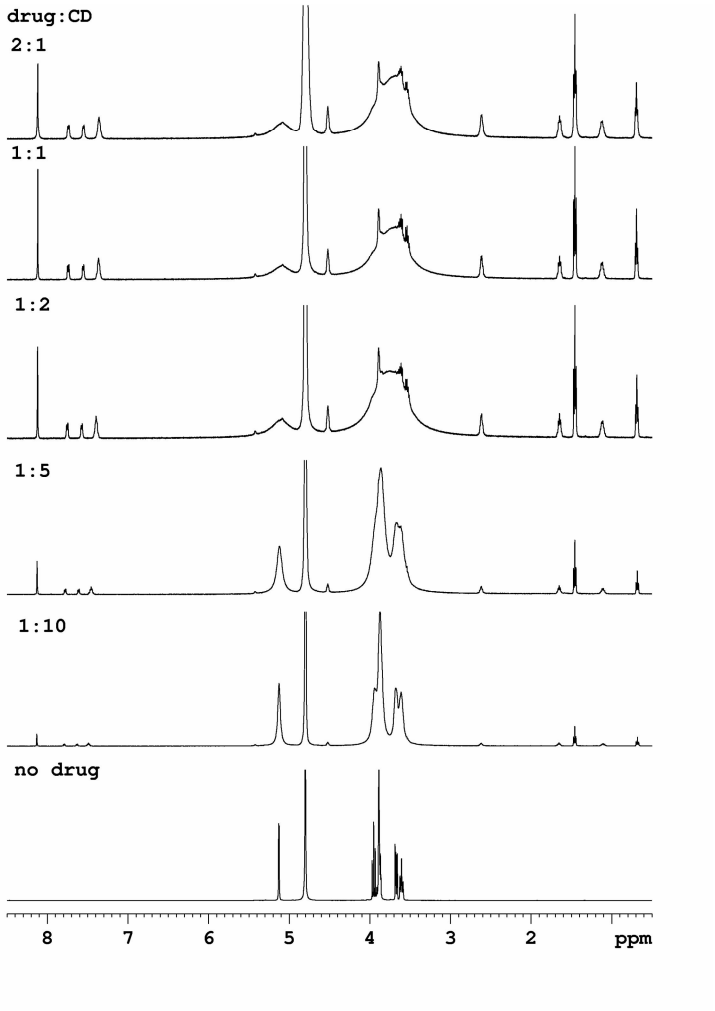

Fig. 7.3: Changes of the ^{1}H NMR spectrum of the amiodarone/γ-CD formulation with increasing the drug:CD molar ratio in the beginning mixture.

The aromatic drug lines shift to higher field up to this point. Measurement of diffusion for different drug concentrations shows that the drug diffusion rate decreases with increasing amount of the drug. From the concentration ratio, where the drug:CD molar ratio is between 1:2 an 1:1, on, the drug diffusion remains constant. These changes of drug diffusion together with the changes of the chemical shift of drug aromatic protons are shown in Fig. 7.4.

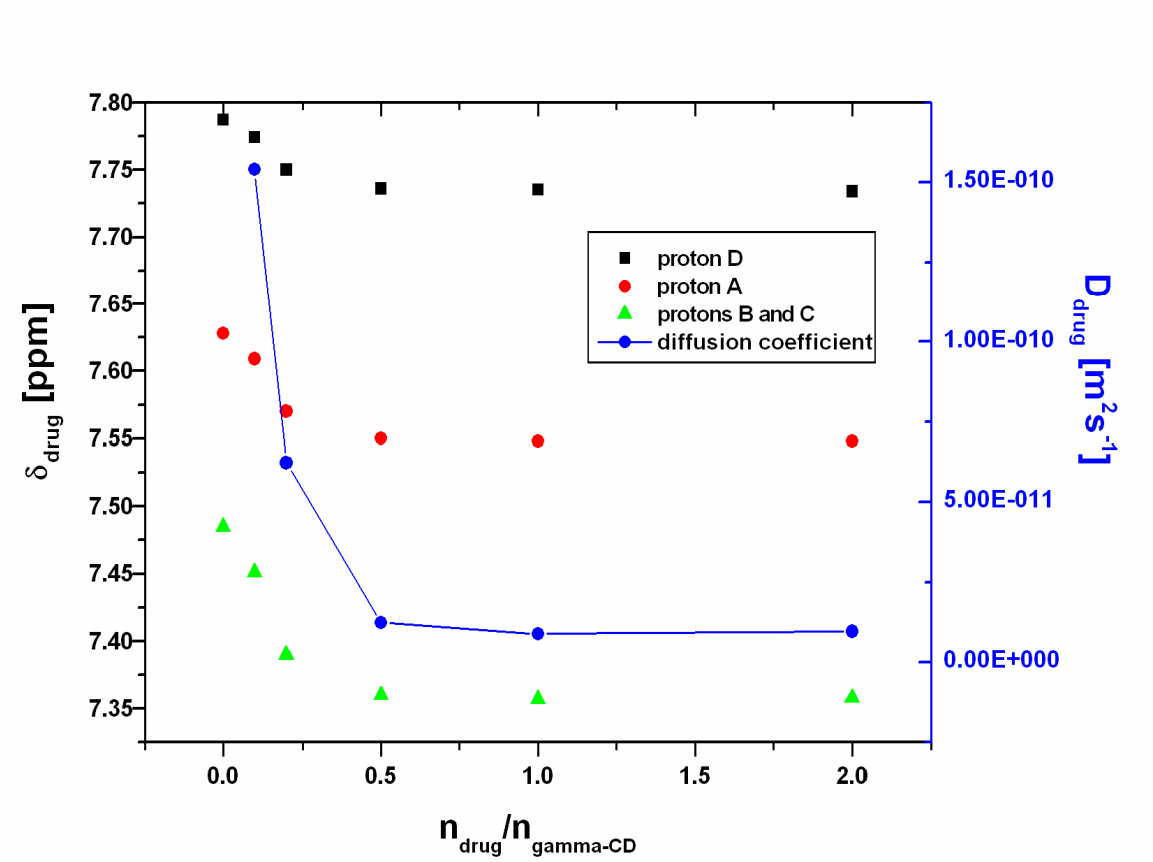

Fig. 7.4: Changes of the chemical shift of three drug aromatic protons and the drug diffusion coefficient with increasing molar fraction of amiodarone in the system. The assignment of the different drug protons is given in the Appendix 9.4.

In order to get better insight into this phenomenon, we investigated how this mixture interacts with polarized light in an optical microscope. Fig. 7.5 shows the microscope images of the sample at different temperatures. The amplification factor was 112. Optical microscopy with polarized light shows that the sample is locally birefringent. At room temperature structures are observed which seem like bundles of fibers. That means that in the mixture locally ordered structures (ordered domains) must exist. By increasing the temperature, the fraction of these ordered domains is decreasing and above 45 ^{0}C the sample does not show the light polarization effects anymore.

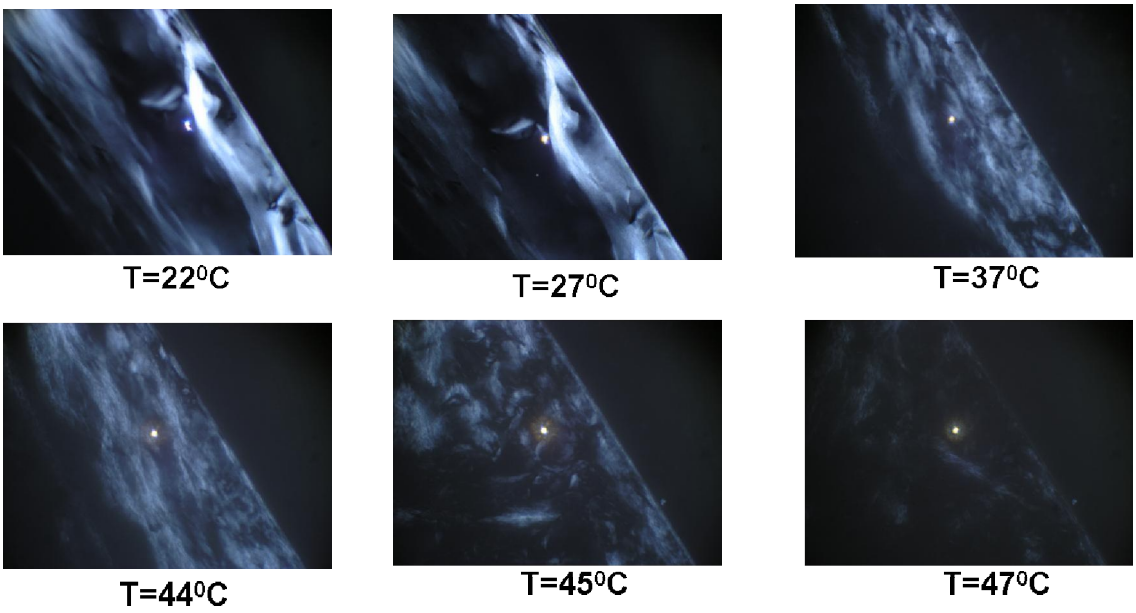

Fig. 7.5: Optical microscopy with polarization light. Images of the amiodarone/γ-CD sample at different temperatures.

It was found also here that after cooling down to the room temperature the ordered structures are again observable.

Intrigued by the presence of liquid-NMR-unobservable drug and CD molecules in the mixture at room temperature a solid state NMR method is applied to attempt to directly detect those rigid components of the amiodarone/γ-CD mixture. Fig. 7.6 shows the ^{13}C CPMAS spectra of solid γ-cyclodextrin and the formulation of amiodarone/γ-CD. In the mixture the resonances of γ-cyclodextrin are clearly observed (60-120 ppm) showing that cyclodextrin is part of the rigid domains in the sample. The drug molecules are hardly observed by the CPMAS method which shows that they must be relatively mobile.

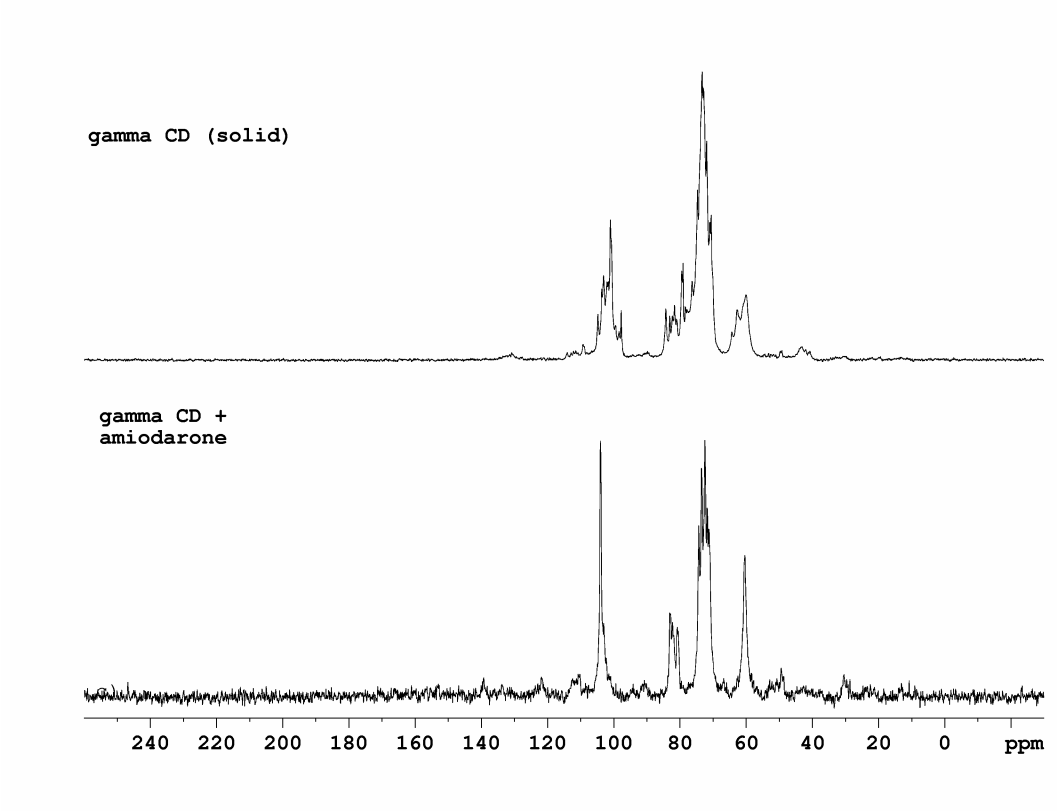

Fig. 7.6: ^{13}C CPMAS spectra of the γ-cyclodextrin powder and the amiodarone/γ-CD mixture (drug/CD molar ratio in the initial mixture is 2:1, T=28 ^{0}C).

By increasing the temperature the intensity of the γ-CD resonances slowly decreases. Fig. 7.7 presents CPMAS spectra of the sample at different temperatures. The supramolecular structures gradually disappear when the temperature is increasing up to 70 ^{0}C.

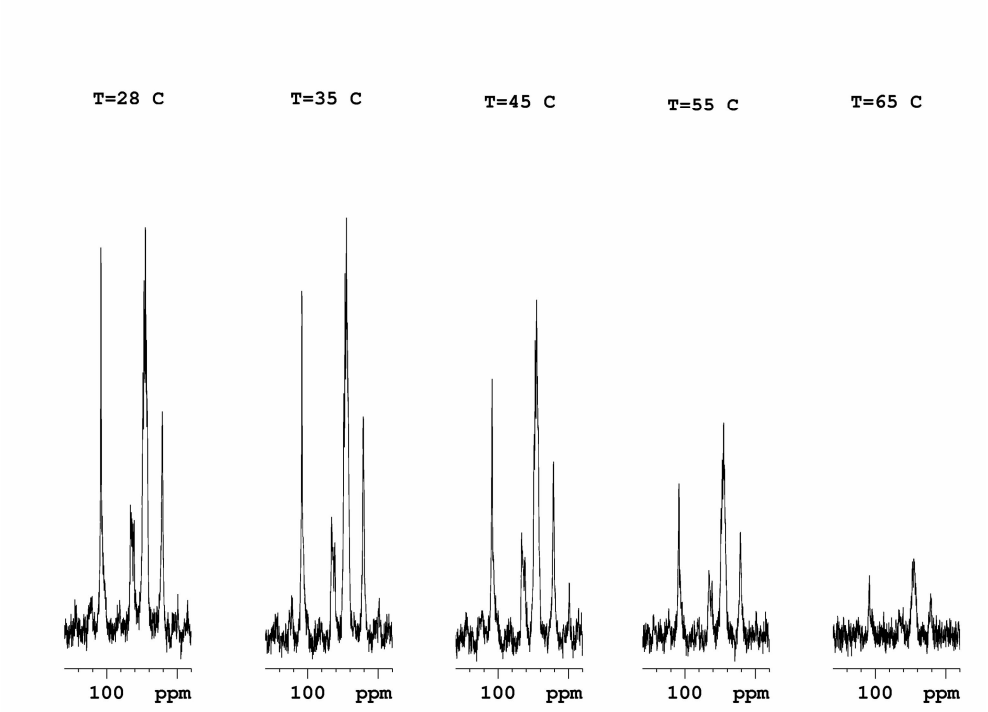

Fig. 7.7: ^{13}C CPMAS spectra of the amiodarone/γ-CD mixture at different temperatures in the range from 28 to 65 C.

A very interesting feature is observed when to the amiodarone/γ-CD formulation another drug is added which possesses the property to build an inclusion compound with γ-cyclodextrin. For example, by addition of flucloxacilline the previously high-viscosity solution becomes very fast a low viscosity liquid. The broad CD lines become narrow and the amiodarone lines can not be observed anymore in the NMR spectrum (Fig. 7.8). The same effect occurs when fluoresceine, which is also able to form inclusion complex with γ-CD, is added. These drugs compete for the cyclodextrin binding and apparently are able to destroy the existing structure with amiodarone and γ-cyclodextrin.

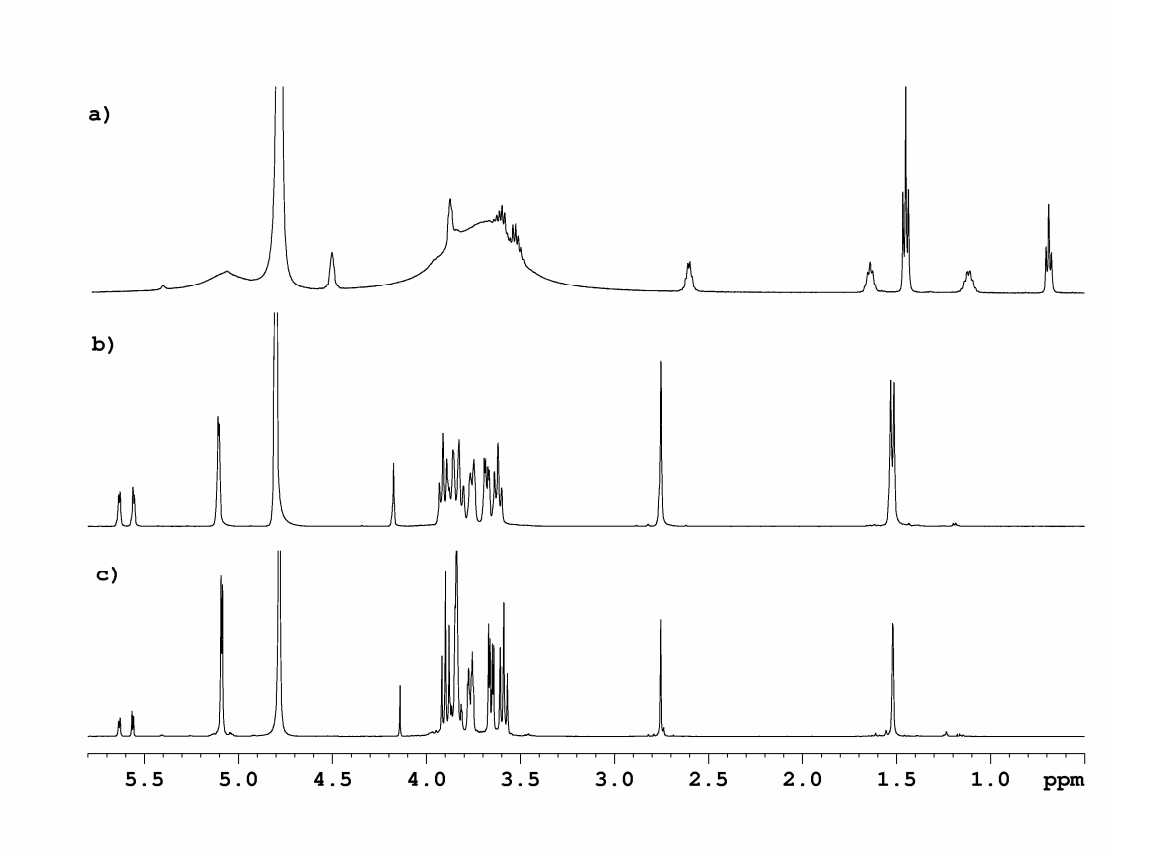

Fig. 7.8: ^{1}H NMR spectra of the amiodarone/γ-CD mixture (a), the same mixture after addition of flucloxacilline (b) and the flucloxacilline/γ-CD complex solution (c).

For a structural elucidation valuable information can be obtained by modeling the interaction between amiodarone and γ-cyclodextrin. The modeling was performed by Dr. B. Coussens from DSM Research. Computations are done using software programs from Accelrys. Dynamics and energy minimizations are performed with MS.Forcite using the COMPASS forcefield. Graphical displays are generated with Materials Studio. The results are shown in the Fig. 7.9. The figure is a minimized structure (minimal energy) using modeling and it shows three cone-shaped CD molecules and two amiodarone molecules. Each drug molecule interacts with two cyclodextrins. The figure indicates that by continuing this pattern, the formation of a chain of CD molecules, held together by amiodarone molecules, seems possible.

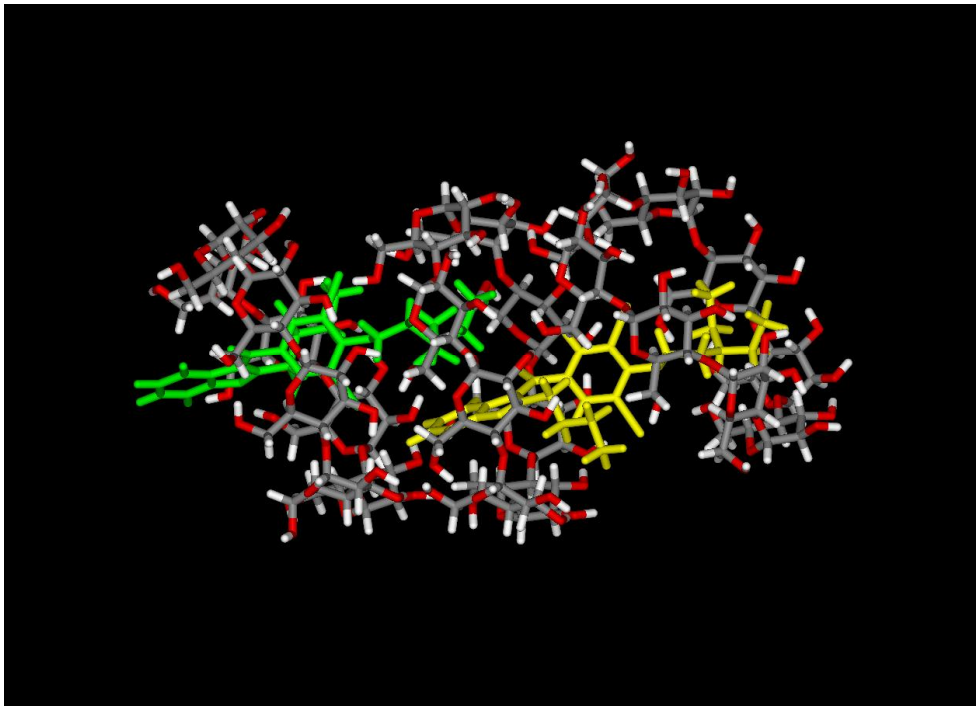

Fig. 7.9: Optimized structure by molecular modeling of the amidarone-γ-CD interactions.

7.3 Discussion

In this chapter we showed that by mixing amiodarone and γ-cyclodextrin at room temperature at a molar ratio somewhere between 1:2 and 1:1 a highly viscous liquid is obtained.

The NMR experiments show that:

a. a fraction of the drug and CD molecules in the mixture is at room temperature NMR invisible by liquid NMR;
b. the CD molecules in that fraction are detectable by solid state NMR;
c. the diffusion of the drug molecules, measured via liquid NMR techniques, is even slower than that of the largest drug molecule in the most cross-linked PEGDA matrix;
d. by increasing the temperature the liquid-NMR-invisible fraction *gradually* decreases till at 70 ^{0}C the rigid fraction has disappeared. At that temperature amiodarone/CD complexes still exist;

e. the optical polarized microscopy images show that the mixture at room temperature is locally birefringent. This birefringence *suddenly* disappears at 45 ^{0}C.

Combining these observations one comes to the conclusion that at room temperature large, rigid supramolecular structures must exist that are much larger than a drug/CD complex. They give the mixture their high viscosity and contain the liquid-NMR-invisible drug and CD fractions.

Akira Harada and coworkers found that α-cyclodextrin can spontaneously be threaded on a linear polyethylene glycol chain to form a crystalline supramolecular complex[92]. In this assembly PEG penetrates the tunnel made of cyclodextrins and such a structure is called a molecular necklace (Fig. 7.10). Later it was also shown that in the presence of linear polymer chains cyclodextrins can act as cross-linking agents[93].

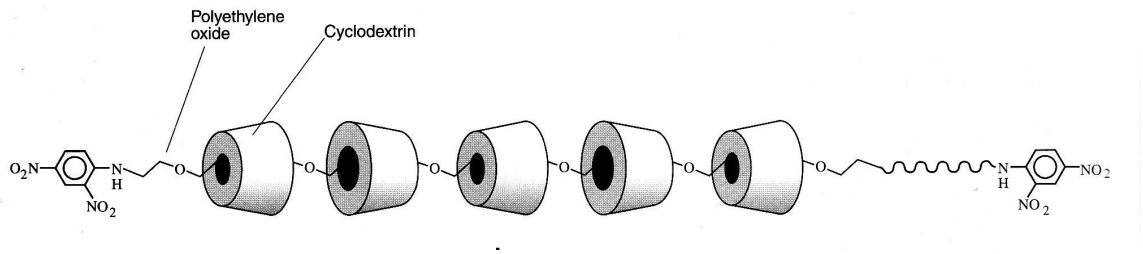

Fig. 7.10: Formation of molecular necklace from cyclodextrins and linear polymer chain[94].

In view of the modeling results we propose a similar process for the amiodarone/γ-CD mixture. Here the amiodarone molecules must form the chain in the necklace. Amiodarone is a relatively large drug molecule which is long and possesses several interaction sites for interaction with cyclodextrin molecules. For this reason one drug molecule is expected to penetrate two cyclodextrins. Continuing this pattern, molecular rods are formed, similarly as in the case of the polymer and cyclodextrin in

Fig. 7.10. Even the formation of cross-links seems possible, turning the liquid mixture into a gel.

The optical polarization experiments suggest that in addition the necklaces locally order to oriented domains, crystalline or liquid-crystalline domains. In that case we locally would have a physically cross-linked gel. The polarization effects are not homogeneous for the whole sample, in other words the ordering is not homogeneous.

We tried to establish with NMR if this ordering was liquid-crystalline like. In that case orientation effects could appear in a magnetic field when the domains would be free to orient, resulting in splitting of NMR lines. Since this did not happen, the ordered structures apparently are too rigid to allow orientation in a magnetic field.

Summarizing all experimental findings we propose that amiodarone and γ-cyclodextrin at room temperature form a gel, consisting of chains of amiodarone-cyclodextrin. Physical cross-linking of these chains occurs by ordered crystalline regions. In a rather narrow temperature range, between 40 and 50 ^{0}C, the crystalline regions are dissolved (the polarization effects disappear). At increasing temperature, between 25 and 70 ^{0}C, the supramolecular structures (chains) gradually dissolve into individual drug/CD complexes.

The hydrogel formed by cyclodextrin and the drug represents a potential drug delivery system for the release and delivery of this important anti-arrhythmic drug amiodarone. The advantage of this system is that the cross-linking in the gel is of physical nature which does not affect the drug molecule. Beside the drug the only components of this supramolecular delivery system are cyclodextrins which are water soluble, non-toxic and biocompatible. This novel hydrogel drug delivery system is temperature sensitive at temperatures near the body temperature and in this way drug diffusion rate can be controlled. The fact that addition of other cyclodextrin-complexing molecules can disturb the gel makes this system very attractive for the targeted drug delivery where it is often necessary to achieve a burst release of the drug at a certain site. Also this gel can be injected through a needle which is for some applications more attractive than implantable hydrogels.

Chapter 8: Summary

The aim of this work was to study the drug mobility and drug-matrix interaction in a hydrogel drug delivery system.

As polymeric drug delivery systems cross-linked PEG-containing polymer gels were used. With increasing cross-link density of the matrix the network mesh size decreases and the polymer exhibits lower swelling (swelling factor decreases). This affects the drug behavior in the gel. Different NMR methods provided information about the drug mobility in the gel and drug-polymer interaction. ^{1}H NMR spectroscopy was employed for the determination of the direct drug-polymer interaction via the drug proton chemical shifts, self-diffusion measurements for the study of translational mobility of drug molecules and water in the network and T_1 and T_2 measurements for the study of drug rotational mobility. All experiments were performed on drug-polymer-water systems that contain more water than the maximum amount the polymer network can take up by swelling. Therefore the systems were composed of two phases: water phase and gel phase. Under these conditions proton NMR spectra show that water soluble drugs partition between the gel phase and the water phase. For the drugs in the gel phase a model has been proposed in which the drug molecule exchanges fast between a state in which the drug is "bound" to the polymer network and a state in which the drug molecule is dissolved in the hydrogel water. This model and the experimental chemical shifts provide a quantitative measure for the drug-network interaction. The differences in chemical shift of protons of the drug bound to polymer and of the drug freely dissolved in water, $\delta_{drug}^{bound} - \delta_{drug}^{free}$, are very small, demonstrating the very weak drug-polymer interaction (van der Waals type), even for the largest drug and the highest cross-link density.

The drug self-diffusion and relaxation experiments show that the translational and rotational diffusional mobility of drug molecules in the investigated polymer networks is a complex function of the drug molecular mass and size and of the network cross-link density. When the cross-link density of the network increases, the diffusion rate of the drug molecules decreases. The translational diffusion is already hindered by the polymer network when the mesh size of the network is still much larger than the drug molecular size. On the other hand, the rotational mobility of the drug molecules is not very much dependent on the network cross-link density, except for the largest drug in the most dense

network, where the network mesh size approaches the drug molecular size. Under such conditions the rotational motion of the drug molecules becomes very anisotropic, as evidenced by the drug proton T_2 relaxation studies.

It has been shown that the network cross-link density represents an important tuning parameter in the polymeric drug delivery. It affects polymer morphology and surface properties of these materials (as shown by AFM), swelling behavior, diffusional mobility of the drug molecules in the gel and thereby the drug release rate.

Our study is also concerned with cyclodextrins, one of the most important molecular drug carriers. Two of the water soluble drugs investigated here form host-guest type inclusion complexes with cyclodextrins. It is found that the complexes also partition between the water phase and the gel phase. In contrast to expectation, the complexation of the drug to the CD does not necessarily slow down the drug diffusion in the gel network. This is explained by extending the model used to describe the diffusion of the drug alone in the network. When the drug-CD complexation is also described as an equilibrium reaction, the drug self-diffusion rate will depend on the equilibrium constants for the drug ↔ cyclodextrin and drug ↔ network equilibria. Combination of these equilibrium constants exist for which the drug diffusivity increases by the presence of a host molecule.

The fact that water insoluble drugs can build an inclusion complex with cyclodextrin is of great importance for the delivery of such drugs. By this means the solubility of the drug is enhanced which enables the introduction of the drug into the polymeric hydrogel as shown for the water insoluble drug ibuprofen. The drug availability and the efficiency of delivery of water insoluble drugs can be thus significantly improved.

Further in this work it was found that in the case of the water insoluble drug amiodarone and γ-cyclodextrin the drug-CD complexation leads to large, rigid supramolecular structures. We propose that the amiodarone molecules connect cyclodextrins to form linear chains. Locally these linear chains can order and probably form crystalline regions, which leads to a physically cross-linked gel. The properties of this complex material are strongly temperature dependent. At ca 45 ^{0}C the ordered local structures, and therefore the gel, disappear, while the supramolecular chain structures

disappear gradually in the temperature range 25 to 70 ^{0}C. This finding is of great importance for improvements in the delivery formulations of this important antiarrhythmic drug.

Chapter 9: Appendices

9.1 ^{1}H NMR spectra of water soluble drugs in swollen matrices

Proxyphylline and fluoresceine exhibit the same behavior as flucloxacilline in ternary drug/polymer/water systems. Figures 9.1 and 9.2 present the proton NMR spectra of proxyphylline and fluoresceine in swollen PEGDA matrices of different cross-link density, respectively.

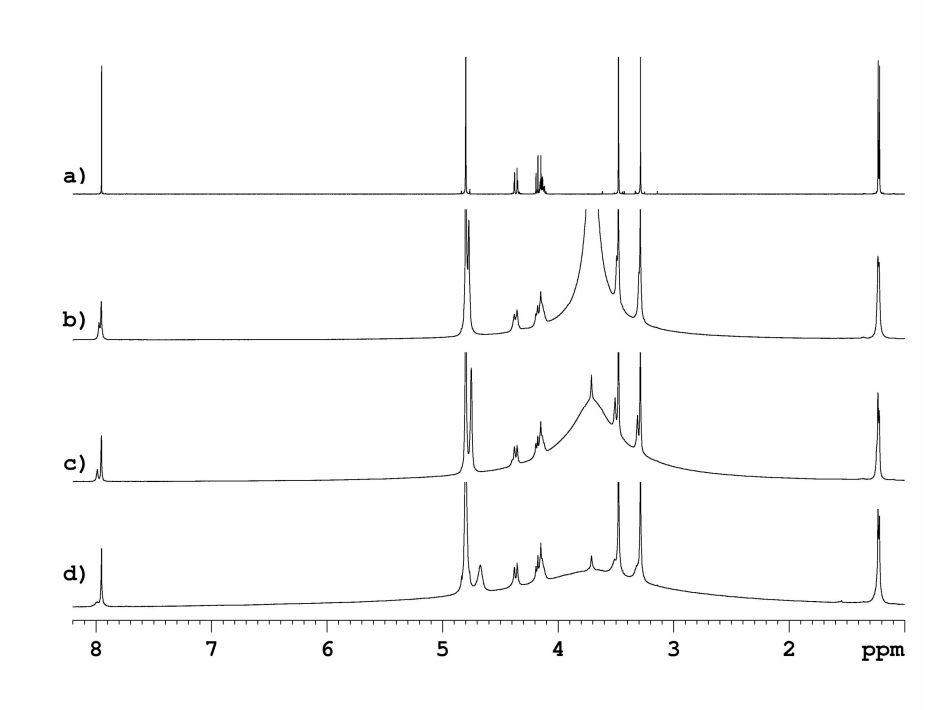

Fig. 9.1: ^{1}H NMR spectra of proxyphylline in water solution (a), in PEGDA 4000 (b), in PEGDA 2000 (c), and in PEGDA 450 (d).

In both cases the spectra show the same pattern as in the case with flucloxacilline. Beside the drug lines at the chemical shift for the drug in water, new lines appear, arising from the drug population in the gel phase of the two-phase systems. The drug and water molecules are partitioned between the water and the gel phase. At higher cross-link densities the lines become broader and the chemical shift difference between the two drug (or water) components increases.

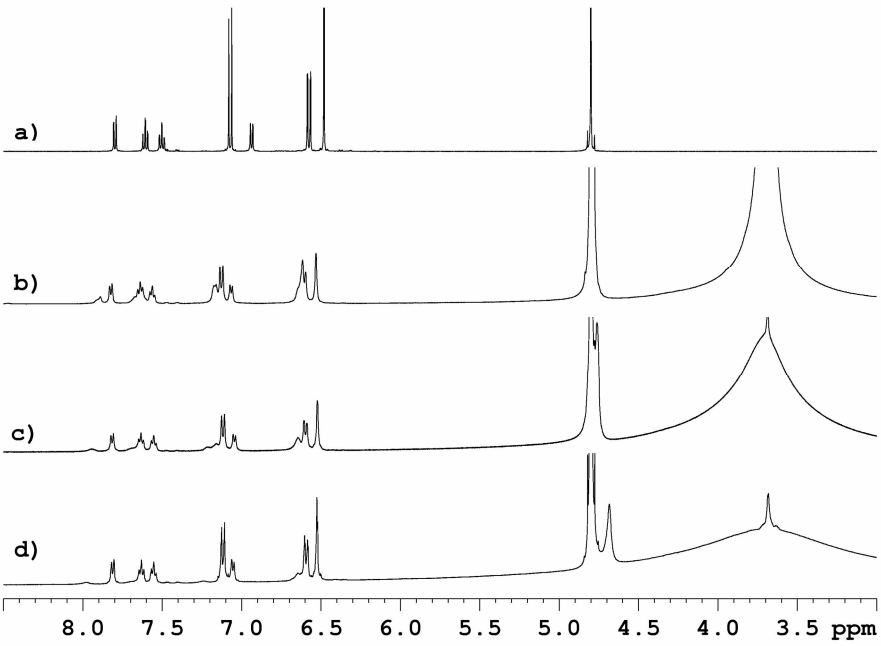

Fig. 9.2: ^{1}H NMR spectra of fluoresceine in water solution (a), in PEGDA 4000 (b), in PEGDA 2000 (c), and in PEGDA 450 (d).

9.2 Activation energies of water soluble drugs

Figures 9.3 and 9.4 represent the temperature dependence of diffusion of proxyphylline and fluoresceine in both the water and hydrogel phase of swollen PEGDA matrices with different cross-link densities. Here as well, the activation energies determined by the slope of the curves, do not change with the cross-link density of the matrix. For a certain degree of cross-linking, activation energies do not differ for the water and the hydrogel phase of the two-phase systems. It can be observed that the drug diffusion in the water phase of PEGDA 4000 system is somewhat slower than the diffusion in the water phase of PEGDA 2000 and PEGDA 450 matrix. This is because for the PEGDA 4000 matrix a slow exchange occurs between the drugs in the two phases of the swollen polymer.

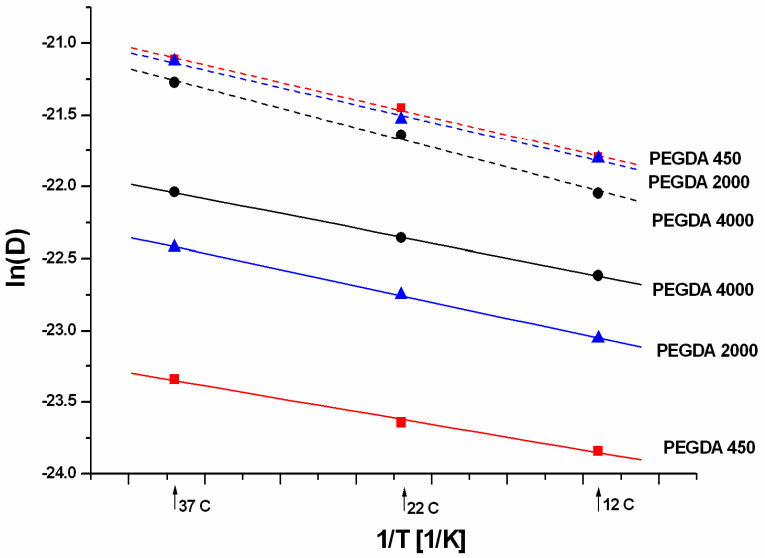

Fig. 9.3: Arrhenius plots of ln(D) of proxyphylline versus the reciprocal of the absolute temperature in different PEGDA matrices. The dashed lines represent the drug diffusion in the water phase, the solid lines the diffusion in the gel phase.

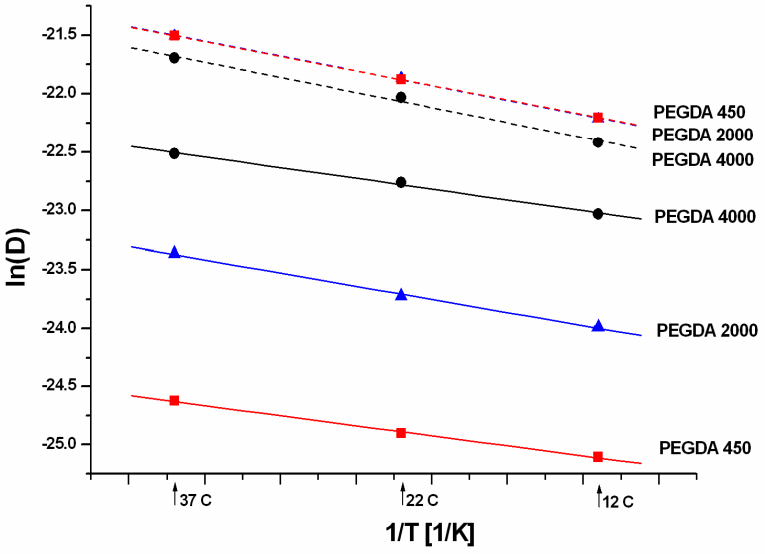

Fig. 9.4: Arrhenius plots of ln(D) of proxyphylline versus the reciprocal of the absolute temperature in different PEGDA matrices. The dashed lines represent the drug diffusion in the water phase, the solid lines the diffusion in the gel phase.

9.3 Structural assignment of cyclodextrin protons

Cyclodextrin protons can be classified as external and internal protons. Fig. 9.5 shows a structure of the glucose unit of a CD molecule with atom numbering.

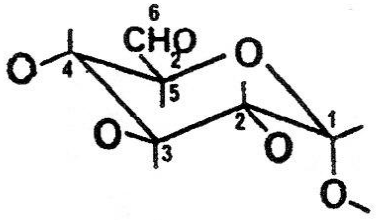

Fig. 9.5: Glucose residue of a cyclodextrin molecule with atom numbering[89]

External protons (H-2, H-4) are located at the outer surface of the torus, while internal protons (H-3, H-5) are placed in the internal hydrophobic cavity. Fig. 9.6 presents the ^{1}H NMR spectrum of α-CD in water including the assignment for different cyclodextrin protons.

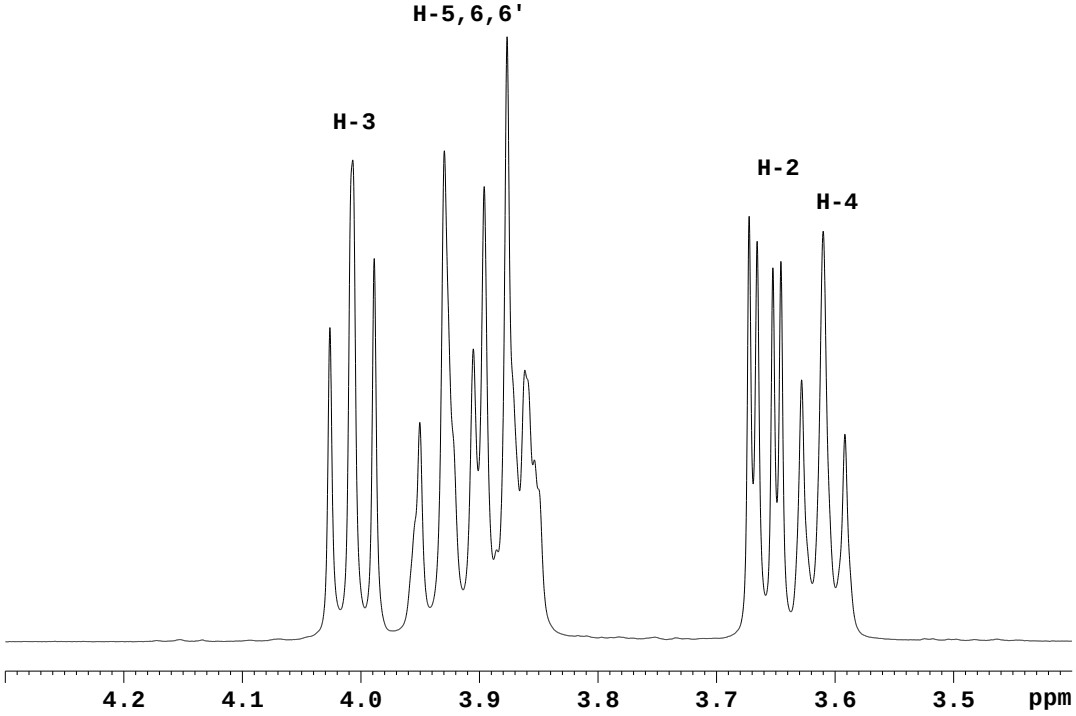

Fig. 9.6: CD spectral region of ^{1}H NMR spectrum of α-cyclodextrin in water

If a guest molecule is at least partly included in the CD cavity it should affect the internal protons of cyclodextrin and its corresponding resonances in the NMR spectrum will be shifted.

9.4 Assigned molecular structure of amiodarone

The 2-dimensional molecular structure of the water insoluble drug amiodarone is shown in Fig. 9.7 along with alphabetical assignment for different drug protons.

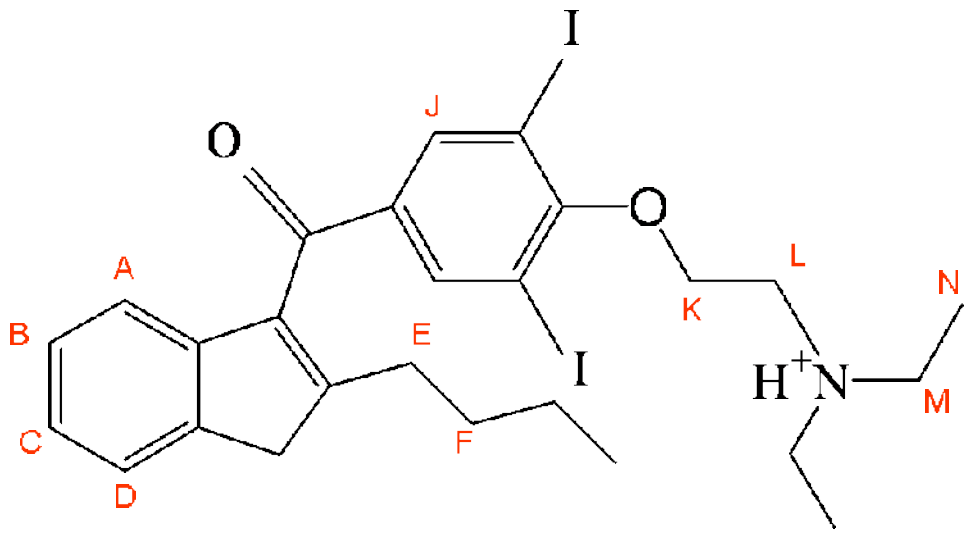

Fig. 9.7: Chemical structure of amiodarone with designated drug protons

The proton NMR spectrum of this drug in the mixture with γ-cyclodextrin is presented in Fig. 9.8. The NMR signals of corresponding drug protons are also alphabetically designated.

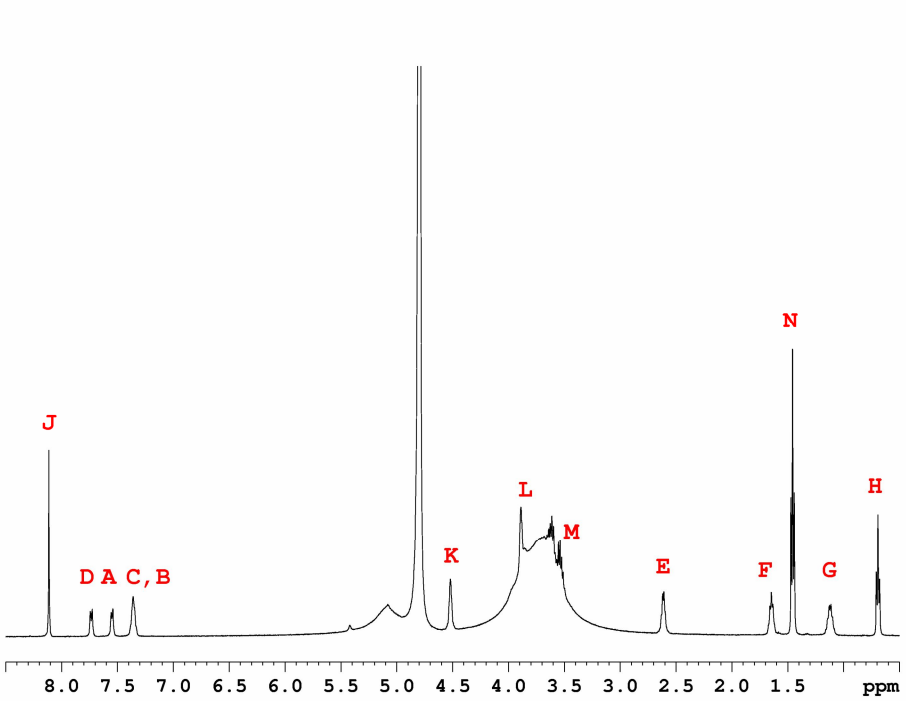

Fig. 9.8: Assigned ^{1}H NMR spectrum of amiodarone in the mixture with γ-CD.

9.5 List of abbreviations

1D	one-dimensional
2D	two-dimensional
3D	three-dimensional
AFM	Atomic Force Microscopy
ATR FTIR	Attenuated Total Reflection Fourier Transform Infrared
CAS	Chemical Shift Anisotropy
CD	Cyclodextrin
CP	Cross Polarization
CW	Continuous Wave
D	Diffusion coefficient
DDS	Drug Delivery System
DP	Degree of polymerization

E_a	Activation energy
FID	Free Induction Decay
FT	Fourier Transformation
ħ	Planck's constant divided by 2π (h/2π)
k_b	Boltzmann constant ($1.381 \cdot 10^{-23}$ J/K)
MAS	Magic Angle Spinning
M_c	Average molecular weight between cross-links
NMR	Nuclear Magnetic Resonance
NOE	Nuclear Overhauser Effect
NOESY	Nuclear Overhauser Enhancement Spectroscopy
OEG	oligo(ethylene glycol)
PEG	poly(ethylene glycol)
PEGDA	poly(ethylene glycol) diacrylate
PEO	poly(ethylene oxide)
PFGE	Pulsed Field Gradient Echo
R	Universal gas constant (8.314 J/mol·K)
STD	Saturation Transfer Difference
TMS	Tetramethylsilane
UV	Ultraviolet

Chapter 10: References

[1] J.G. Webster. Encyclopedia of medical devices and instrumentations. John Wiley & Sons, Inc., New York, 2006.

[2] E. E. Schmitt and R. A. Polistina. Surgical sutures. In U.S. Patent, Pat. No. 3,297,033. 1967.

[3] www.pharmaceutical-technology.com/contractors/drug_delivery/gallery.html

[4] K. E. Uhrich, S. M. Cannizzaro, R. S. Langer and K. M. Shakesheff. Polymeric systems for controlled drug release. Chem. Rev., 99:3181-3198, 1999.

[5] A. S. Hoffman. Hydrogels for biomedical applications. Adv. Drug Deliv. Rev., 43:3-12, 2002.

[6] S. Hamai. Inclusion of 2-Chloronaphtalene by α-Cyclodextrin and Room-Temperature Phosphorescence of 2-Chloronaphtalene in Aqueous D-Glucose Solutions Containing α-Cyclodextrin. J. Phys. Chem., 101:1707-1712, 1997.

[7] Y. Liu, L. Li, H. Zhang, Z. Fan and X. Guan. Selective binding of chiral molecules of cinchona alkaloid by β- and γ-cyclodextrins and organoselenium-bridged bis(β-cyclodextrin)s. Bioorg. Chem., 31:11-23, 2003.

[8] S. Bekiroglu, L. Kenne and C. Sandström. ^{1}H NMR Studies of Maltose, Maltoheptaose, α-, β-, and γ-Cyclodextrins, and Complexes in Aqueous Solutions with Hydroxy Protons as Structural Probes. J. Org. Chem., 68:1671-1678, 2003.

[9] MicroFab: Technology. www.microfab.com/technology/biomedical/Stents.html

[10] N. A. Peppas, K. B. Keys, M. Torres-Lugo and A. M. Lowman. Poly(ethylene glycol)-containing hydrogels in drug delivery. J. Control. Release, 62:81-87, 1999.

[11] L. Bromberg. Crosslinked poly(ethylene glycol) networks as reservoirs for protein delivery. J. Appl. Polym. Sci., 59:459-466, 1996.

[12] J. L. Stringer and N. A. Peppas. Diffusion of small molecular weight drugs in radiation-crosslinked poly(ethylene oxide) hydrogels. J. Control. Release, 42:195-202, 1996.

[13] C. P. Pathak, A. S. Sawhney and J. A. Hubbell. Rapid photopolymerization of immunoprotective gels in contact with cells and tissue. J. Am. Chem. Soc., 114:8311-8312, 1992.

[14] A. S. Sawhney, C. P. Pathak and J. A. Hubbell. Bioerodible hydrogels based on photopolymerized poly(ethylene glycol)-co-poly(α-hydroxy acid) diacrylate macromers. Macromolecules, 26:581-587, 1993.

[15] G. M. Cruise, D. S. Scharp and J. A. Hubbell. Characterization of permeability and network structure of interfacially photopolymerized poly(ethylene glycol) diacrylate hydrogels. Biomaterials, 19:1287-1294, 1998.

[16] R. A. Scott and N. A. Peppas. Highly crosslinked, PEG-containing copolymers for sustained solute delivery. Biomaterials, 20:1371-1380, 1999.

[17] M. B. Mellott, K. Searcy and M. V. Pishko. Release of protein from highly cross-linked hydrogels of poly(ethylene glycol) diacrylate fabricated by UV polymerization. Biomaterials, 22:929-941, 2001.

[18] V. M. Litvinov and A. A. Dias. Analysis of Network Structure of UV-Cured Acylates by ^{1}H NMR Relaxation, ^{13}C NMR Spectroscopy and Dynamic Mechanical Experiments. Macromolecules, 34: 4051-4060, 2001.

[19] M. Wulff and M. Aldén. Solid state studies of drug-cyclodextrin inclusion complexes in PEG 6000 prepared by a new method. Eur. J. Pharm. Sci., 8:269-281, 1999.

[20] E. Vallés, D. Durando, I. Katime, E. Mendizábal and J. E. Puig. Equillibrium swelling and mechanical properties of acrylamide and itaconic acid or its esters. Pollymer Bulletin, 44:109-114, 2000.

[21] K. S. Anseth, C. N. Bowman and L. Brannon-Peppas. Mechanical properties of hydrogels and their experimental determination. Biomaterials, 17:1647-1657, 1996.

[22] B. D. Ratner, A. S. Hoffman, F. J. Schoen and J. E. Lemons. Biomaterials science. An Introduction to Materials in Medicine. Elsevier Academic Press, San Diego, 2004.

[23] P. J. Flory and J. Rehner. Statistical Mechanics of Cross-Linked Polymer Networks. II Swelling. J. Chem. Phys., 11:521-526, 1943.

[24] P. J. Flory. Principles of polymer chemistry. Cornell University Press, London, 1978.

[25] J. C. Bray and E. W. Merrill. Poly(vinyl Alcohol) Hydrogels. Formation by Electron Beam Irradiation of Aqueous Solutions and Subsequent Crystallization. J. Appl. Pol. Sci., 17:3779-3794, 1973.

[26] T. Canal and N. A. Peppas. Correlation between mesh size and equilibrium degree of swelling of polymeric networks. J. Biomed. Mater. Res., 23:1183-1193, 1989.

[27] W. Borchard and U. Steinbrecht. Theory of swelling of a crosslinked substance in equilibrium with a solvent in various phases. Colloid. Polym. Sci., 269:95-104, 1991.

[28] L. T. Fan and S. K. Singh. Controlled Release: a Quantitative Treatment. Springer Verlag, Berlin Heidelberg, 1989.

[29] P. Colombo, R. Bettini, P. Santi and N. A. Peppas. Swellable matrices for controlled drug delivery: gel-layer behaviour, mechanisms and optimal performance. Pharm. Sci. Technol. Today, 3:198-204, 2000.

[30] P. L. Ritger and N. A. Peppas. A simple equation for description of solute release II. Fickian and anomalous release from swellable devices. J. Controlled Release, 5:37-42, 1986.

[31] J. Kärger and D. M. Ruthven. Diffusion in Zeolites and Other Microporous Solids. John Wiley & Sons, Inc., New York, 1992.

[32] P. T. Callaghan. Principles of Nuclear Magnetic Resonance Microscopy. Oxford University Press Inc., New York, 1991.

[33] L. Masaro, X. X. Zhu and P. M. Macdonald. Study of the Self-Diffusion of Poly(ethylene glycol)s in Poly(vinyl alcohol) Aqueous Systems. J. Polym. Sci. B: Polym. Phys., 37:2396-2403, 1999.

[34] L. Masaro and X. X. Zhu. Physical models of diffusion for polymer solutions, gels and solids. Prog. Polym. Sci., 24:731-775, 1999.

[35] J. S. Mackie and P. Meares. The diffusion of electrolytes in a cation-exchange resin membrane. Proc. R. Soc. Lond. A, 232:498-509, 1955.

[36] A. G. Ogston, B. N. Preston and J. D. Wells. On the transport of compact particles through solutions of chain polymers, Proc. R. Soc. Lond. A, 333:297-316, 1973.

[37] H. Yasuda, C. E. Lamaze and L. D. Ikenberry. Permeability of Solutes through Hydrated Polymer Membranes. Makromol. Chem., 118:19-35, 1968.

[38] G. D. J. Philies. Universal Scaling Equation for Self-Diffusion by Macromolecules in Solution. Macromolecules, 19:2367-2376, 1986.

[39] R. A. Dwek and R. E. Richards. Study of Molecular Motion in Liquids by Measurement of Nuclear Relaxation. Discuss. Faraday Soc., 43:196-204, 1967.

[40] A. Abragam. The principles of nuclear magnetism. Oxford University Press, London, 1961.

[41] R. J. Abraham, J. Fisher and P. Loftus. Introduction to NMR Spectroscopy. John Wiley & Sons, New York, 1988.

[42] D. E. Woessner. Nuclear Spin Relaxation in Ellipsoids Undergoing Rotational Brownian Motion. J. Chem. Phys., 37:647-654, 1962.

[43] R. Witt, L. Sturz and A. Dölle. Molecular Dynamics of Benzene in Neat Liquid and a Solution Containing Polystyrene. ^{13}C Nuclear Magnetic Relaxation and Molecular Dynamics Simulation Results. J. Phys. Chem. A, 104:5716-5725, 2000.

[44] W. A. Freeman. Structures of p-xylylenediammonium chloride and calcium hydrogensulfat adducts of the cavitand 'cucurbituril', $C_{36}H_{36}N_{24}O_{12}$. Acta Cryst. B, 40:382-387, 1984.

[45] R. Challa, A. Ahuja, J. Ali and R. K. Khar. Cyclodextrins in Drug Delivery: An Updated Review. PharmSciTech., 6:329-357, 2005.

[46] M. Wulff and M. Aldén. Solid state studies of drug-cyclodextrin inclusion complexes in PEG 6000 prepared by a new method. Eur. J. Pharm. Sci., 8:269-281, 1999.

[47] M. Wulff, M. Alden and J. Tegenfeldt. Solid-State NMR Investigation of Indomethacin-Cyclodextrin Complexes in PEG 6000 Carrier. Bioconjugate Chem., 13:240-248, 2002.

[48] T. Loftsson and M. E. Brewster. Pharmaceutical Applications of Cyclodextrins. 1. Drug Solubilization and Stabilization. J. Pharm. Sci., 85:1017-1025, 1996.

[49] C. Rodriguez-Tenreiro, C. Alvarez-Lorenzo, A. Rodriguez-Perez, A. Concheiro and J. J. Torres-Labandeira. New Cyclodextrin Hydrogels Cross-Linked with Diglycidylethers with a High Drug Loading and Controlled Release Ability. Pharm. Res., 23:121-130, 2006.

[50] H. Friebolin. Basic One- and Two-Dimensional NMR Spectroscopy. VCH Publishers, New York, 1993.

[51] W. S. Veeman, NMR Spektroskopie. Lecture Notes.

[52] J. Kärger. The Benefit of Microscopic Measuring Techniques for Unveiling Structure-Mobility Relations in Molecular Diffusion under Confinement. Diffusion Fundamentals, 1:5.1-5.107, 2005.

[53] E. O. Stejskal and E. J. Tanner. Spin diffusion measurements: Spin echoes in the presence of a time-dependent field gradient. J. Chem. Phys., 42:288-292, 1965.

[54] K. I. Momot and P. W. Kuchel. Pulsed Field Gradient Nuclear Magnetic Resonance as a Tool for Studying Drug Delivery Systems. Concepts Magn. Reson. A, 19:51-64, 2003.

[55] S. Matsukawa and I. Ando. A study of Self-Diffusion of Molecules in Polymer Gel by Pulsed-Gradient Spin-Echo ^{1}H NMR. Macromolecules, 29:7136-7140, 1996.

[56] H. Walderhaug, B. Nyström, F. K. Hansen and B. Lindman. Interactions of Ionic Surfactants with a Nonionic Cellulose Ether in Solution and in the Gel State Studied by Pulsed Field Gradient NMR. J. Phys. Chem., 99:4672-4678, 1995.

[57] J. Kříž. Diffusion of Molecules Confined in Semipenetrable Nanoscale Carriers Probed by Pulsed Field Gradient NMR. Langmuir, 20:9560-9564, 2004.

[58] M. Mayer and B. Meyer. Group Epitope Mapping by Saturation Transfer Difference NMR to Identify Segments of a Ligand in Direct Contact with a Protein Receptor. J. Am. Chem. Soc., 123:6108-6117, 2001.

[59] J. H. Streiff, N. O. Juranic, S. I. Macura, D. O. Warner, K. A. Jones and W. J. Perkins. Saturation Transfer Difference Nuclear Magnetic Resonance Spectroscopy As a Method for Screening Proteins for Anesthetic Binding. Mol. Pharmacol., 66:929-935, 2004.

[60] D. Neuhaus and M. P. Williamson. The Nuclear Overhauser Effect in Structural and Conformational Analysis. John Wiley & Sons, New York, 2000.

[61] G. Jeschke. High-Resolution Solid-State NMR: Magic Angle Spinning and Cross Polarization. Lecture notes, WS 2003/04.

[62] W. S. Veeman. Syllabus solid state NMR course paon:basics. Lecture notes.

[63] C. S. Yanoni. High resolution NMR in solids: the CPMAS experiment. IBM Research Laboratory, San Jose, California.

[64] P. E. West. Introduction to Atomic Force Microscopy. Theory, Practice, Applications. Pacific Nanotechnology site, www.pacificnanotech.com, 2007.

[65] JPK Instruments AG. Tutorial for Scanning Probe Microscopy in Life Science. www.jpk.com.

[66] K. Tomić, W. S. Veeman, M. Boerakker, V. M. Litvinov and A. A. Dias. Lateral and Rotational Mobility of Some Drug Molecules in a Poly(Ethylne Glycol) Diacrylate Hydrogel and the Effect of Drug-Cyclodextrin Complexation. J. Pharm. Sci., published online (early view), DOI 10.1002/jps 21251, 2007.

[67] J. L. Hill-West, S. M. Chowdhury, M. J. Slepian and J. A. Hubbell. Inhibition of thrombosis and intimal thickening by in situ photopolymerization of thin hydrogel barriers. Proc. Natl. Acad. Sci. USA, 91:5967-5971, 1994.

[68] J. L. West and J. A. Hubbell. Separation of the arterial wall from blood contact using hydrogel barriers reduces intimal thickening after balloon injury in the rat: The roles of medial and luminal factors in arterial healing. Proc. Natl. Acad. Sci. USA, 93:13188-13193, 1996.

[69] J. Elisseeff, K. Anseth, D. Sims, W. McIntosh, M. Randolph and R. Langer. Transdermal photopolymerization for minimally invasive implantation. Proc. Natl. Acad. Sci. USA, 96:3104-3107, 1999.

[70] K. T. Nguyen and J. L. West. Photopolymerizable hydrogels for tissue engineering applications. Biomaterials, 23:4307-4314, 2002.

[71] S. Lu and K. S. Anseth. Photopolymerization of multilaminated poly(HEMA) hydrogels for controlled release. J. Control. Release, 57:291-230, 1999.

[72] T. Cserháti and E. Smith. Cyclodextrins in Chromatography. Athenaeum Press Ltd, Gateshead, UK, 2003.

[73] K. Uekama. Design and Evaluation of Cyclodextrin-Based Drug Formulation. Chem. Pharm. Bull., 52:900-915, 2004.

[74] A. P. Mukne and M. S. Nagarsenker. Triamterene-β-cyclodextrin Systems:Preparation, Characterization and In Vivo Evaluation. Pharm. Sci. Tech., 5:1-19, 2004.

[75] E. Sabadini and T. Cosgrove. Inclusion Complex Formed between Star-Poly(ethylene glycol) and Cyclodextrins. Langmuir, 19:9680-9683, 2003.

[76] D. R. Kioussis and P. Kofinas. Characterization of network morphology in anion binding hydrogels used for wastewater remediation. Polymer, 46:10167-10172, 2005.

[77] A. Suzuki, M. Yamazaki and Y. Kobiki. Direct observation of polymer gel surfaces by atomic force microscopy. J. Chem. Phys., 104:1751-1757, 1996.

[78] G. Reiter and J.U. Sommer. Crystallization of Adsorbed Polymer Monolayers. Phys. Rev. Lett., 80:3771-3774, 1998.

[79] G. Reiter and J.U. Sommer. Polymer crystallization in quasi-two dimensions. I. Experimental results. J. Chem. Phys., 112:4376-4382, 2000.

[80] D. L. Gilbert, T. Okano, T. Miyata and K. W. Sim. Macromolecular diffusion through collagen membranes. Int. J. Pharm., 47:79-88, 1988.

[81] S. Lu and K. S. Anseth. Release behavior of high molecular weight solutes from poly(ethylene glycol)-based degradable networks. Macromolecules, 33:2509-2515, 2000.

[82] E. W. Merrill, K. A. Dennison and C. Sung. Partitioning and diffusion of solutes in hydrogels of poly(ethylene oxide). Biomaterials, 14:1117-1126, 1993.

[83] I. Calderara, R. Gougeon, L. Delmotte, V. Lemee and D. J. Lougnot. NMR study of the structure and properties of poly(MMA-co-VP) crosslinked hydrogels. J. Polym. Sci. A Polym. Chem., 35:3619-3625, 1997.

[84] R. A. Dwek. Nuclear magnetic resonance in biochemistry: Applications to enzyme systems. Clarendon Press, Oxford, 1973.

[85] V. M. Rao, J. L. Haslam and V. J. Stella. Controlled and complete release of a model poorly water-soluble drug, prednisolone, from hydroxypropyl methylcellulose matrix tablets using $(SBE)_{7m}$-β-cyclodextrin as a solubilizing agent. J Pharm. Sci., 90:807-816, 2001.

[86] S. M. Ali, A. Maheshwari, F. Asmat and M. Koketsu. Complexation of enalapril maleate with β-cyclodextrin: NMR spectroscopic study in solution. Quim. Nova, 29:685-688, 2006.

[87] I. Bratu, J. M. Gavira-Vallejo and A. Hernanz. ^{1}H-NMR Study of the Inclusion Processes for α- and γ-Cyclodextrin with Fenbufen. Biopolymers, 77:361-367, 2005.

[88] C. Sicard-Roselli, B. Perly and G. le Bas. The Respective Benefits of X-ray Crystallography and NMR for the Structural Determination of the Inclusion Complex Between Butyl-isothiocyanate and Alpha-cyclodextrin. J. Inclusion Phenom. Macrocycl. Chem., 39:333-337, 2001.

[89] A. F. Casy and A. D. Mercer. Application of Cyclodextrins to Chiral Analysis by ^{1}H NMR Spectroscopy. Magn. Reson. Chem., 26:765-774, 1988.

[90] P. Gao and P. Fagerness. Diffusion in HPMC gels. I. Determination of drug and water diffusivity by pulsed-field-gradient spin-echo NMR. Pharm. Res., 12:955-964, 1995.

[91] F. Quaglia, G. Varicchio, A. Miro, M. I. La Rotonda, D. Larobina and G. Mensitieri. Modulation of drug release from hydrogels by using cyclodextrins: The case of nicardipine/β-cyclodextrin system in cross-linked polyethyleneglycol. J. Control. Release, 71:329-337, 2001.

[92] A. Harada, J. Li and M. Kamachi. The molecular necklace: a rotaxane containing many threaded α-cyclodextrins. Nature, 356:325-327, 1992.

[93] J. Li, X. Ni and K. W. Leong. Injectable drug-delivery systems based on supramolecular hydrogels formed by poly(ethylene oxide)s and α-cyclodextrin. J. Biomed. Mater. Res., 65:196-202, 2003.

[94] N. Hall. The new chemistry. Cambridge University Press, 2000.